PHYSICAL REVIEW C **88**, 035209 (2013)

Nucleon resonances within a dynamical coupled-channels model of πN and γN reactions

H. Kamano,[1] S. X. Nakamura,[2] T.-S. H. Lee,[3] and T. Sato[4]
[1]*Research Center for Nuclear Physics, Osaka University, Ibaraki, Osaka 567-0047, Japan*
[2]*Yukawa Institute for Theoretical Physics, Kyoto University, Kyoto 606-8502, Japan*
[3]*Physics Division, Argonne National Laboratory, Argonne, Illinois 60439, USA*
[4]*Department of Physics, Osaka University, Toyonaka, Osaka 560-0043, Japan*
(Received 23 May 2013; published 27 September 2013)

The nucleon resonances are investigated within a dynamical coupled-channels model of πN and γN reactions up to the invariant mass $W = 2$ GeV. The meson-baryon (MB) channels included in the calculations are $MB = \pi N$, ηN, $K\Lambda$, $K\Sigma$, and $\pi\pi N$ that has $\pi\Delta$, ρN, and σN resonant components. The meson-baryon amplitudes $T_{M'B',MB}(W)$ are calculated from solving a set of coupled-channels integral equations defined by an interaction Hamiltonian consisting of (a) meson-exchange interactions $v_{M'B',MB}$ derived from phenomenological Lagrangian and (b) vertex interactions $N^* \to MB$ for describing the transition of a bare excited nucleon state N^* to a meson-baryon channel MB. The parameters of $v_{M'B',MB}$ are mainly constrained by the fit to the data of $\pi N \to \pi N$ in the low-energy region up to $W = 1.4$ GeV. The bare masses of N^* and the $N^* \to MB$ parameters are then determined in simultaneous fits to the data of $\pi N \to \pi N$ up to $W = 2.3$ GeV and those of $\pi N \to \eta N$, $K\Lambda$, $K\Sigma$ and $\gamma N \to \pi N$, ηN, $K\Lambda$, $K\Sigma$ up to $W = 2.1$ GeV. The pole positions and residues of nucleon resonances are extracted by analytically continuing the meson-baryon amplitudes $T_{M'B',MB}(W)$ to the complex Riemann energy surface. From the extracted residues, we have determined the $N^* \to \pi N$, γN, ηN, $K\Lambda$, $K\Sigma$ transition amplitudes at resonance poles. We compare the resonance pole positions from our analysis with those given by the Particle Data Group and the recent coupled-channels analyses by the Jülich and Bonn-Gatchina groups. Four results agree well only for the first N^* in each spin-parity-isospin (J^P, I) channel. For higher mass states, the number of states and their resonance positions from four results do not agree well. We discuss the possible sources of the discrepancies and the need of additional data from new hadron facilities such as the Japan Proton Accelerator Research Complex.

DOI: 10.1103/PhysRevC.88.035209 PACS number(s): 14.20.Gk, 13.75.Gx, 13.60.Le, 24.10.Eq

I. INTRODUCTION

One of the important problems in hadron physics is to understand the structure of the nucleon within quantum chromodynamics (QCD). Because the nucleon is a composite particle, its properties are closely related to the spectrum and the structure of its excited states. From the available data, we know that all of the excited nucleon states (denoted collectively as N^*) are unstable and couple strongly with the meson-baryon continuum states to form resonances in πN and γN reactions. Therefore, the study of the N^* resonances in πN and γN reactions has been a well-recognized important task in advancing our understanding of the structure of baryons. It can also provide important information for understanding how the confinement and chiral symmetry breaking emerge from QCD.

In this work, we report on the results from an investigation of N^* resonances with an extension of the dynamical coupled-channels (DCC) model developed in Ref. [1]. Schematically, the following coupled-channels integral equations in each partial wave are solved within the DCC model of Ref. [1],

$$T_{\beta,\alpha}(p_\beta, p_\alpha; W) = V_{\beta,\alpha}(p_\beta, p_\alpha; W) + \sum_\gamma \int p^2 dp V_{\beta,\gamma}(p_\beta, p; W) \times G_\gamma(p; W) T_{\gamma,\alpha}(p, p_\alpha; W), \quad (1)$$

with

$$V_{\beta,\alpha}(p_\beta, p_\alpha; W) = v_{\beta,\alpha}(p_\beta, p_\alpha) + \sum_{N^*} \frac{\Gamma^\dagger_{N^*,\beta}(p_\beta)\Gamma_{N^*,\alpha}(p_\alpha)}{W - M^0_{N^*}}, \quad (2)$$

where $\alpha, \beta, \delta = \gamma N, \pi N, \eta N$, and $\pi\pi N$ that has the unstable $\pi\Delta$, ρN, and σN components, $G_\delta(p; W)$ is the Green's function of the channel δ, $M^0_{N^*}$ is the mass of a bare excited nucleon state N^*, $v_{\beta,\alpha}$ is defined by the meson-exchange mechanisms, and the vertex interaction $\Gamma_{N^*,\alpha}$ defines the $\alpha \to N^*$ transition. We describe in Sec. II how Eqs. (1) and (2) can be cast into a form that is most convenient for extracting the nucleon resonances from the amplitude $T_{\beta,\alpha}(p_\beta, p_\alpha; W)$. In the past few years, we have applied this DCC model to analyze πN and γN reactions with πN [2–4], ηN [5], and $\pi\pi N$ [6,7] final states. The method for extracting the nucleon resonances within the considered DCC model was developed in Refs. [8,9] with the results presented in Refs. [9–11]. During this developing stage, the DCC model parameters were not determined by *simultaneous* fits to all of the considered data. In addition, the very extensive data of $K\Lambda$ and $K\Sigma$ photoproduction reactions were not included in the analysis. As a step in improving our analysis, we have extended these earlier efforts to perform a *combined* analysis of the available data for $\pi N, \gamma N \to \pi N, \eta N, K\Lambda$, and $K\Sigma$. The purpose of this paper is to report on the results from this effort.

 ©2013 American Physical Society

The starting point of our analysis is to extend the model, defined by Eqs. (1) and (2), to include the $K\Lambda$ and $K\Sigma$ channels. We then apply the same numerical procedures detailed in our previous publications [1–3,8,9] to perform the calculations. Our main effort is to determine the parameters of the interactions $V_{\beta,\alpha}$ of Eq. (2) by fitting simultaneously all of the rather extensive data, as explained later. The nucleon resonances are then extracted from the resulting model by using the analytic continuation method developed in Refs. [8,9].

The extraction of nucleon resonances has a long history and several different approaches have been developed. To see the main features of our approach, as well as the other dynamical models [12–20], we briefly discuss how the nucleon resonances are extracted by the other analysis groups. It is common to parametrize [21–29] the partial-wave amplitudes in terms of polynomial functions, the Breit-Wigner forms, the tree diagrams of phenomenological Lagrangian, or various combinations of them. The K-matrix method is used in these analyses to unitarize the constructed amplitudes. In most cases, the resulting forms of partial-wave amplitudes depend algebraically on the energy variable W and hence it is rather efficient numerically to fit the data and extract the resonances. The analyses [30–32] based on the unitary Carnegie-Mellon-Berkeley model also only involve solving algebraic equations in extracting the resonances from the partial-wave amplitudes. In an approach based on a DCC model, such as the one defined by Eqs. (1) and (2), the partial-wave amplitudes are calculated by solving a set of coupled-channels integral equations. Thus, the computation effort needed in fitting the meson production data is considerably more complex than that of the K-matrix analyses. Furthermore, the resulting partial-wave amplitudes, defined by the coupled-channels integral equations such as Eqs. (1) and (2) used in our analysis, have complicated analytic structure and must be analyzed carefully to develop a correct procedure for extracting the nucleon resonances.

Compared with the models [21–24,30–32] with polynomial parameterizations of the partial-wave amplitudes, our approach, as well as all dynamical models, have an important constraint in fitting the data. In the polynomial fits, the parameters in each partial wave of each channel are adjusted independently. However, the dynamical models have much less freedom in adjusting the parameters to fit the data because the partial-wave amplitudes in all partial waves and in all reaction channels are related to the same parameters of the meson-exchange mechanisms.

Obviously, a DCC approach is much more complex and difficult than the other approaches [21–32]. This, however, is needed to investigate the dynamical origin and the internal structure of the nucleon resonances. As can be seen from the ingredients of the interaction $V_{\beta,\alpha}(p_\beta, p_\alpha; W)$ in Eq. (2), the dynamical model considered in our approach is aimed at exploring a question whether a nucleon resonance can be interpreted as a system of a core state surrounded by a meson cloud, a moleculelike meson-baryon state, or a mixture of them. Such an interpretation has been obtained for the Δ (1232) resonance in various meson-exchange models of πN and γN reactions up to $W = 1.3$ GeV. An example can be found in Ref. [15], where $\Delta(1232)$ was interpreted as a baryon made of a core state and a pion cloud. The resulting core state can be identified, qualitatively, with the Δ of a hadron structure model with only constituent-quark degrees of freedom. Our earlier DCC analysis [10,11] has also provided useful information on the dynamical origin of the Roper resonance and has provided an interpretation of the mass of the first excited nucleon state with isospin-spin-parity $I(J^P) = 1/2(1/2^+)$ predicted by most of the hadron structure models such as the model based on the Dyson-Schwinger equation of QCD [33]. The DCC analysis performed in this work is a necessary step toward improving our understanding of the dynamical origins and the structure of all nucleon resonances with mass below 2 GeV.

In Sec. II, we briefly describe the formulation of the DCC model used in our analysis. The formula for extracting nucleon resonances developed in Refs. [8,9] are reviewed in Sec. III. The procedures for determining the model parameters are explained in Sec. IV. The fits to the data are presented and discussed in Sec. V. The extracted nucleon resonances are given in Sec. VI. In Sec. VII, we discuss the possible future developments. For completeness, we also explain the essential details of our calculations in Appendixes A–D. The determined model parameters are given in Appendix E.

II. DYNAMICAL COUPLED-CHANNELS MODEL

Because the formulation of the DCC model employed in this work has been given in detail in Refs. [1–4,6,7], here we only briefly describe the relevant equations that are needed to define the notations for presenting our results. We also indicate several improvements we have made for performing the combined analysis of pion- and photon-induced πN, ηN, $K\Lambda$, and $K\Sigma$ production reactions.

A. Hadronic amplitudes

Within the formulation of Ref. [1], we apply the projection operator method [34] to cast the partial-wave components of the T-matrix elements of the meson-baryon reactions, $M(\vec{k}) + B(-\vec{k}) \to M'(\vec{k}') + B'(-\vec{k}')$, into the form

$$T_{M'B',MB}(k', k; W) = t_{M'B',MB}(k', k; W) + t^R_{M'B',MB}(k', k; W), \tag{3}$$

where W is the total energy, k and k' are the meson-baryon relative momenta in the center of mass frame, and MB, $M'B' = \pi N, \eta N, \pi\Delta, \rho N, \sigma N, K\Lambda, K\Sigma$ are the reaction channels included in this analysis. [The label "MB" also specifies quantum numbers (spin, parity, isospin, etc.) associated with the channel MB.]

The "nonresonant" amplitude $t_{M'B',MB}(k', k; W)$ in Eq. (3) is defined by a set of coupled-channels integral equations,[1]

[1]Because of the perturbative nature of the electromagnetic interactions, it is only necessary to solve the coupled-channels equations in the channel space excluding the γN channel. The $\gamma N \to \pi N$ amplitude up to the order of $e = \sqrt{4\pi/137}$ can then be calculated perturbatively, as can be seen in Sec. II B.

TABLE I. Branch points of the meson-baryon Green's functions $G_{MB}(k;W)$ for unstable channels $MB = \pi\Delta, \sigma N, \rho N$. For the calculation of the Green's functions, we take $m_N = 938.5$ MeV and $m_\pi = 138.5$ MeV.

	Branch point (MeV)
$\pi\Delta$	$(1211.5 - i55.0) + m_\pi$
σN	$(483.7 - i185.8) + m_N$
	$(1032.3 - i247.7) + m_N$
ρN	$(765.5 - i75.0) + m_N$

$$t_{M'B',MB}(k',k;W) = V_{M'B',MB}(k',k;W) + \sum_{M''B''}\int_{C_{M''B''}} k''^2 dk'' V_{M'B',M''B''}(k',k'';W) \times G_{M''B''}(k'';W) t_{M''B'',MB}(k'',k;W). \quad (4)$$

Here $C_{M''B''}$ is the integration path, which is taken from 0 to ∞ for the physical W; the summation $\sum_{MB}$ runs over the orbital angular momentum and total spin indices for all MB channels allowed in a given partial wave; $G_{M''B''}(k;W)$ are the meson-baryon Green's functions. Defining $E_\alpha(k) = [m_\alpha^2 + k^2]^{1/2}$ with m_α being the mass of a particle α, the meson-baryon Green's functions in the above equations are

$$G_{MB}(k;W) = \frac{1}{W - E_M(k) - E_B(k) + i\epsilon}, \quad (5)$$

for the stable πN, ηN, $K\Lambda$, and $K\Sigma$ channels, and

$$G_{MB}(k;W) = \frac{1}{W - E_M(k) - E_B(k) - \Sigma_{MB}(k;W)}, \quad (6)$$

for the unstable $\pi\Delta$, ρN, and σN channels. The details of the self-energy $\Sigma_{MB}(k;W)$ in Eq. (6) are given in Appendix A. The branch points of the meson-baryon Green's functions $G_{MB}(k;W)$, as defined by zeros of the denominator of Eqs. (5) and (6), are related closely to the search of resonance positions on the complex energy surface, as explained in Sec. III. In Table I, we list the branch points of the $\pi\Delta$, ρN, and σN channels within the model considered here.

The driving terms of Eq. (4) are

$$V_{M'B',MB}(k',k;W) = v_{M'B',MB}(k',k) + Z^{(E)}_{M'B',MB}(k',k;W). \quad (7)$$

Here the potentials $v_{M'B',MB}(k',k)$ are meson-exchange interactions derived from the tree diagrams, as illustrated in Fig. 1, of phenomenological Lagrangian. Within the unitary transformation method [15,35–37] used in the derivation, those

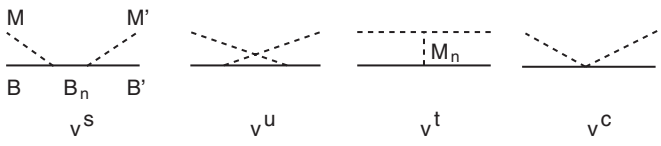

FIG. 1. Meson-exchange mechanisms.

FIG. 2. Z-diagram mechanisms.

potentials are energy independent and free of singularities. In Appendix B, we list the Lagrangian used in our derivations. The resulting forms of $v_{M'B',MB}(k',k)$ and their partial-wave expansions are given in Appendix C.

The energy-dependent $Z^{(E)}_{M'B',MB}(k',k;W)$ terms in Eq. (7), as illustrated in Fig. 2, contain the *moving* singularities owing to the three-body $\pi\pi N$ cut. These Z-diagram terms were neglected in the fit of Ref. [2] and are now included in this combined analysis. With this inclusion of the Z-diagram terms, we have confirmed that our model satisfies the three-body $\pi\pi N$ unitarity perfectly within the numerical accuracy. The procedures for evaluating the partial-wave matrix elements of $Z^{(E)}_{M'B',MB}(k',k;W)$ are explained in detail in Appendix E of Ref. [1].

The second term on the right-hand-side of Eq. (3) is the N^*-excitation term defined by

$$t^R_{M'B',MB}(k',k;W) = \sum_{N^*_n,N^*_m} \bar\Gamma_{M'B',N^*_n}(k';W)[D(W)]_{n,m}\bar\Gamma_{N^*_m,MB}(k;W). \quad (8)$$

Here the dressed $N^* \to MB$ and $MB \to N^*$ vertices are, respectively, defined by

$$\bar\Gamma_{MB,N^*}(k;W) = \Gamma_{MB,N^*}(k) + \sum_{M'B'}\int q^2 dq t_{MB,M'B'}(k,q;W) \times G_{M'B'}(q,W)\Gamma_{M'B',N^*}(q), \quad (9)$$

$$\bar\Gamma_{N^*,MB}(k;W) = \Gamma_{N^*,MB}(k) + \sum_{M'B'}\int q^2 dq \Gamma_{N^*,M'B'}(q) \times G_{M'B'}(q,W) t_{M'B',MB}(q,k;W), \quad (10)$$

with $\Gamma_{MB,N^*}(k)$ being the bare $N^* \to MB$ decay vertex [note that $\Gamma_{N^*,MB}(k) = \Gamma^\dagger_{MB,N^*}(k)$]; the inverse of the dressed N^* propagator is defined by

$$[D^{-1}(W)]_{n,m} = \left(W - M^0_{N^*_n}\right)\delta_{n,m} - [\Sigma_{N^*}(W)]_{n,m}, \quad (11)$$

where $M^0_{N^*}$ is the mass of the bare N^* state and the N^* self-energies $\Sigma_{N^*}(W)$ are given by

$$[\Sigma_{N^*}(W)]_{n,m} = \sum_{MB}\int_{C_{MB}} k^2 dk \Gamma_{N^*_n,MB}(k) \times G_{MB}(k;W)\bar\Gamma_{MB,N^*_m}(k;W). \quad (12)$$

We emphasize here that the N^* propagator $D(W)$ can have off-diagonal terms owing to the meson-baryon interactions.

Equations (3)–(12) define the DCC model used in our analysis. In the absence of theoretical input, the DCC model, as well as all hadron reaction models, has parameters that

can only be determined phenomenologically from fitting the data. The meson-exchange interactions $v_{M'B',MB}$ depend on the coupling constants and the cutoffs of form factors that regularize their matrix elements. While the values of some of the coupling constants can be estimated from the flavor SU(3) relations, we allow most of them to vary in the fits. The s-channel and u-channel mechanisms of $v_{M'B',MB}$ (v^s and v^u in Fig. 1) include at each meson-baryon-baryon vertex a form factor of the form

$$F(\vec{k},\Lambda)=\left(\frac{\Lambda^2}{\vec{k}^2+\Lambda^2}\right)^2, \tag{13}$$

with $\vec{k}$ being the meson momentum. For the meson-meson-meson vertex of t-channel mechanism (v^t), the form Eq. (13) is also used with $\vec{k}$ being the momentum of the exchanged meson. For the contact term (v^c) we regularize it by $F(\vec{k}',\Lambda')F(\vec{k},\Lambda)$. The bare vertex functions in Eqs. (9) and (10) are parametrized as

$$\Gamma_{MB(LS),N^*}(k)=\frac{1}{(2\pi)^{3/2}}\frac{1}{\sqrt{m_N}}C_{MB(LS),N^*} \times\left(\frac{\Lambda_{N^*}^2}{\Lambda_{N^*}^2+k^2}\right)^{(2+L/2)}\left(\frac{k}{m_\pi}\right)^L, \tag{14}$$

where L and S denote the orbital angular momentum and spin of the MB state, respectively. All of the possible (L,S) states in each partial wave included in our coupled-channels calculations are listed in Table II. The vertex function (14) behaves as k^L at $k\sim 0$ and k^{-4} for $k\to\infty$. The coupling constant $C_{MB(LS),N^*}$ and the cutoff Λ_{N^*} are adjusted along with the bare masses $M^0_{N^*}$ in the fits. It is noted that in our early analysis [2], the different cutoffs were introduced for each $MB(LS)$ state of a given bare N^*, and those were allowed to vary independently in the fit. In this analysis, however, we use a single cutoff Λ_{N^*} for all $MB(LS)$ states. This drastically reduces the number of parameters associated with the hadronic interaction of the bare N^* states.

B. Electromagnetic amplitudes

With the hadronic amplitudes $t_{M'B',MB}(k',k;W)$ defined in Eq. (4), the partial-wave amplitudes for the $\gamma(\vec{q})+N(-\vec{q})\to M'(\vec{k}')+B'(-\vec{k}')$ reactions are expressed as [1]

$$T_{M'B',\gamma N}(k',q;W)=t_{M'B',\gamma N}(k',q;W)+t^R_{M'B',\gamma N}(k',q;W), \tag{15}$$

with

$$t_{M'B',\gamma N}(k',q;W)=v_{M'B',\gamma N}(k',q) +\sum_{M''B''}\int p^2dp\, t_{M'B',M''B''}(k',p;W) \times G_{M''B''}(p;W)v_{M''B'',\gamma N}(p,q), \tag{16}$$

TABLE II. The orbital angular momentum (L) and total spin (S) of each MB channel allowed in a given partial wave. In the first column, partial waves are denoted with the conventional notation l_{2I2J}, as well as (I,J^P).

l_{2I2J} (I,J^P)	(L,S) of the considered partial waves									
	πN	ηN	$\pi\Delta$		σN	ρN			$K\Lambda$	$K\Sigma$
			$(\pi\Delta)_1$	$(\pi\Delta)_2$		$(\rho N)_1$	$(\rho N)_2$	$(\rho N)_3$		
S_{11} $(1,\frac{1}{2}^-)$	$(0,\frac{1}{2})$	$(0,\frac{1}{2})$	$(2,\frac{3}{2})$	–	$(1,\frac{1}{2})$	$(0,\frac{1}{2})$	$(2,\frac{3}{2})$	–	$(0,\frac{1}{2})$	$(0,\frac{1}{2})$
S_{31} $(3,\frac{1}{2}^-)$	$(0,\frac{1}{2})$	–	$(2,\frac{3}{2})$	–	–	$(0,\frac{1}{2})$	$(2,\frac{3}{2})$	–	–	$(0,\frac{1}{2})$
P_{11} $(1,\frac{1}{2}^+)$	$(1,\frac{1}{2})$	$(1,\frac{1}{2})$	$(1,\frac{3}{2})$	–	$(0,\frac{1}{2})$	$(1,\frac{1}{2})$	$(1,\frac{3}{2})$	–	$(1,\frac{1}{2})$	$(1,\frac{1}{2})$
P_{13} $(1,\frac{3}{2}^+)$	$(1,\frac{1}{2})$	$(1,\frac{1}{2})$	$(1,\frac{3}{2})$	$(3,\frac{3}{2})$	$(2,\frac{1}{2})$	$(1,\frac{1}{2})$	$(1,\frac{3}{2})$	$(3,\frac{3}{2})$	$(1,\frac{1}{2})$	$(1,\frac{1}{2})$
P_{31} $(3,\frac{1}{2}^+)$	$(1,\frac{1}{2})$	–	$(1,\frac{3}{2})$	–	–	$(1,\frac{1}{2})$	$(1,\frac{3}{2})$	–	–	$(1,\frac{1}{2})$
P_{33} $(3,\frac{3}{2}^+)$	$(1,\frac{1}{2})$	–	$(1,\frac{3}{2})$	$(3,\frac{3}{2})$	–	$(1,\frac{1}{2})$	$(1,\frac{3}{2})$	$(3,\frac{3}{2})$	–	$(1,\frac{1}{2})$
D_{13} $(1,\frac{3}{2}^-)$	$(2,\frac{1}{2})$	$(2,\frac{1}{2})$	$(0,\frac{3}{2})$	$(2,\frac{3}{2})$	$(1,\frac{1}{2})$	$(2,\frac{1}{2})$	$(0,\frac{3}{2})$	$(4,\frac{3}{2})$	$(2,\frac{1}{2})$	$(2,\frac{1}{2})$
D_{15} $(1,\frac{5}{2}^-)$	$(2,\frac{1}{2})$	$(2,\frac{1}{2})$	$(2,\frac{3}{2})$	$(4,\frac{3}{2})$	$(3,\frac{1}{2})$	$(2,\frac{1}{2})$	$(2,\frac{3}{2})$	$(4,\frac{3}{2})$	$(2,\frac{1}{2})$	$(2,\frac{1}{2})$
D_{33} $(3,\frac{3}{2}^-)$	$(2,\frac{1}{2})$	–	$(0,\frac{3}{2})$	$(2,\frac{3}{2})$	–	$(2,\frac{1}{2})$	$(0,\frac{3}{2})$	$(2,\frac{3}{2})$	–	$(2,\frac{1}{2})$
D_{35} $(3,\frac{5}{2}^-)$	$(2,\frac{1}{2})$	–	$(2,\frac{3}{2})$	$(4,\frac{3}{2})$	–	$(2,\frac{1}{2})$	$(2,\frac{3}{2})$	$(4,\frac{3}{2})$	–	$(2,\frac{1}{2})$
F_{15} $(1,\frac{5}{2}^+)$	$(3,\frac{1}{2})$	$(3,\frac{1}{2})$	$(1,\frac{3}{2})$	$(3,\frac{3}{2})$	$(2,\frac{1}{2})$	$(3,\frac{1}{2})$	$(1,\frac{3}{2})$	$(3,\frac{3}{2})$	$(3,\frac{1}{2})$	$(3,\frac{1}{2})$
F_{17} $(1,\frac{7}{2}^+)$	$(3,\frac{1}{2})$	$(3,\frac{1}{2})$	$(3,\frac{3}{2})$	$(5,\frac{3}{2})$	$(4,\frac{1}{2})$	$(3,\frac{1}{2})$	$(3,\frac{3}{2})$	$(5,\frac{3}{2})$	$(3,\frac{1}{2})$	$(3,\frac{1}{2})$
F_{35} $(3,\frac{5}{2}^+)$	$(3,\frac{1}{2})$	–	$(1,\frac{3}{2})$	$(3,\frac{3}{2})$	–	$(3,\frac{1}{2})$	$(1,\frac{3}{2})$	$(3,\frac{3}{2})$	–	$(3,\frac{1}{2})$
F_{37} $(3,\frac{7}{2}^+)$	$(3,\frac{1}{2})$	–	$(3,\frac{3}{2})$	$(5,\frac{3}{2})$	–	$(3,\frac{1}{2})$	$(3,\frac{3}{2})$	$(5,\frac{3}{2})$	–	$(3,\frac{1}{2})$
G_{17} $(1,\frac{7}{2}^-)$	$(4,\frac{1}{2})$	$(4,\frac{1}{2})$	$(2,\frac{3}{2})$	$(4,\frac{3}{2})$	$(3,\frac{1}{2})$	$(4,\frac{1}{2})$	$(2,\frac{3}{2})$	$(4,\frac{3}{2})$	$(4,\frac{1}{2})$	$(4,\frac{1}{2})$
G_{19} $(1,\frac{9}{2}^-)$	$(4,\frac{1}{2})$	$(4,\frac{1}{2})$	$(4,\frac{3}{2})$	$(6,\frac{3}{2})$	$(5,\frac{1}{2})$	$(4,\frac{1}{2})$	$(4,\frac{3}{2})$	$(6,\frac{3}{2})$	$(4,\frac{1}{2})$	$(4,\frac{1}{2})$
G_{37} $(3,\frac{7}{2}^-)$	$(4,\frac{1}{2})$	–	$(2,\frac{3}{2})$	$(4,\frac{3}{2})$	–	$(4,\frac{1}{2})$	$(2,\frac{3}{2})$	$(4,\frac{3}{2})$	–	$(4,\frac{1}{2})$
G_{39} $(3,\frac{9}{2}^-)$	$(4,\frac{1}{2})$	–	$(4,\frac{3}{2})$	$(6,\frac{3}{2})$	–	$(4,\frac{1}{2})$	$(4,\frac{3}{2})$	$(6,\frac{3}{2})$	–	$(4,\frac{1}{2})$
H_{19} $(1,\frac{9}{2}^+)$	$(5,\frac{1}{2})$	$(5,\frac{1}{2})$	$(3,\frac{3}{2})$	$(5,\frac{3}{2})$	$(4,\frac{1}{2})$	$(5,\frac{1}{2})$	$(3,\frac{3}{2})$	$(5,\frac{3}{2})$	$(5,\frac{1}{2})$	$(5,\frac{1}{2})$
H_{39} $(3,\frac{9}{2}^+)$	$(5,\frac{1}{2})$	$(5,\frac{1}{2})$	$(3,\frac{3}{2})$	$(5,\frac{3}{2})$	–	$(5,\frac{1}{2})$	$(3,\frac{3}{2})$	$(5,\frac{3}{2})$	–	$(5,\frac{1}{2})$

$$t^R_{M'B',\gamma N}(k',q;W) = \sum_{n,m} \bar{\Gamma}_{M'B',N^*_n}(k';W)[D(W)]_{n,m} \times \bar{\Gamma}_{N^*_m,\gamma N}(q;W), \quad (17)$$

$$\bar{\Gamma}_{N^*,\gamma N}(q;W) = \Gamma_{N^*,\gamma N}(q) + \sum_{M'B'} \int p^2 dp \Gamma_{N^*,M'B'}(p) \times G_{M'B'}(p,W) t_{M'B',\gamma N}(p,q;W). \quad (18)$$

Here $v_{MB,\gamma N}$ is the meson-exchange potential for the $\gamma N \to MB$ processes, and $\bar{\Gamma}_{N^*,\gamma N}(q;W)$ is the dressed $\gamma N \to N^*$ vertex (Fig. 3). The procedures for calculating $v_{MB,\gamma N}$ are detailed in Ref. [1] and also given here in Appendix D. In the latter, the ingredients associated with KY channels are newly added.

For the bare $\gamma N \to N^*$ vertex, we depart from the simple parametrization given in Ref. [1] and write it in the helicity representation as

$$\Gamma_{N^*,\gamma N}(q) = \frac{1}{(2\pi)^{3/2}} \sqrt{\frac{m_N}{E_N(q)}} \sqrt{\frac{q_R}{|q_0|}} A^{N^*}_\lambda \delta_{\lambda,(\lambda_\gamma - \lambda_N)}, \quad (19)$$

where λ_γ (λ_N) is the helicity quantum number of the photon (nucleon) and q_R and q_0 are defined by $M_{N^*} = q_R + E_N(q_R)$ and $W = q_0 + E_N(q)$, respectively. The helicity amplitudes $A^{N^*}_\lambda$ in the above equation are related to the multipole amplitudes $E^{N^*}_{l\pm}$ and $M^{N^*}_{l\pm}$ of $\gamma N \to N^*$ processes as

$$A^{N^*}_{3/2} = \frac{\sqrt{l(l+2)}}{2}\left[- M^{N^*}_{l+} + E^{N^*}_{l+}\right], \quad (20)$$

$$A^{N^*}_{1/2} = -\frac{1}{2}\left[l M^{N^*}_{l+} + (l+2) E^{N^*}_{l+}\right], \quad (21)$$

for $j = l + 1/2$, and

$$A^{N^*}_{3/2} = -\frac{\sqrt{(l-1)(l+1)}}{2}\left[M^{N^*}_{l-} + E^{N^*}_{l-}\right], \quad (22)$$

$$A^{N^*}_{1/2} = +\frac{1}{2}\left[(l+1) M^{N^*}_{l-} - (l-1) E^{N^*}_{l-}\right], \quad (23)$$

for $j = l - 1/2$. The multipole amplitudes are parametrized as

$$M^{N^*}_{l\pm}(q) = \left(\frac{q}{m_\pi}\right)^l \left(\frac{\left(\Lambda^{\rm e.m.}_{N^*}\right)^2 + m_\pi^2}{\left(\Lambda^{\rm e.m.}_{N^*}\right)^2 + q^2}\right)^{(2+l/2)} \tilde{M}^{N^*}_{l\pm}, \quad (24)$$

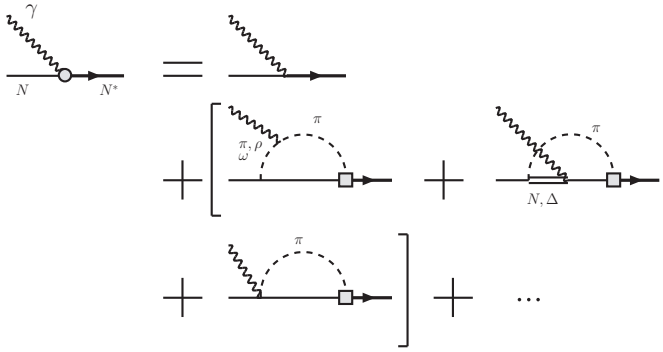

FIG. 3. Dressed $\gamma N \to N^*$ vertex defined by Eq. (18).

$$E^{N^*}_{l\pm}(q) = \left(\frac{q}{m_\pi}\right)^{(l\pm1)} \left(\frac{\left(\Lambda^{\rm e.m.}_{N^*}\right)^2 + m_\pi^2}{\left(\Lambda^{\rm e.m.}_{N^*}\right)^2 + q^2}\right)^{[2+(l\pm1)/2]} \tilde{E}^{N^*}_{l\pm}, \quad (25)$$

where the cutoff $\Lambda^{\rm e.m.}_{N^*}$ and the coupling constants $\tilde{M}^{N^*}_{l\pm}$ and $\tilde{E}^{N^*}_{l\pm}$ are determined in fitting the data. One significant difference between this work and our previous analysis [3] is that the multipole amplitudes, or equivalently the helicity amplitudes, for the $\gamma N \to N^*$ processes now have momentum dependence. To compare with our previous works [15] on $\Delta(1232)$, however, we depart from the above parametrization and use the following forms for the first bare state in P_{33}:

$$A^{1{\rm st}P_{33}}_{3/2} = -x_{A_{3/2}} \frac{\sqrt{3}}{2} A\left[G^{SL}_M(0) - (1-N) G^{SL}_E(0)\right], \quad (26)$$

$$A^{1{\rm st}P_{33}}_{1/2} = -x_{A_{1/2}} \frac{1}{2} A\left[G^{SL}_M(0) - (1+N) G^{SL}_E(0)\right], \quad (27)$$

with

$$A = \frac{e}{2m_N} \sqrt{\frac{Wq}{m_N}} \frac{W + m_N}{M_{N^*} + m_N}, \quad (28)$$

$$N = 2\left(\frac{W - m_N}{M_{N^*} - m_N}\right)^2, \quad (29)$$

where $G^{SL}_M(0) = 1.85$ and $G^{SL}_E(0) = 0.025$ [15]. The factors $x_{A_{3/2}}$ and $x_{A_{1/2}}$ in Eqs. (26) and (27) are treated as free parameters in our fitting processes.

III. EXTRACTIONS OF NUCLEON RESONANCES

We follow the earlier works [38,39] to define that a nucleon resonance with a complex mass M_R is an "eigenstate" of a Hamiltonian $H|\psi^R_{N^*}\rangle = M_R|\psi^R_{N^*}\rangle$ under the so-called outgoing boundary condition. Then from the spectral expansion of the Low equation for reaction amplitude $T(W) = H' + H'(W - H)^{-1}H'$, where we have defined $H' = H - H_0$, with H_0 being the noninteracting free Hamiltonian, we have

$$T_{M'B',MB}\left(k^0_{M'B'}, k^0_{MB}; W \to M_R\right) = \frac{\left\langle k^0_{M'B'}\middle|H'\middle|\psi^R_{N^*}\right\rangle \left\langle \psi^R_{N^*}\middle|H'\middle|k^0_{MB}\right\rangle}{W - M_R} + \cdots, \quad (30)$$

where k^0_{MB} and $k^0_{M'B'}$ are the on-shell momenta defined by

$$W = E_M\left(k^0_{MB}\right) + E_B\left(k^0_{MB}\right) = E_{M'}\left(k^0_{M'B'}\right) + E_{B'}\left(k^0_{M'B'}\right). \quad (31)$$

Therefore, the resonance masses M_R can be defined as the pole positions of the meson-baryon amplitude $T_{M'B',MB}(k^0_{M'B'}, k^0_{MB}; W)$ on the complex Riemann W surface. Because of the quadratic relation between the energy and momentum variables, each MB channel for a given W can have a physical (p) sheet characterized by $\mathrm{Im}(k^0_{MB}) > 0$ and an unphysical (u) sheet by $\mathrm{Im}(k^0_{MB}) < 0$. Like all previous works, we only look for the poles close to the physical region and/or having large effects on scattering observables. All of these poles are on the unphysical sheet of the πN channel, but could be on either (u) or (p) sheets of other channels. To find the

resonance poles, we analytically continue Eqs. (3)–(12) to the complex W plane by using the method detailed in Refs. [8,9]. The main step is to choose appropriate momentum-integration paths in solving Eqs. (3)–(12).

As derived in Refs. [8,9], we can write Eq. (30) in terms of $t_{M'B',MB}(k',k;W)$, which is the solution of Eq. (4), $t^R_{M'B',MB}(k',k;W)$ defined by Eq. (8), and $\bar{\Gamma}_{MB,N^*}$ [$\bar{\Gamma}_{N^*,MB}$] defined by Eq. (9) [Eq. (10)]. Explicitly, as the energy approaches a resonance position in the complex W plane, the total meson-baryon amplitudes can be written as

$$T_{M'B',MB}\left(k^R_{M'B'},k^R_{MB};W\to M_R\right) = \tilde{B}_{M'B',MB}(M_R)+\frac{\tilde{R}_{M'B',MB}(M_R)}{W-M_R}, \tag{32}$$

where the on-shell momenta k^R_{MB} and $k^R_{M'B'}$ are defined by Eq. (31) with $W=M_R$, and

$$\tilde{B}_{M'B',MB}(M_R) = t_{M'B',MB}\left(k^R_{M'B'},k^R_{MB};M_R\right) + \frac{d}{dW}\left[(W-M_R)t^R_{M'B',MB}\left(k^R_{M'B'},k^R_{MB};W\right)\right]_{W=M_R}, \tag{33}$$

$$\tilde{R}_{M'B',MB}(M_R) = \bar{\Gamma}^R_{M'B'}\left(k^R_{M'B'},M_R\right)\bar{\Gamma}^R_{MB}\left(k^R_{MB},M_R\right), \tag{34}$$

with

$$\bar{\Gamma}^R_{MB}\left(k^R_{MB},M_R\right)=\sum_i \chi_i \bar{\Gamma}_{MB,N^*_i}\left(k^R_{MB},M_R\right). \tag{35}$$

Here χ_i represents ith "bare" resonance component of the dressed N^* and satisfies

$$\sum_j [D^{-1}(M_R)]_{ij}\chi_j = \sum_j\left[\left(M_R-M_{N^*_i}\right)\delta_{ij}-\Sigma(M_R)_{ij}\right]\chi_j = 0. \tag{36}$$

If there is only one bare N^* state, with $D^{-1}(W)=W-M_{N^*}-\Sigma(W)$, it is easy to see that

$$\chi=\frac{1}{\sqrt{1-\Sigma'(M_R)}}, \tag{37}$$

where $\Sigma'(M_R)=[d\Sigma/dW]_{W=M_R}$.

With the normalizations we employ, the S matrix in each partial wave is related to $T_{M'B',MB}(k^0_{M'B'},k^0_{MB};W)$ by

$$S_{M'B',MB}(W)=\delta_{M'B',MB}+2iF_{M'B',MB}(W), \tag{38}$$

where

$$F_{M'B',MB}(W) = -[\rho_{M'B'}(W)]^{1/2}T_{M'B',MB}\left(k^0_{M'B'},k^0_{MB};W\right)[\rho_{MB}(W)]^{1/2}, \tag{39}$$

with

$$\rho_{MB}(W)=\pi\frac{k^0_{MB}E_M\left(k^0_{MB}\right)E_B\left(k^0_{MB}\right)}{W}. \tag{40}$$

For the later use, we denote the residue of the scattering amplitude $F_{M'B',MB}(W)$ at a resonance pole as $R_{M'B',MB}$,

$$F_{M'B',MB}(W\to M_R)=\frac{S_{M'B',MB}(W\to M_R)-\delta_{M'B',MB}}{2i} = -\left[\frac{R_{M'B',MB}}{W-M_R}\right]_{W\to M_R}. \tag{41}$$

From Eqs. (32), (34), (38), (39), and (41) we have

$$R_{M'B',MB}=[\rho_{M'B'}(M_R)]^{1/2}\bar{\Gamma}^R_{M'B'}\left(k^R_{M'B'},M_R\right) \times\bar{\Gamma}^R_{MB}\left(k^R_{MB},M_R\right)[\rho_{MB}(M_R)]^{1/2}. \tag{42}$$

Here it is noted that we have fixed a sign freedom of χ_i in $\bar{\Gamma}^R_{MB}(k^R_{MB},M_R)$ in such a way that $\bar{\Gamma}^R_{\pi N}(k^R_{\pi N},M_R)$ is given by $[\rho_{\pi N}(M_R)]^{1/2}\bar{\Gamma}^R_{\pi N}(k^R_{\pi N},M_R)=[R_{\pi N,\pi N}]^{1/2}$ with $-\pi<\arg(R_{\pi N,\pi N})<\pi$. The πN elasticity of a resonance is then defined as

$$\eta_e=\frac{|R_{\pi N,\pi N}|}{-\mathrm{Im}(M_R)}. \tag{43}$$

With a similar procedure, we have the helicity amplitudes of $\gamma N\to N^*$ at the resonance pole M_R as [9]

$$A_{3/2}=C\times\bar{\Gamma}^R_{\gamma N}(M_R,\lambda_\gamma=1,\lambda_N=-1/2), \tag{44}$$

$$A_{1/2}=C\times\bar{\Gamma}^R_{\gamma N}(M_R,\lambda_\gamma=-1,\lambda_N=-1/2), \tag{45}$$

where λ_N and λ_γ are the helicities of the initial nucleon and photon, respectively, and

$$C=\sqrt{\frac{E_N(\vec{q})}{m_N}}\frac{1}{\sqrt{2K}}\sqrt{\frac{(2J^R+1)(2\pi)^3(2q_0)}{4\pi}}, \tag{46}$$

where J^R is the spin of the resonance state, $q_0=|\vec{q}|$, and $K=(M_R^2-m_N^2)/(2M_R)$.

IV. FITTING PROCEDURES

The model parameters specified in Sec. II are determined by fitting the data of pion- and photon-induced πN, ηN, $K\Lambda$, and $K\Sigma$ production reactions off a proton. One of the difficult tasks in the analysis is to decide the data we fit. For the $\pi N\to\pi N$ data, we rely on the database of SAID [40]. For simplicity, we fit their single energy solutions of πN partial-wave amplitudes

TABLE III. Number of the data points of $\pi N\to\pi N$ amplitudes included in our fits. The data are from a SAID analysis [40].

Partial wave		Partial wave		
S_{11}	65×2	S_{31}	65×2	
P_{11}	65×2	P_{31}	61×2	
P_{13}	61×2	P_{33}	65×2	
D_{13}	61×2	D_{33}	59×2	
D_{15}	61×2	D_{35}	40×2	
F_{15}	48×2	F_{35}	43×2	
F_{17}	32×2	F_{37}	44×2	
G_{17}	42×2	G_{37}	32×2	
G_{19}	28×2	G_{39}	32×2	
H_{19}	34×2	H_{39}	31×2	
Sum	994		944	1938

TABLE IV. Number of data points of hadronic processes included in our fits. See Refs. [5,23] for the data references.

	$d\sigma/d\Omega$	P	β	Sum
$\pi^- p \to \eta p$	294	–	–	294
$\pi^- p \to K^0\Lambda$	544	262	43	849
$\pi^- p \to K^0\Sigma^0$	160	70	–	230
$\pi^+ p \to K^+\Sigma^+$	552	312	7	871
Sum	1550	644	50	2244

instead of fitting the original πN elastic scattering data. There is always a question on whether this is a reliable procedure. We justify this by observing that the πN partial-wave amplitudes determined by using a very different approach based on the dispersion-relations [41,42] are not so different from that of SAID. Thus, the SAID amplitudes, which are extracted from much more data than the previous analyses, can be considered as fairly reliable representations of the original πN elastic scattering data (about 30 000 data points as compiled in SAID).

In this work, we want to determine the spectrum of the N^* resonances with masses only up to 2 GeV and widths less than 400 MeV. Because the N^* resonances can affect the observables over the energy range of their widths, we include the data of $\pi N \to \pi N$ up to $W = 2.3$ GeV to make sure that the N^* resonances with masses near about 1.9 GeV are properly identified within our model. In Table III, we list the data points of the SAID energy-independent solutions included in our fits. In the fitting process, we check the resulting parameters by comparing the predicted observables with the original πN scattering data.

For the data of $\pi N \to \eta N, K\Lambda, K\Sigma$ and $\gamma N \to \pi N, \eta N, K\Lambda, K\Sigma$, we use the database of the Bonn-Gatchina group [23] with some differences: (i) we only include the data up to $W = 2.1$ GeV; (ii) following the discussion in Ref. [5] (the references of the data are also found in Ref. [5]), the data for $\pi^- p \to \eta n$ differential cross sections used in our analysis are different from those of Bonn-Gatchina group; and (iii) we include the new data of the polarization G of $\gamma p \to \pi^0 p$ from CBELSA/TAPS Collaboration [43]. The data of $\pi N \to \eta N, K\Lambda, K\Sigma$ and $\gamma N \to \pi N, \eta N, K\Lambda, K\Sigma$ included in our fit are listed in Tables IV and V. It is known [44,45] that the determinations of the multipole amplitudes of pseudoscalar meson photoproductions need at least eight observables, i.e., $d\sigma/d\Omega$, Σ, T, P, and appropriately chosen four double-spin polarizations. We see from Table V that the polarization observables, in particular the double-spin polarizations, do not have enough data points. Thus, it is rather difficult to fit these data because they have much less weights in the χ^2-minimization processes.

We next discuss how we perform the minimization of χ^2. We follow the most commonly used definition,

$$\chi^2 = \sum_O \sum_{i,j} \frac{[O^{\rm model}(W_i,\theta_j) - O^{\rm exp.}(W_i,\theta_j)]^2}{[\delta O^{\rm exp.}(W_i,\theta_j)]^2}, \quad (47)$$

where $O^{\rm model}(W_i,\theta_j)$ is the observable O at energy W_i and angle θ_j calculated from our DCC model, while $O^{\rm exp.}(W_i,\theta_j)$ and $\delta O^{\rm exp.}(W_i,\theta_j)$ are the central value and the statistical error of the experimental data, respectively. (Note that the πN partial-wave amplitudes depend only on the energy.) There are more sophisticated minimization procedures accounting separately for the systematic and statistical errors. Thus, some of the discrepancies between our final results and the data, as presented in the next section, could be partly attributed to our use of Eq. (47) for χ^2. Such a more careful fitting procedure will be desirable when we move to our next analysis including more complete data from future experiments, as discussed later.

In the absence of theoretical input, our main challenge is to determine the bare N^* mass $M^0_{N^*}$, the strong $N^* \to MB$ bare vertex functions defined by Eq. (14), and the electromagnetic $N^* \to \gamma N$ bare vertex functions defined by Eq. (19). For each partial wave, the number of the N^* parameters contained is $N_{N^*} \times (3 + N^{\rm str.}_{\rm c.c.} + N^{\rm e.m.}_{\rm c.c.})$. Here N_{N^*} is the number of the bare N^* states included in the partial wave, and the numbers in the parentheses are those of the parameters each bare N^* state has: 3 comes from the bare mass $M^0_{N^*}$ and the cutoffs Λ_{N^*} and $\Lambda^{\rm e.m.}_{N^*}$ of the hadronic and electromagnetic decay vertex functions, and $N^{\rm str.}_{\rm c.c.}$ ($N^{\rm e.m.}_{\rm c.c.}$) is the number of coupling constants of the hadronic (electromagnetic) interactions, which can be $5 \leqslant N^{\rm str.}_{\rm c.c.} \leqslant 10$ ($N^{\rm e.m.}_{\rm c.c.} = 1$ or 2). We thus face a many-parameters problem in fitting the data, which is also present in all existing coupled-channels analysis of nucleon resonances. This common problem poses difficulties in assigning the errors for the determined model parameters.

Here we have additional difficulties owing to the long computation time in solving the coupled-channels integral equations (4), as mentioned in the previous sections. We thus follow all previous works on dynamical model analyses and do not try to resolve this difficult problem here. We therefore

TABLE V. The number of data points of photoproduction processes included in our fits. See Refs. [23,43] for the data references.

	$d\sigma/d\Omega$	Σ	T	P	$\hat{E}$	G	H	$O_{x'}$	$O_{z'}$	C_x	C_z	Sum
$\gamma p \to \pi^0 p$	4381	1128	380	589	140	125	49	7	7	–	–	6806
$\gamma p \to \pi^+ n$	2315	747	678	222	231	86	128	–	–	–	–	4407
$\gamma p \to \eta p$	3221	235	50	–	–	–	–	–	–	–	–	3506
$\gamma p \to K^+\Lambda$	800	86	66	865	–	–	–	66	66	79	79	2107
$\gamma p \to K^+\Sigma^0$	758	62	–	169	–	–	–	–	–	40	40	1069
$\gamma p \to K^0\Sigma^+$	220	15	–	36	–	–	–	–	–	–	–	271
Sum	11 695	2273	1174	1881	371	211	177	73	73	119	119	18166

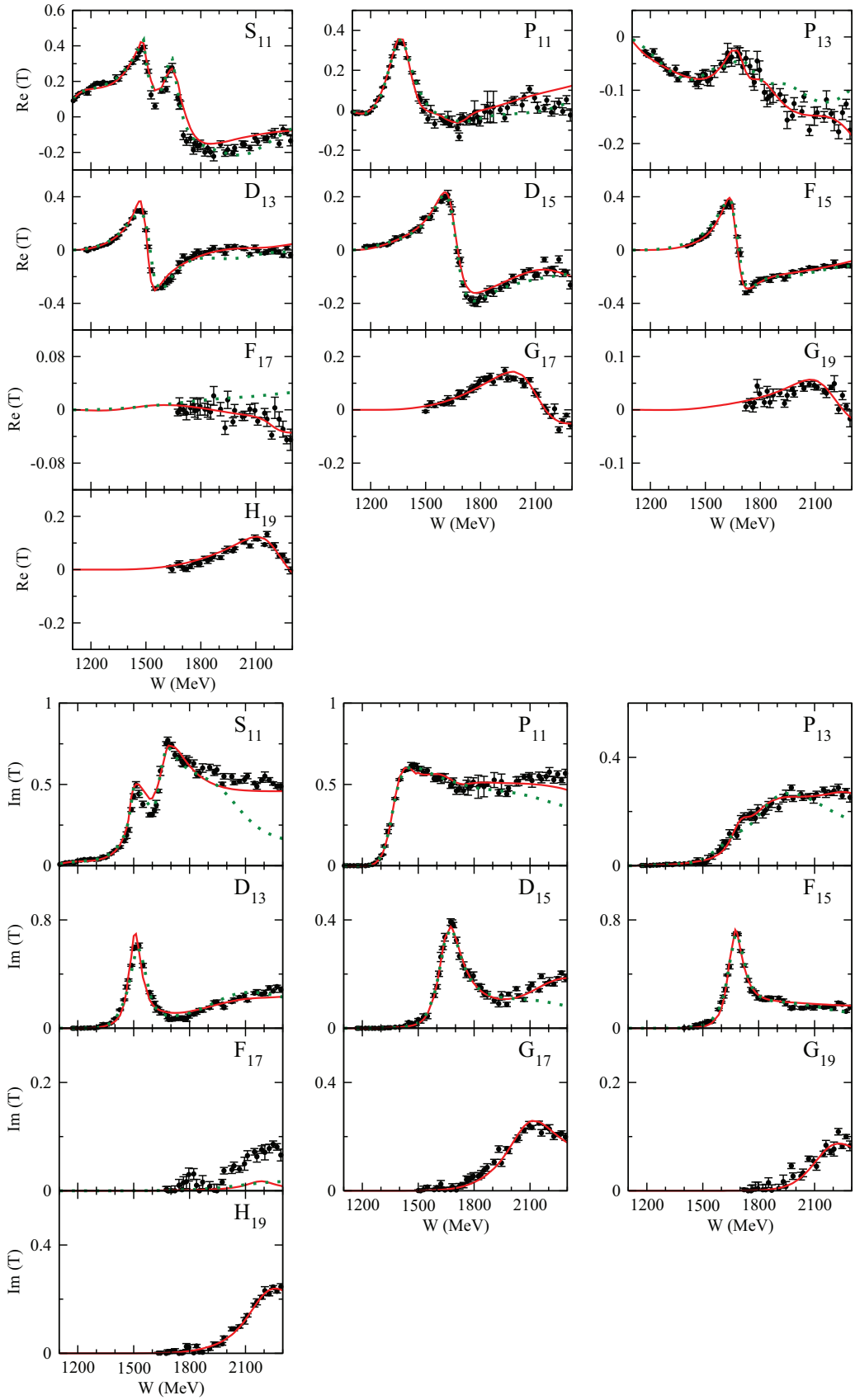

FIG. 4. (Color online) Partial-wave amplitudes of πN scattering with isospin $I = 1/2$. Upper (lower) panels are for real (imaginary) parts of the amplitudes. Red solid curves, current results; green dotted curves, results from our previous analysis [2].

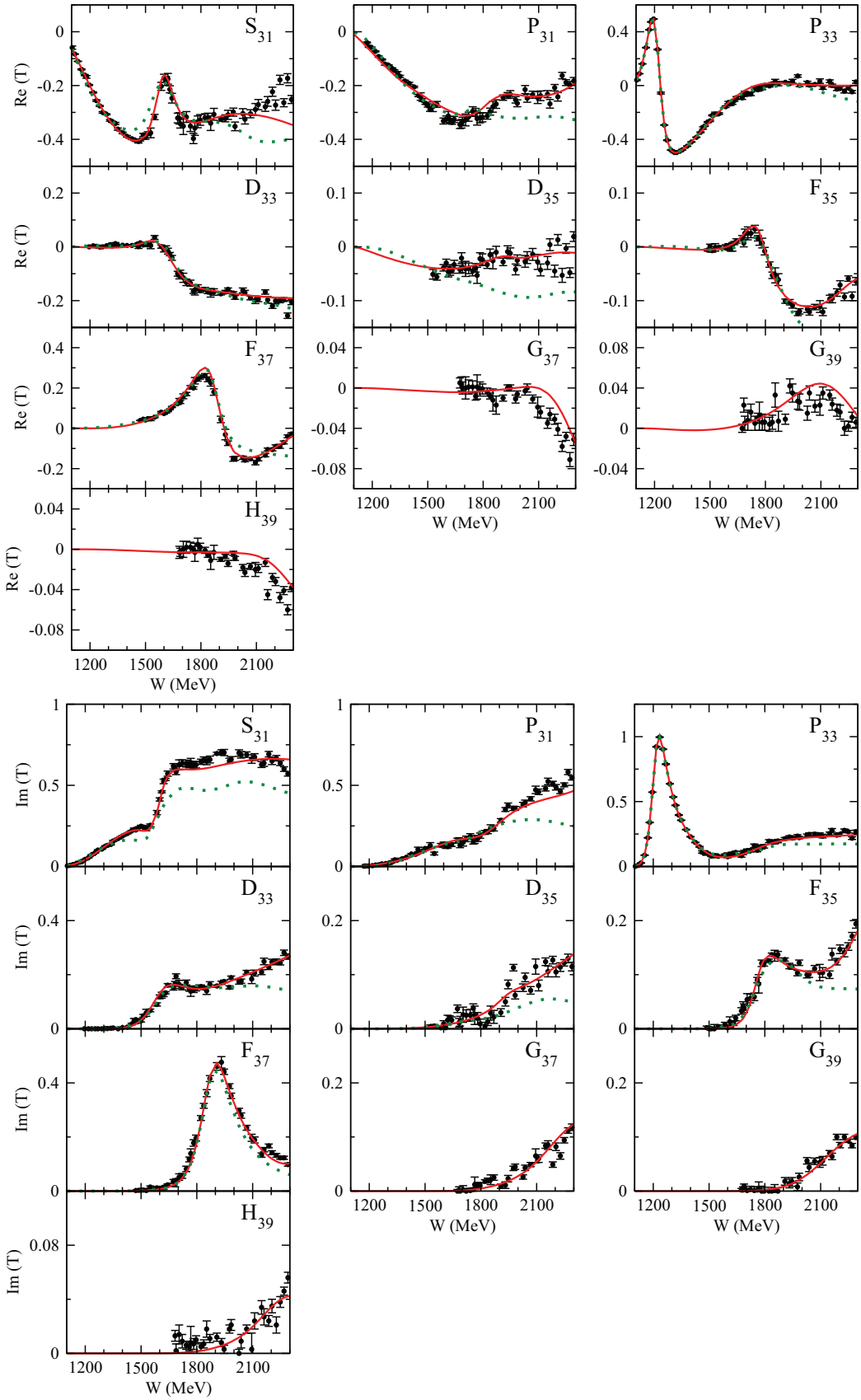

FIG. 5. (Color online) Partial-wave amplitudes of πN scattering with isospin $I = 3/2$. Upper (lower) panels are for real (imaginary) parts of the amplitudes. Red solid curves, current results; green dotted curves, results from our previous analysis [2].

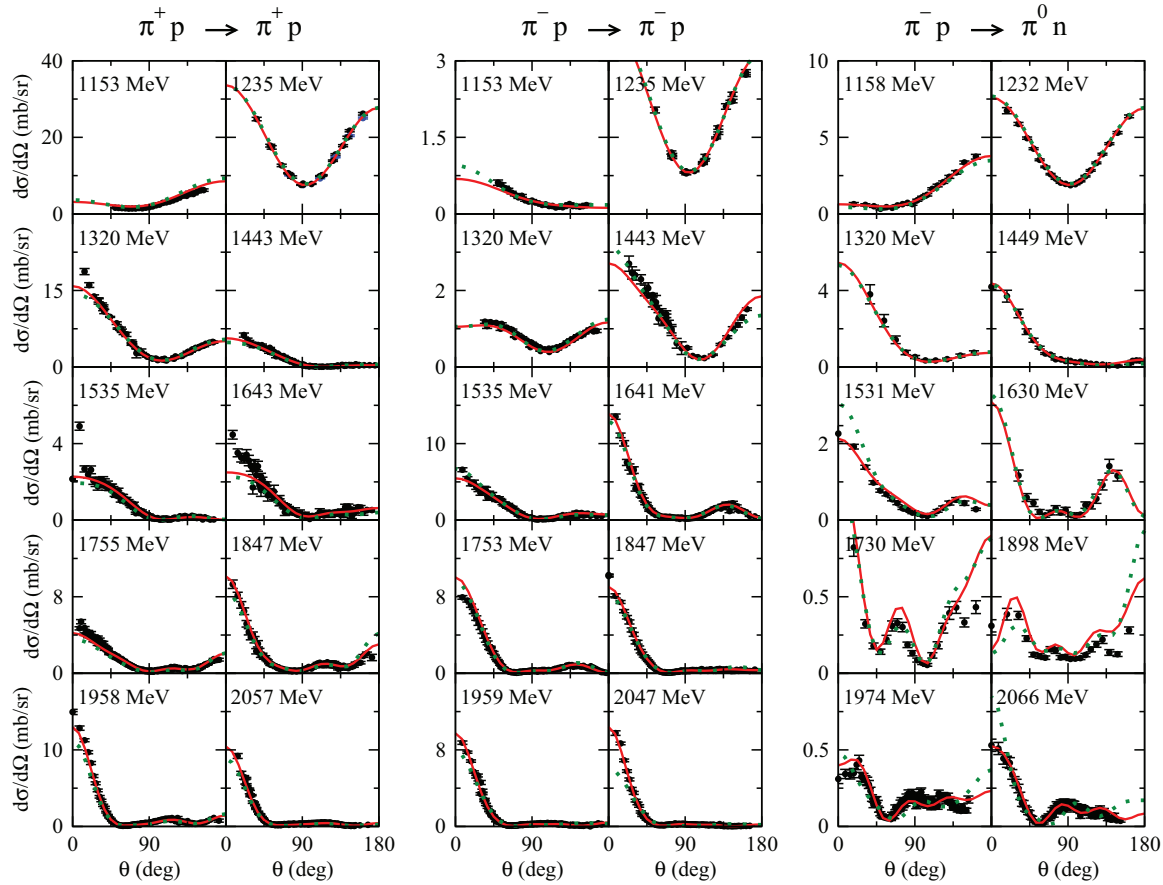

FIG. 6. (Color online) Differential cross section $d\sigma/d\Omega$ of $\pi N \to \pi N$. Red solid curves, current results; green dotted curves, results from our previous analysis [2]. The corresponding values of W are indicated in each panel. The same applies to the rest of figures.

are not able to provide the errors of the determined resonance parameters. This must be improved in the future.

Owing to the many-parameters problem mentioned above and the limitation of the current computation power in the χ^2 minimization, it is practically not possible to get convergent results if all of the model parameters are allowed to vary *simultaneously* in the χ^2-minimization processes. We therefore take the following strategy. First we determine the parameters associated with the meson-exchange potentials $v_{M'B',MB}$ to some extent. The parameters associated with the bare N^* states are then determined. In the latter step the parameters of $v_{M'B',MB}$ may be varied only when it is necessary to fine tune the fits. This two-step procedure is essential because the most time-consuming part of the computation is to calculate the meson-exchange amplitude $t_{M'B',MB}$ from the meson-exchange potentials $v_{M'B',MB}$ by solving the coupled-channels equations (4). Hence, the computation time is drastically increased if the parameters of $v_{M'B',MB}$ are varied in the χ^2-minimization processes.

Concretely, our fitting procedure is as follows. Guided by the success of the meson-exchange models [12–20] in the $\Delta(1232)$ region, we first adjust the parameters associated with the meson-exchange potentials $v_{M'B',MB}$ to fit the data of the πN partial-wave amplitudes at low energies with $W \leqslant 1.4$ GeV, where one bare N^* state in the P_{33} partial wave is included to incorporate the $\Delta(1232)$ contribution. Fortunately, we find that most of the parameters in $v_{M'B',MB}$ are heavily constrained by the πN partial-wave amplitudes at low energies and do not have to be varied too much in the later fitting processes. Once a good πN partial-wave amplitudes in the $W \leqslant 1.4$ GeV region is obtained, we extend the fits of the amplitudes to $W = 2.3$ GeV by including the bare N^* states in each partial wave. To minimize the number of the bare N^* states, we first include only one bare N^* state in each partial wave and try to fit the data of the πN partial-wave amplitudes in the entire considered energy region by adjusting its bare mass, $M^0_{N^*}$, and vertex function parameters, $C_{N^*,MB(LS)}$ and Λ_{N^*}. If this fails, we then also allow the parameters associated with $v_{MB,M'B'}$ to vary in some limited ranges. If this fails again, we then include one more bare N^* state in some partial waves and repeat the process. After completing the fit of the πN partial-wave amplitudes, we extend our global fit step by step: first include the πN reaction data of Table IV, and then include the γN reaction data of Table V. This procedure has to be repeated many times to make sure that we have reached the limitation of the model in the χ^2 minimization. The resulting masses, coupling constants, and cutoff parameters for the meson-exchange potentials are given in Tables XI–XIII of Appendix E. We find that the considered data can be fitted to a very large extent with one or two bare N^* states in

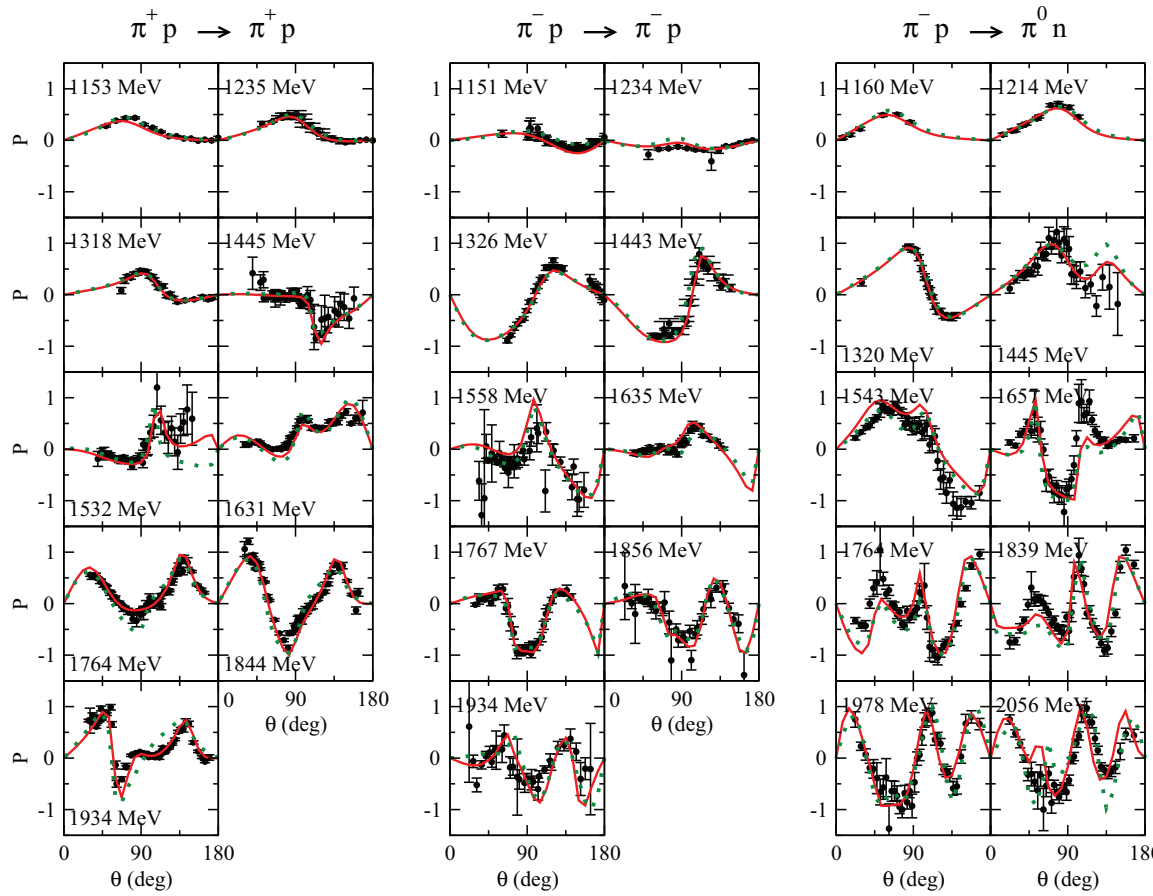

FIG. 7. (Color online) Target polarization P of $\pi N \to \pi N$. Red solid curves, current results; green dotted curves, results from our previous analysis [2].

each partial wave. All the resulting cutoff parameters for the nonresonant and N^* interactions are in the range of 500–2000 MeV, which are similar to those in typical meson-exchange models [12–20].

As seen in Tables III–V, the numbers of the data points of each reaction are very different. The observables with much fewer data points are hard to fit because they have little effects on χ^2 minimization. Thus, in calculating Eq. (47) for the fitting, we need to put "artificial" weights on χ^2 for those observables such as polarization observables. This procedure, which is highly undesirable, is, however, necessary before those data become more extensive. Also for this reason, we cannot give meaningful χ^2 values. To show the quality of our fits, in the next section we present detailed comparisons with the data for all processes considered. Hopefully, the situation, in particular the scarce data for the pion-induced inelastic reactions, can be improved with new experiments at the Japan Proton Accelerator Research Complex (J-PARC).

V. RESULTS

In this section we present the results from our fits to 22 348 data points listed in Tables III–V. The resulting values of the model parameters are presented in Tables XI–XVI of Appendix E. The formulas for calculating the considered observables of the $\pi N, \gamma N \to \pi N, \eta N, K\Lambda, K\Sigma$ from the partial-wave amplitudes defined in Sec. II can be straightforwardly derived following the formulas given in Refs. [1,44] and will not be given here. Here it should be noted that in the literature various notations have been employed for the polarization observables of pseudoscalar photoproduction reactions (see Ref. [46] for the summary of such notations used by different analysis groups). In this work, we follow the notation defined in Ref. [44]. In the following sections, we discuss separately the results for each considered reaction.

A. $\pi N \to \pi N$

In Figs. 4 and 5, we present our results for the $\pi N \to \pi N$ partial-wave amplitudes up to $W = 2.3$ GeV. Clearly, very good fits to the data of SAID [40] have been obtained. Comparing with the green dotted curves of our previous analysis (JLMS) [2], which were obtained by the fit to the data of the πN amplitudes only up to F wave ($L = 3$) and $W = 2$ GeV, there are significant improvements in the S_{31}, P_{31}, D_{35} partial waves, as seen in Fig. 5. The large improvement in the P_{31} and D_{35} waves in this analysis is mainly because we have introduced more bare N^* states than JLMS for those partial waves. These improvements are also perhaps attributable to the change of our fitting strategy by using the data below 1.4 GeV to constrain the parameters

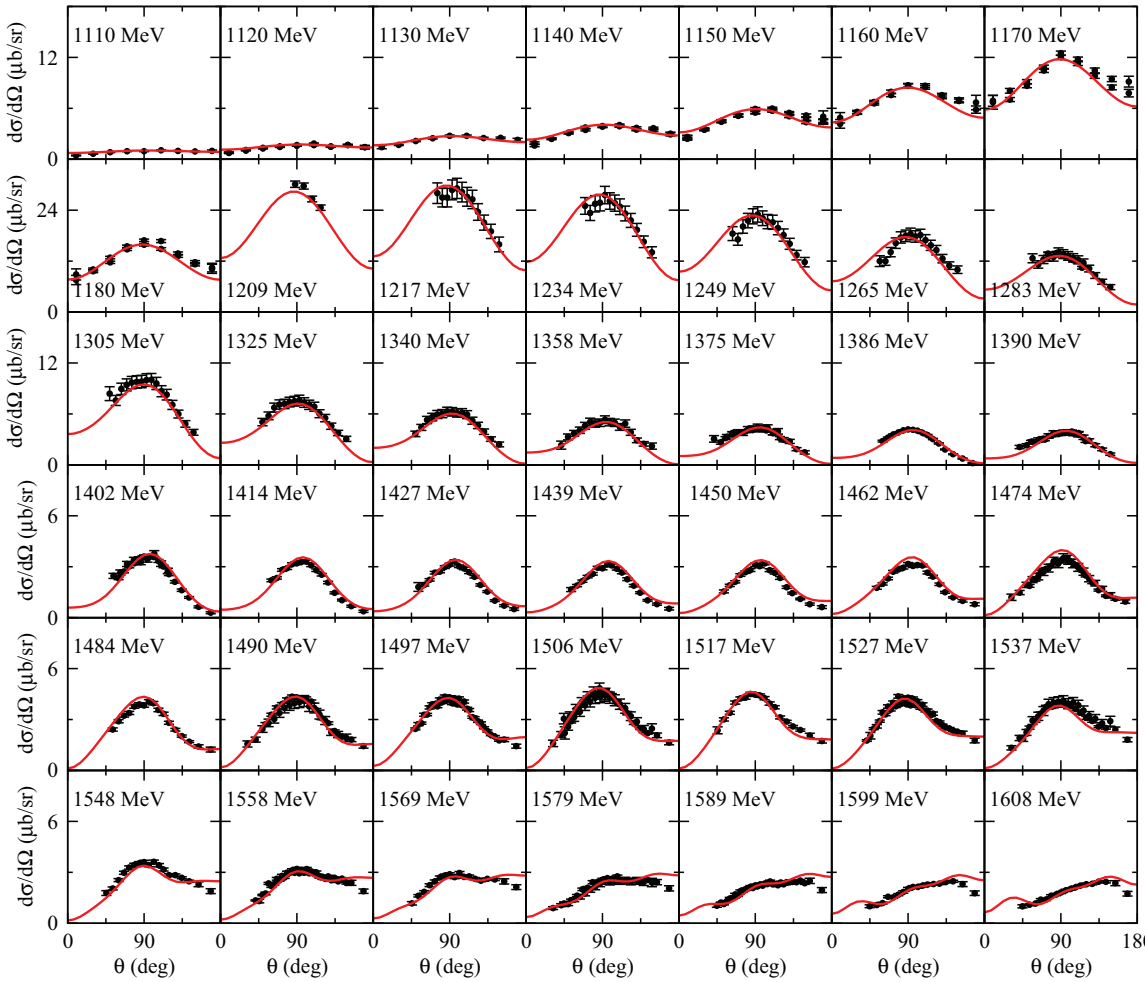

FIG. 8. (Color online) $d\sigma/d\Omega$ of $\gamma p \to \pi^0 p$.

of the meson-exchange potentials $v_{M'B',MB}$. We also find that this procedure prevents the model from generating undesirable bound states through the strong coupling with the bare N^* states in the low-energy region. We also note that the data of the G and H partial waves with the orbital angular momentum $L \geqslant 4$, which were not included in the fit of JLMS, are also fitted very well. These high-L partial waves become important in fitting the meson production data in the high-W region.

To test our model directly with the experimental data, we have also calculated the observables of πN scattering. Some results of the predicted πN elastic scattering observables are shown in Figs. 6 and 7. Clearly, good agreements have been obtained. Thus, our model parameters are consistent with the ~30 000 data points of πN scattering compiled in SAID.

B. $\gamma N \to \pi N$

In our previous analysis [3], we only considered the data of differential cross section $d\sigma/d\Omega$ and photon asymmetry Σ of the $\gamma N \to \pi N$ reactions. Also, the fits were performed by only adjusting the bare $N^* \to \gamma N$ parameters, and all other parameters of the model were fixed at the values determined in the fits to the $\pi N \to \pi N$ data [2]. It was found that only the data below $W = 1.6$ GeV can be fitted well by using such a very restricted procedure. In this work, we allow all of the model parameters to vary to fit simultaneously the data of $\pi N \to \pi N, \eta N, K\Lambda, K\Sigma$ and $\gamma N \to \pi N, \eta N, K\Lambda, K\Sigma$. This change of the fitting strategy gives us more freedom to fit the data at higher energies above 1.6 GeV and other polarization observables comprehensively.

The $\gamma N \to \pi N$ data included in our fits are listed in the first two rows of Table V. We see that the data points of $d\sigma/d\Omega$ and Σ of $\gamma p \to \pi^0 p$ are much more than those for the other considered pion photoproduction observables. Thus, these two data sets have similar large weights in determining the parameters in our coupled-channels analysis. In Figs. 8–11, we see that these rather extensive data below about $W = 1.9$ GeV can be fitted very well. We, however, are not able to account for the forward peaks in $d\sigma/d\Omega$ at $W \geqslant 1.933$ GeV. Similar difficulty is also encountered in fitting the data of Σ at $W \gtrsim 1.9$ GeV. We expect that such data in the forward-angle region are affected mainly by the t-channel processes rather than the s-channel resonance ones. This might suggest a need for an incorporation of Regge-type processes at high energies.

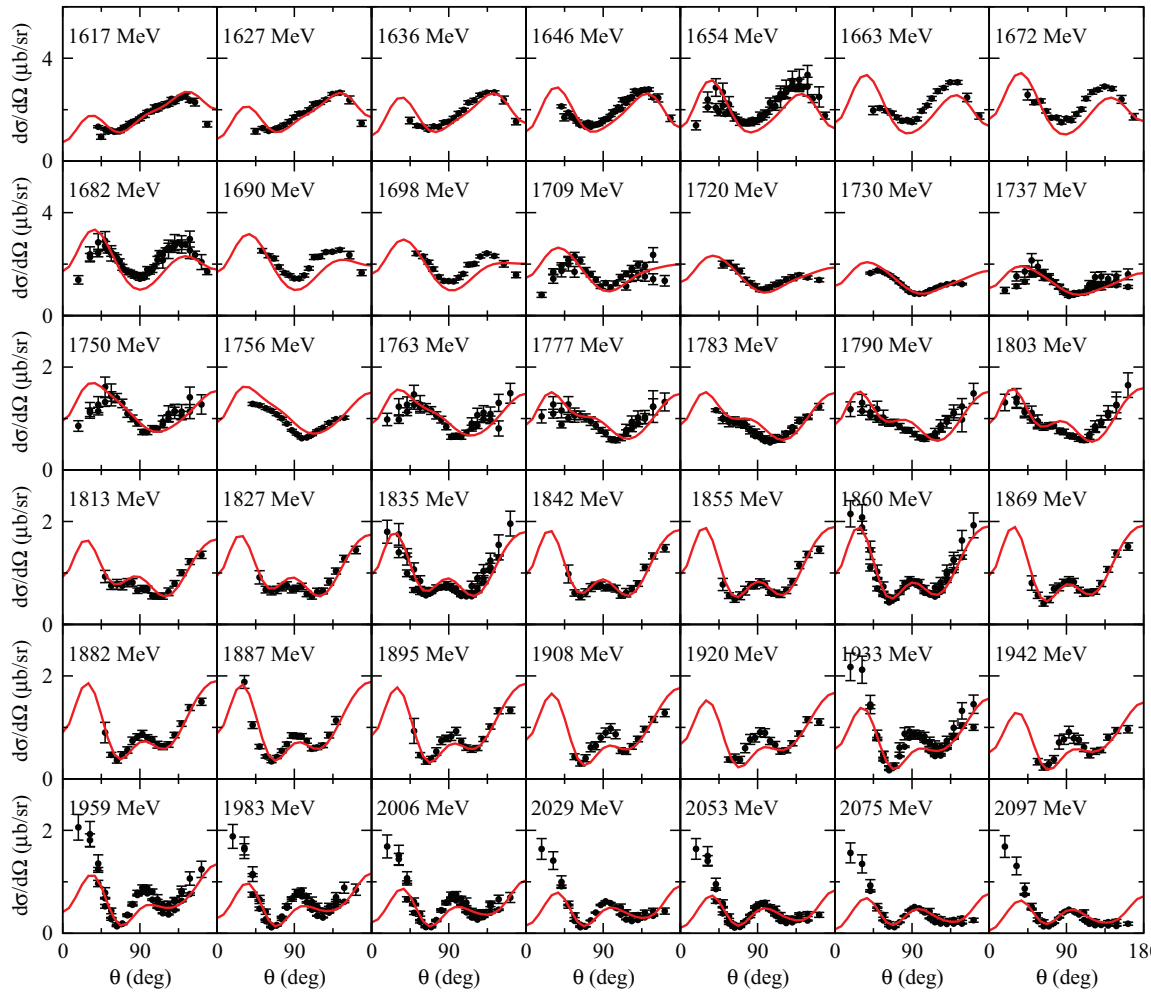

FIG. 9. (Color online) $d\sigma/d\Omega$ of $\gamma p \to \pi^0 p$ (continued).

The fits to the other polarization observables, P, T, $\hat{E}$, G, and H, of $\gamma p \to \pi^0 p$ are shown in Figs. 12–15. [Note that the beam-target polarization $\hat{E}$ defined in Ref. [44] and the quantity Δ_{31} measured and presented in Ref. [47], which are used as the data in our fits, are related with each other by $\hat{E} = -(1/2)\Delta_{31}$.] As seen in Table V, the numbers of these data points are much less than those of $d\sigma/d\Omega$ and Σ; it is therefore not easy to improve the fits to these polarization observables, in particular $\hat{E}$, G, and H (Figs. 14 and 15). While we need to improve our fits, more precise data of the polarization observables are also needed to make further progress.

Our fits to the data of $d\sigma/d\Omega$ of $\gamma p \to \pi^+ n$ are shown in Figs. 16 and 17. The fits are good in most of the considered energy region. The data at forward angles in the $W \gtrsim 1.8$ GeV region cannot be accounted for. The origin of this difficulty is perhaps related to the similar problem in $d\sigma/d\Omega$ for $\gamma p \to \pi^0 p$. Our fits to the polarization observables of $\gamma p \to \pi^+ n$ become less accurate as W increases, as seen in Figs. 18–23.

Overall, we are able to fit more data of $\gamma p \to \pi^0 p, \pi^+ n$ than the JLMS analysis [3]. Not only do we cover the $W \geqslant 1.6$ GeV region, our fits to the data in the low-energy region with $W \leqslant 1.2$ GeV are much better. We, however, still cannot fit accurately the data in the W region close to 2.0 GeV. Here we note that in this high-W region, the data for the ηN, $K\Lambda$, and $K\Sigma$ channels play a very significant role in the analysis through the coupled-channels effects. Thus, the discrepancies with the data in the high-W region cannot be trivially removed.

C. $\pi^- p \to \eta n$

The $\pi^- p \to \eta n$ is simpler than πN elastic scattering because it depends only on the isospin $I = 1/2$ partial waves. As mentioned in Sec. IV, the data for this reaction used in our fits are chosen carefully according to the discussion in Ref. [5] because some inconsistency exists among the data sets from different experiments. In Fig. 24, we show our fits to the data of $d\sigma/d\Omega$ data of $\pi^- p \to \eta n$. Clearly, our results reproduce the considered $d\sigma/d\Omega$ data well.

D. $\gamma p \to \eta p$

Our fits to the data of $\gamma p \to \eta p$ up to $W = 2.1$ GeV are shown in Figs. 25–28. Clearly, both the differential cross sections $d\sigma/d\Omega$ and the polarization observables Σ and T can be described well in the considered energy region. Our results for Σ above $W = 1.7$ GeV are smaller than the data in the

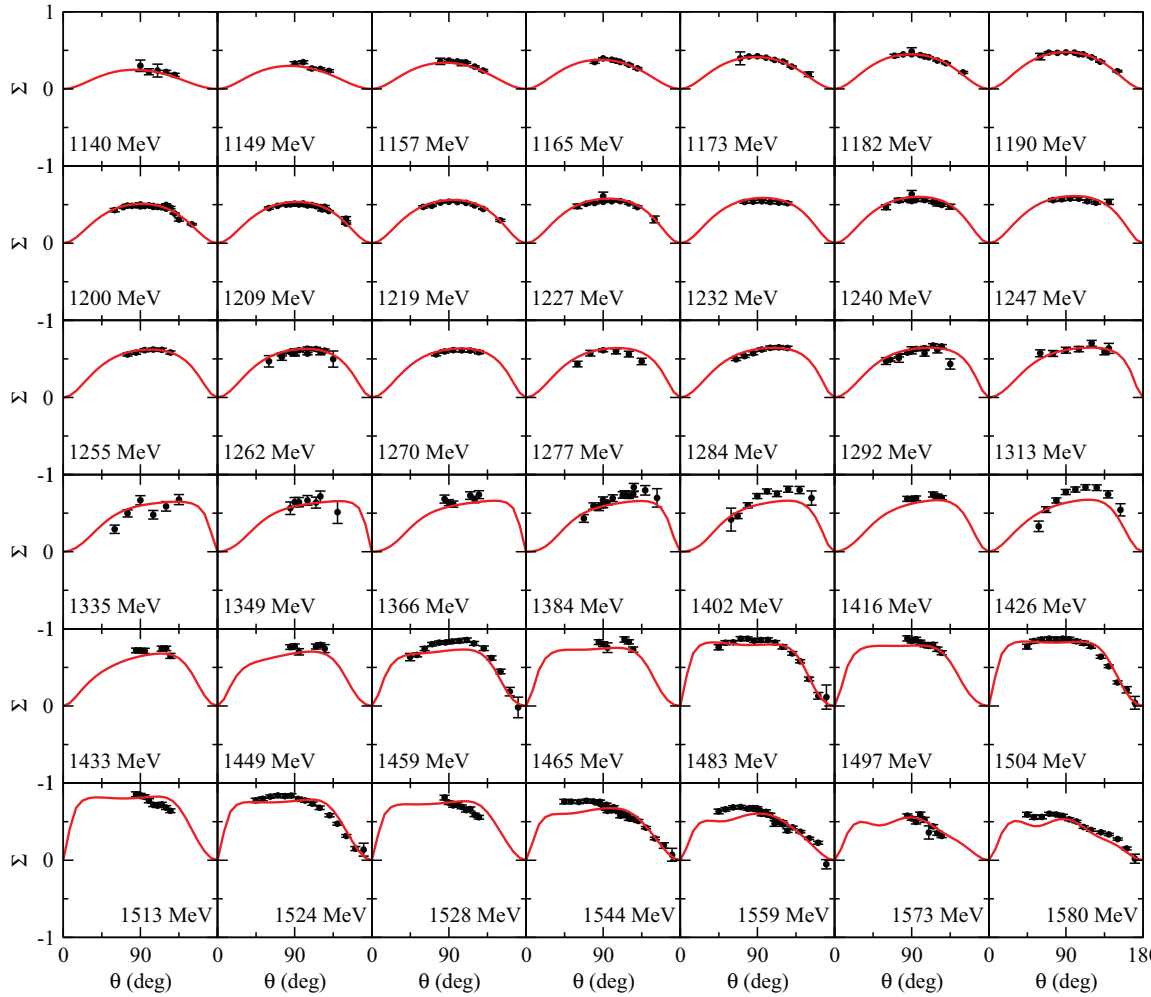

FIG. 10. (Color online) Σ of $\gamma p \to \pi^0 p$.

$0^\circ \lesssim \theta \lesssim 90^\circ$ region, although the positive values of the data are reproduced to a large extent.

E. $\pi^+ p \to K^+\Sigma^+$

The $\pi^+ p \to K^+\Sigma^+$ reaction depends only on the isospin $I = 3/2$ partial waves, and hence the $I = 1/2$ N^* states cannot contribute. Our fits to both $d\sigma/d\Omega$ and P up to $W = 2106$ MeV are good, as shown in Figs. 29 and 30. In Fig. 31, we present the spin-rotation β. This quantity is modulo 2π, and here we plot it in the range $[-\pi, \pi]$. At present, almost no data is available for β of this reaction and these few data points hardly affect the χ^2 minimization. We thus are not able to improve our results shown in Fig. 31.

F. $\pi^- p \to K^0\Lambda^0$

In contrast with the $\pi^+ p \to K^+\Sigma^+$ discussed in the above section, the $\pi^- p \to K^0\Lambda^0$ only involves the isospin $I = 1/2$ mechanism. Our fits to $d\sigma/d\Omega$ and P of this reaction are shown in Figs. 32 and 33, respectively. Clearly, our fits are very good. Our results for the spin rotation β (Fig. 34) reproduce the main feature of the data while these few data points, like those in the $\pi^+ p \to K^+\Sigma^+$ reaction, have practically no effect in the χ^2 minimization. More data for β will be necessary to improve the situation.

G. $\pi^- p \to K^0\Sigma^0$

The $\pi^- p \to K^0\Sigma^0$ reaction is more complex than $\pi^+ p \to K^+\Sigma^+$ and $\pi^- p \to K^0\Lambda^0$, because it involves interfering contributions from both the isospin $I = 1/2$ and $I = 3/2$ mechanisms. Our fits to the data of $d\sigma/d\Omega$ and P of this reaction are shown in Figs. 35 and 36, respectively. We see that our results reproduce the data to a large extent in the considered energy region, although the $d\sigma/d\Omega$ data in the near-threshold region are underestimated.

Here we note that all of the $\pi N \to KY$ data used in our fits are from old measurements more than a quarter of century ago. Their statistical errors are, in general, quite large compared with the recent photoproduction data. Furthermore, the amount of data is scarce in the kinematical region relevant to N^* above 1.6 GeV, in particular for the $\pi^- p \to K^0\Sigma^0$ reaction. An experiment planned at J-PARC [48] is quite encouraging, where the high-precision data for $\pi N \to \pi\pi N$ and $\pi N \to KY$ will be obtained in the wide energy region.

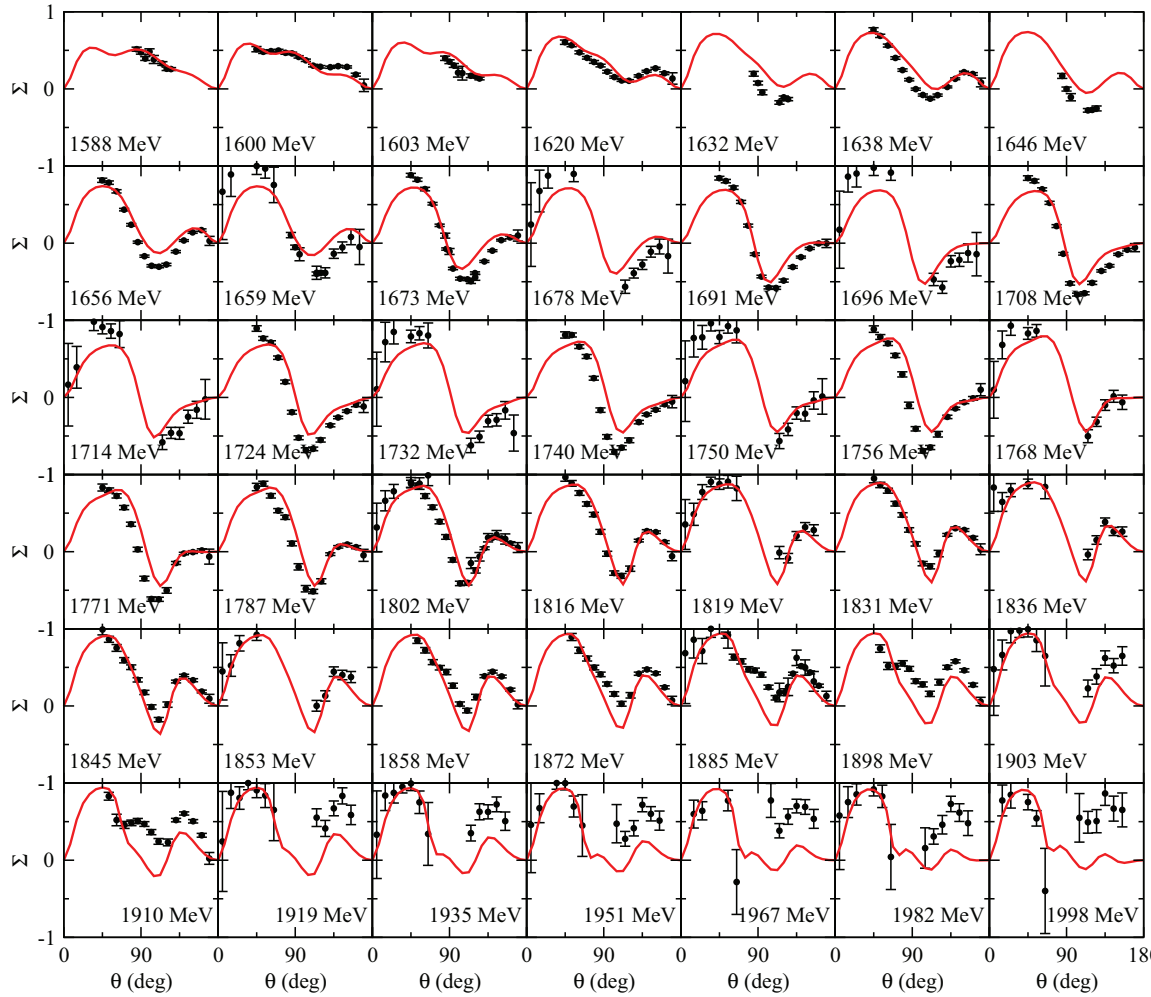

FIG. 11. (Color online) Σ of $\gamma p \to \pi^0 p$ (continued).

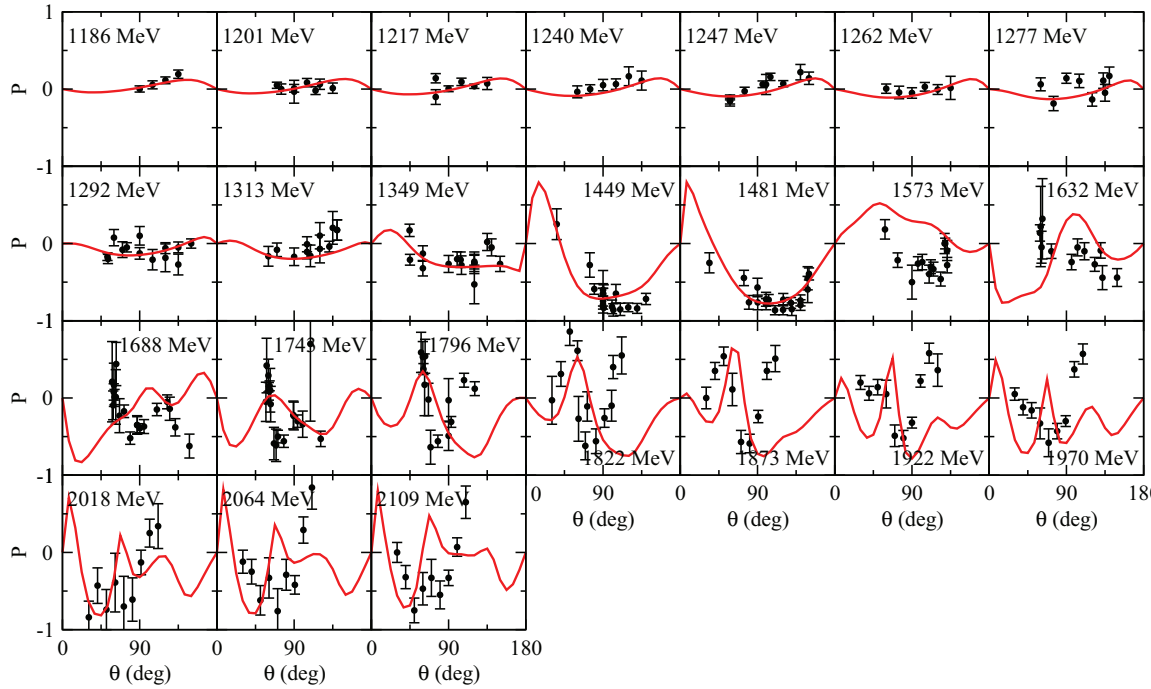

FIG. 12. (Color online) P of $\gamma p \to \pi^0 p$.

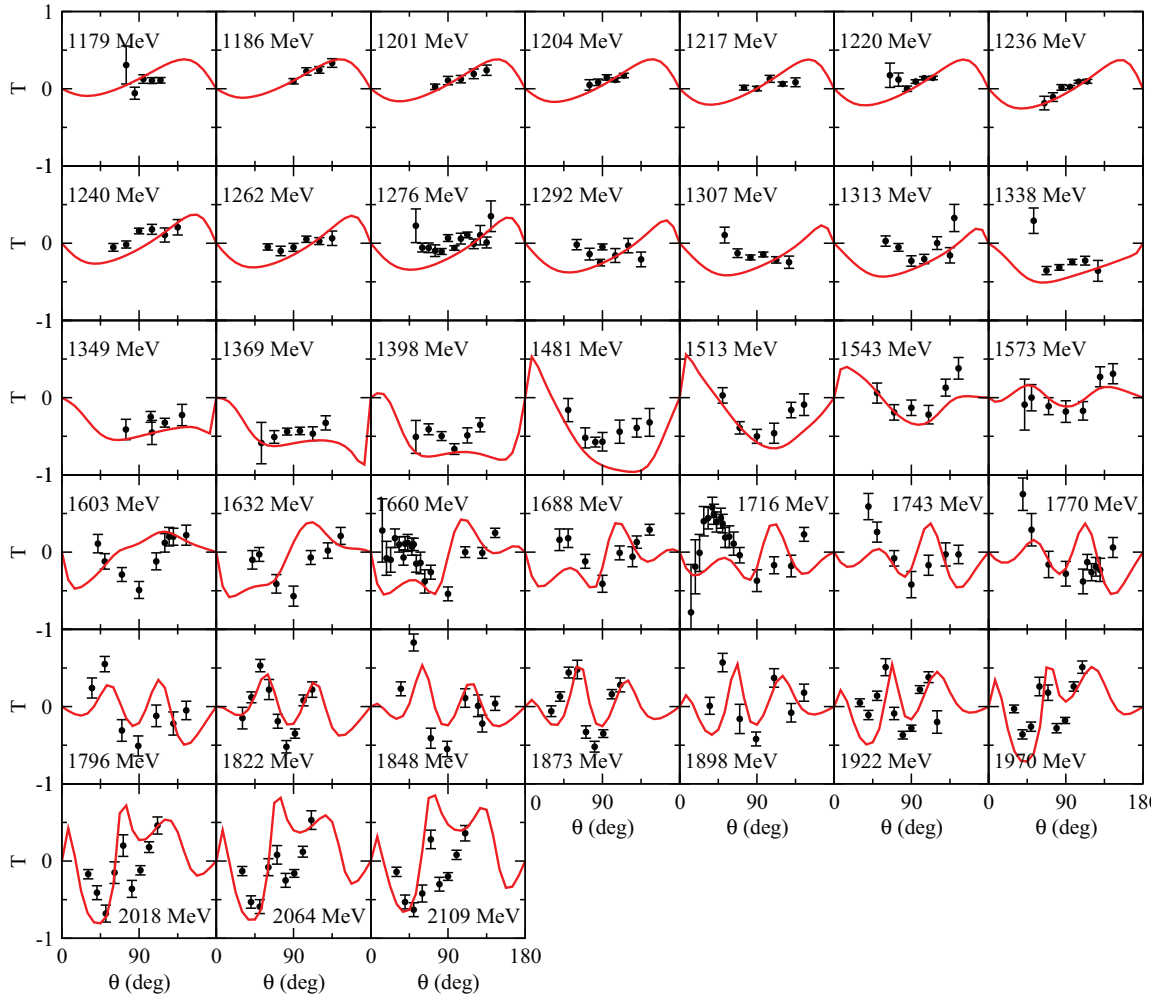

FIG. 13. (Color online) T of $\gamma p \to \pi^0 p$.

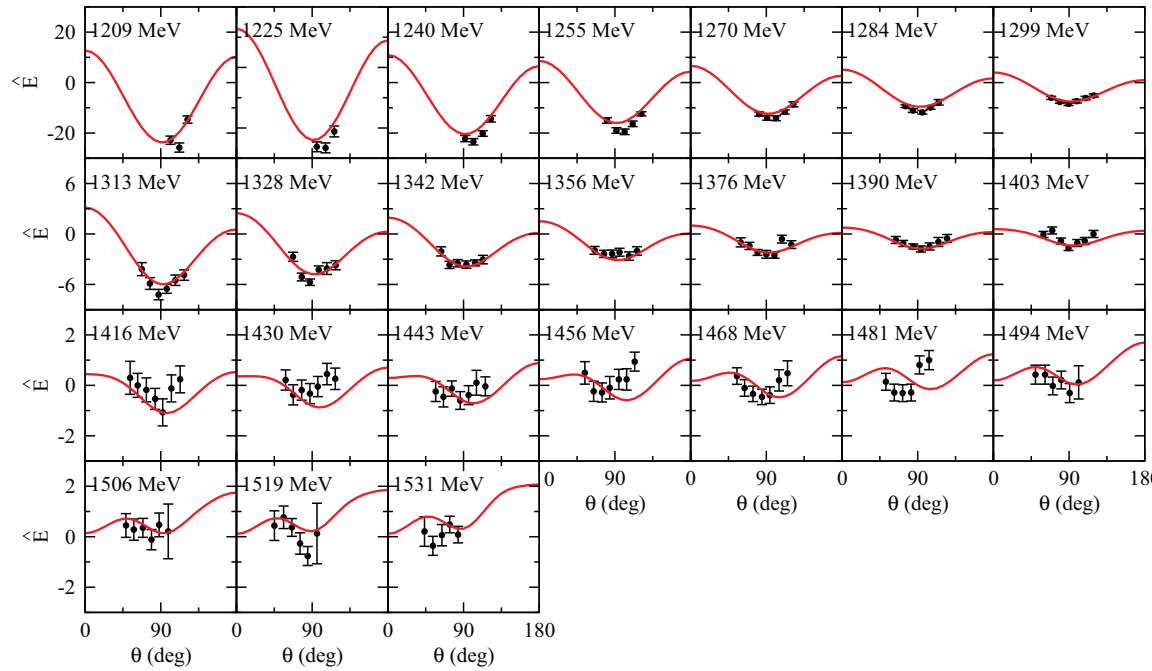

FIG. 14. (Color online) $\hat{E}$ of $\gamma p \to \pi^0 p$.

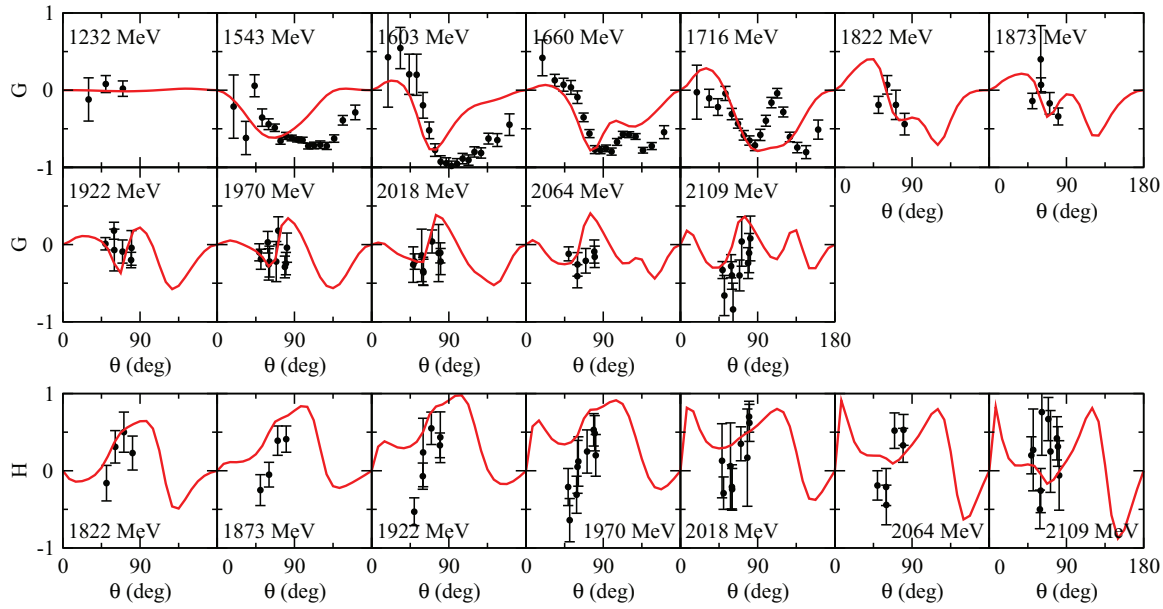

FIG. 15. (Color online) G and H of $\gamma p \to \pi^0 p$.

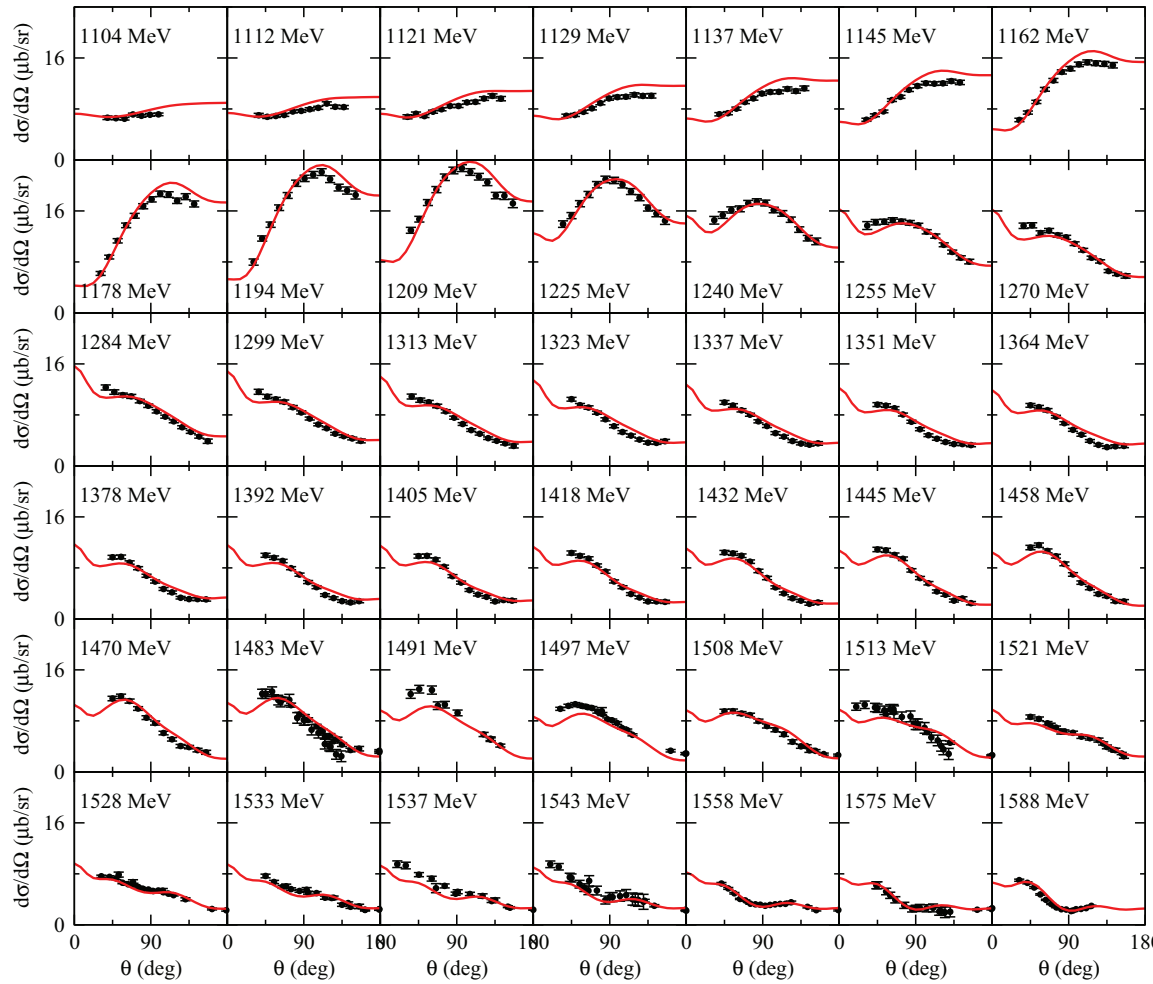

FIG. 16. (Color online) $d\sigma/d\Omega$ of $\gamma p \to \pi^+ n$.

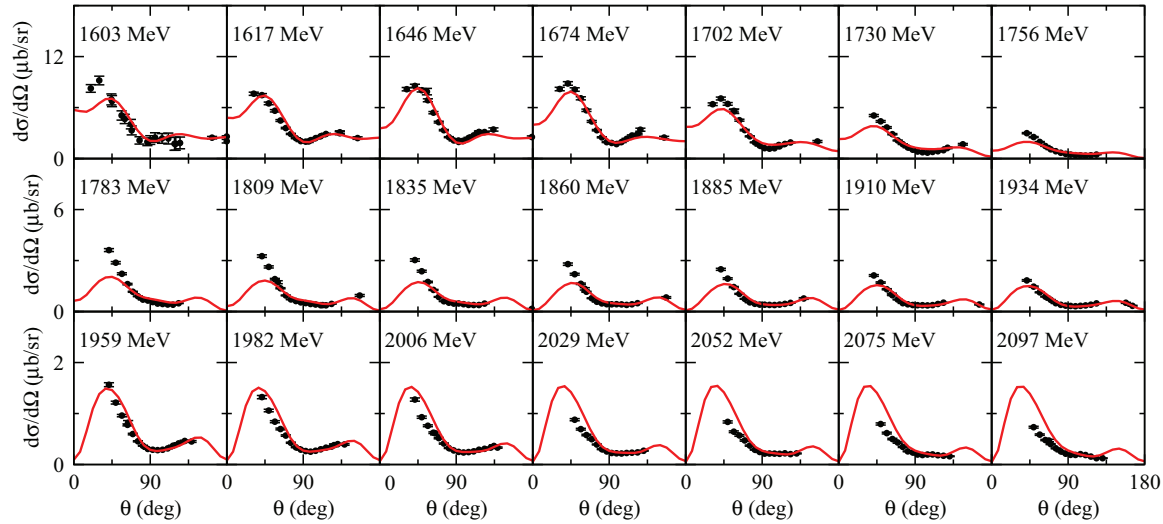

FIG. 17. (Color online) $d\sigma/d\Omega$ of $\gamma p \to \pi^+ n$ (continued).

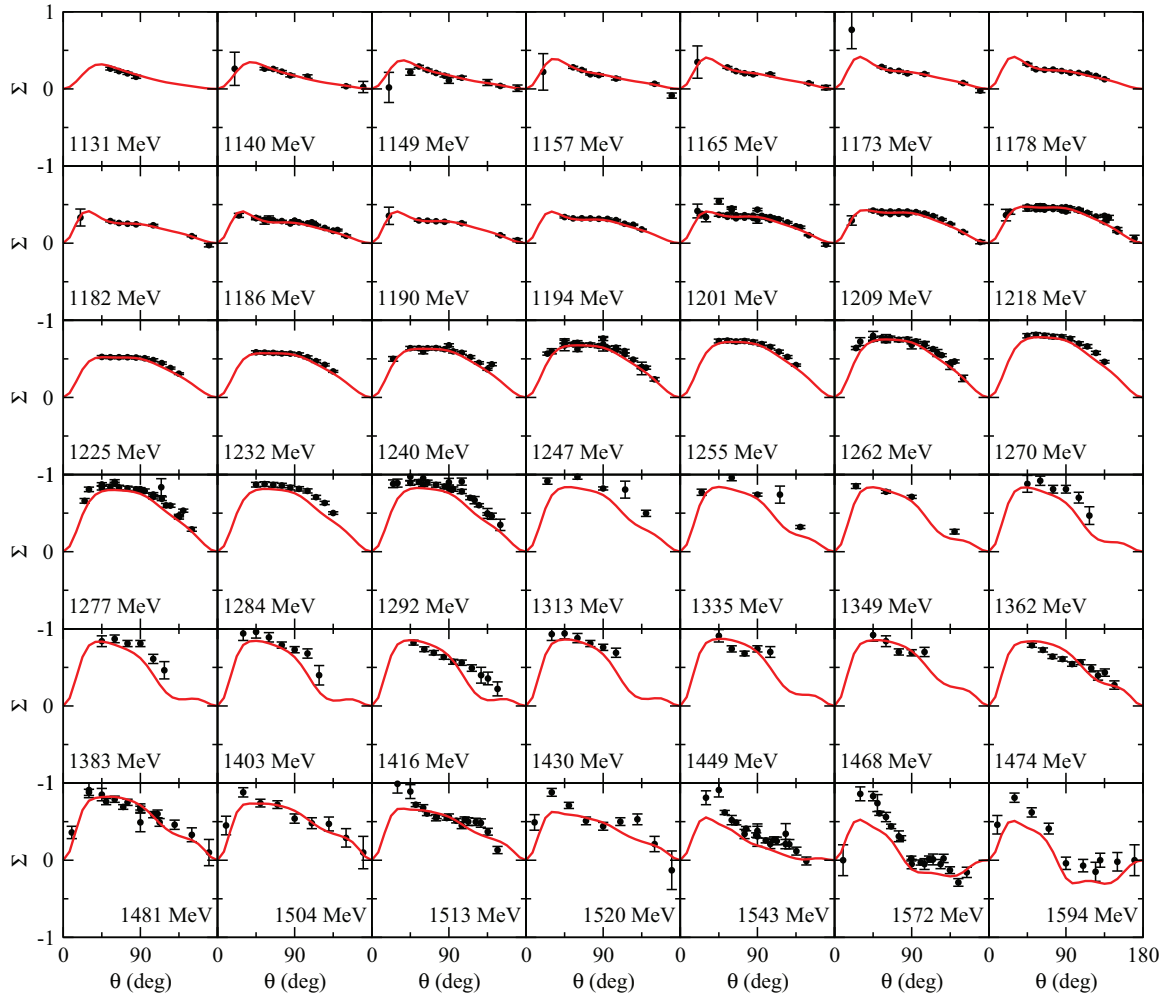

FIG. 18. (Color online) Σ of $\gamma p \to \pi^+ n$.

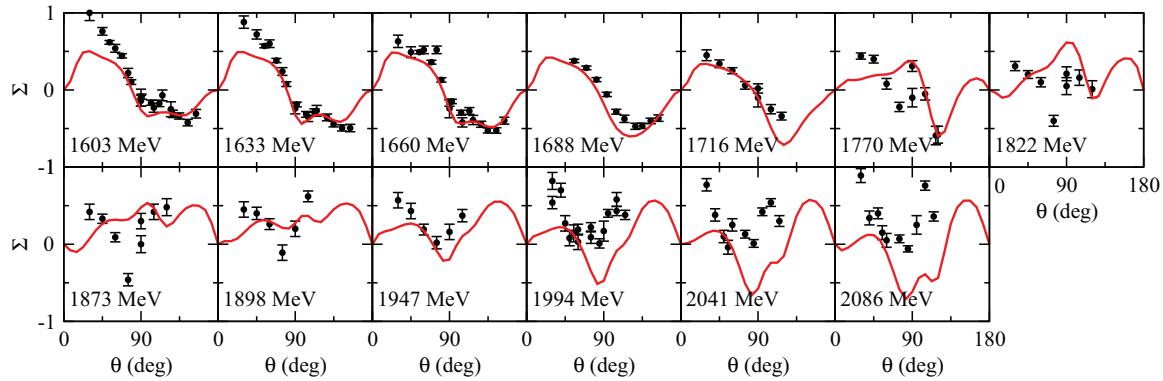

FIG. 19. (Color online) Σ of $\gamma p \to \pi^+ n$ (continued).

H. $\gamma p \to K^+\Lambda$

Our fits to the $d\sigma/d\Omega$ data of $\gamma p \to K^+\Lambda$ are shown in Figs. 37 and 38. The main features of the data up to $W = 2106$ MeV are reproduced reasonably well, in particular in the $45^\circ \lesssim \theta \lesssim 135^\circ$ region where the s-channel processes with the isospin $I = 1/2$ N^* resonances are found to be important. However, our results at forward and backward angles underestimate the data in the $W \gtrsim 1.9$ GeV high-energy region. This situation is similar to the $\gamma p \to \pi N$ reactions and further suggests that the inclusion of additional mechanisms would be necessary for improving our combined analysis at high energies.

Because of the self-analyzing property of the recoil Λ baryon, the single- and double-polarization observables of $\gamma p \to K^+\Lambda$ have been extensively measured in recent years. More data of the polarization observables of $\gamma p \to K^+\Lambda$ will soon become available from JLab and other photon/electron beam facilities. Actually, all of the 15 possible polarization observables for this reaction have already been measured at CLAS [49].

The fits to the available polarization data, as listed in Table V, are already highly nontrivial because they are attributable to delicate interferences between different partial waves. Nevertheless, as seen in Figs. 39 and 40, our fits can

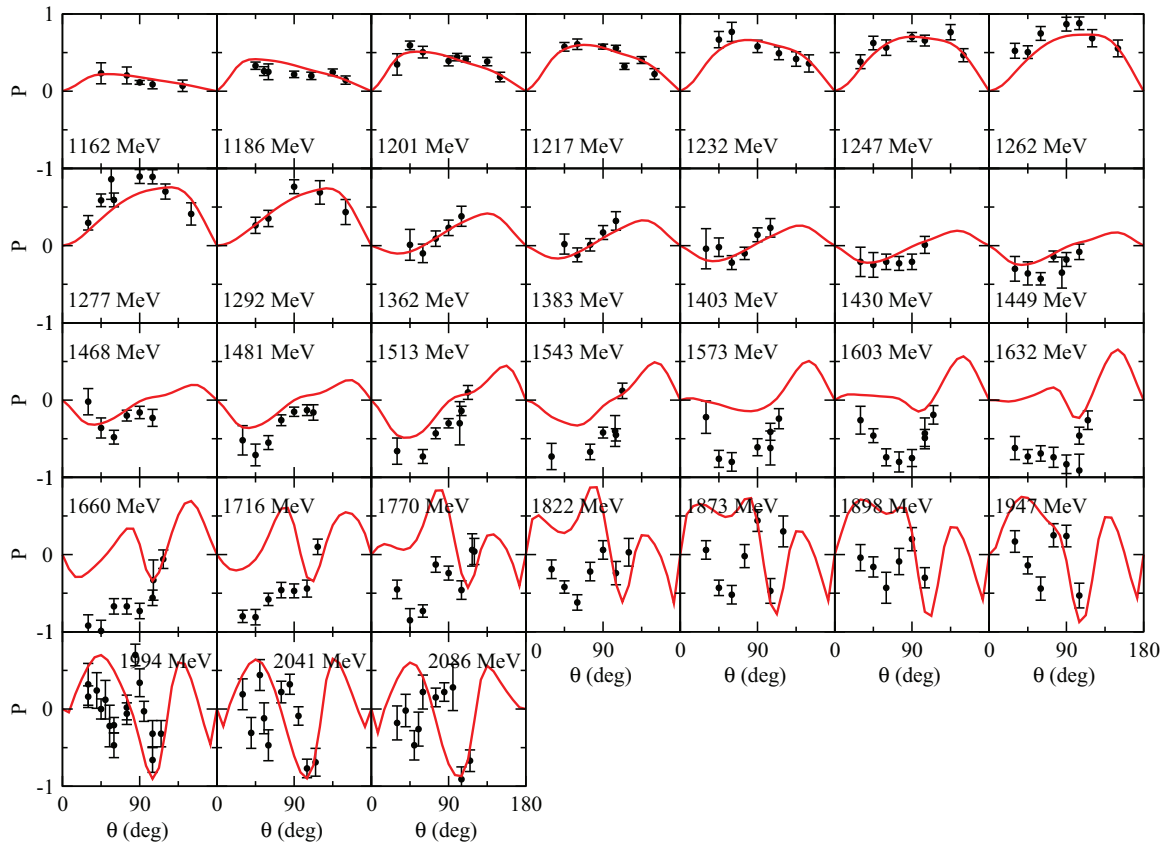

FIG. 20. (Color online) P of $\gamma p \to \pi^+ n$.

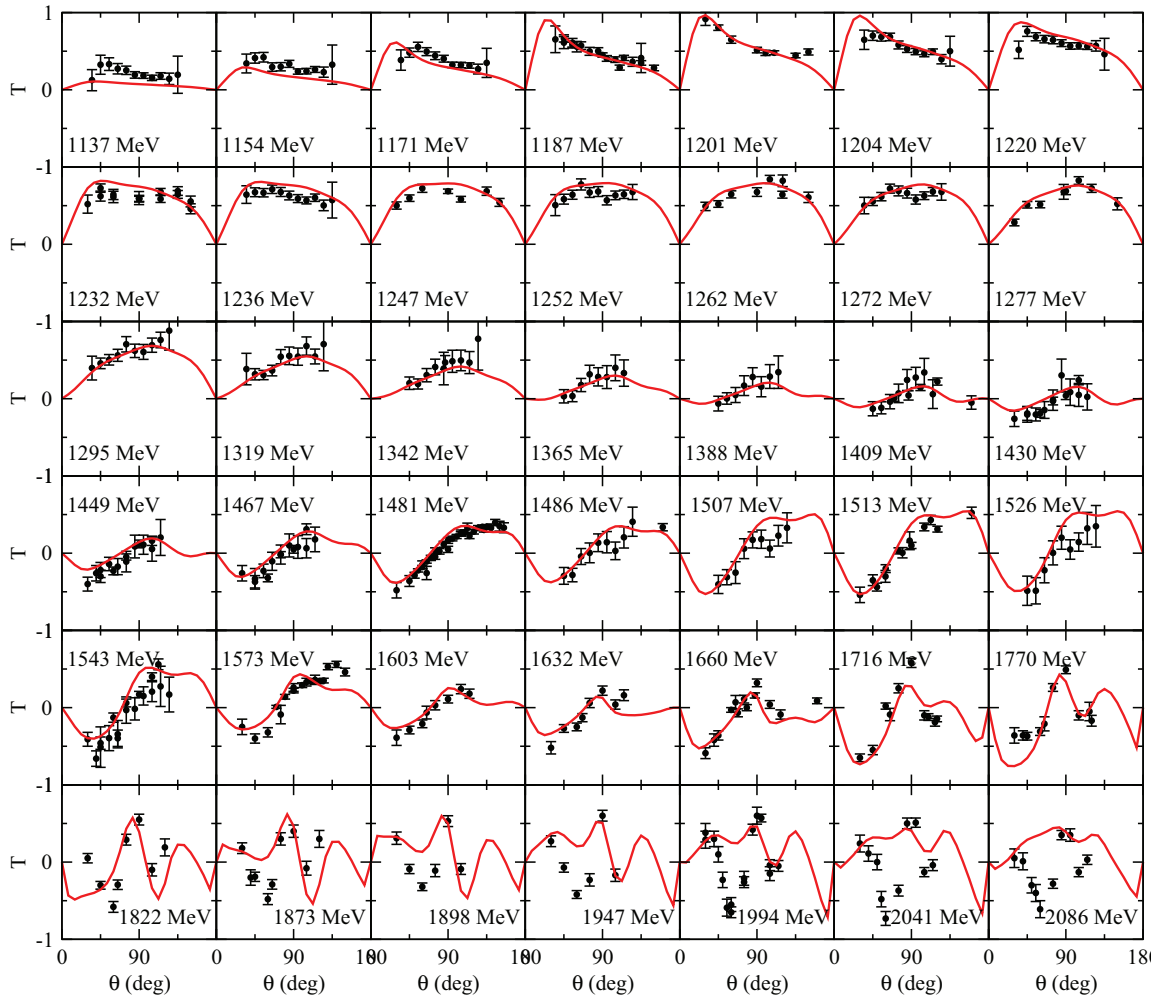

FIG. 21. (Color online) T of $\gamma p \to \pi^+ n$.

reproduce the main features of these polarization data to a very large extent. Here it is noted that for the double polarizations C_x and C_z, we have plotted them in the *primed* coordinate system as $C_{x'}$ and $C_{z'}$, by using the relation

$$C_{x'} = +C_x \cos\theta - C_z \sin\theta, \tag{48}$$

$$C_{z'} = +C_x \sin\theta + C_z \cos\theta, \tag{49}$$

as done in the analysis of Ref. [44].

I. $\gamma p \to K^+\Sigma^0, K^0\Sigma^+$

It is more difficult to fit the data of $\gamma p \to K^+\Sigma^0$ and $\gamma p \to K^0\Sigma^+$ than that of $\gamma p \to K^+\Lambda^0$ presented in the previous section, because here the isospin $I = 3/2$ N^* resonances also contribute. In particular, we have found that the $d\sigma/d\Omega$ data for both $\gamma p \to K^+\Sigma^0$ and $\gamma p \to K^0\Sigma^+$ can be fitted well only when the $K\Sigma N$ coupling constant $g_{K\Sigma N}$ is allowed to vary far off the SU(3) relation, as given in Eqs. (B31), in the fits. This implies that $\gamma p \to K\Sigma$ reaction could be an important source of learning about the validity of the SU(3) relation. This, however, can be done rigorously only when more complete data for these two photoproduction reactions become available.

Our fits to the data of differential cross sections $d\sigma/d\Omega$ and polarization observables P, Σ, C_x, C_z of $\gamma p \to K^+\Sigma^0$ are shown in Figs. 41–43. Again we have plotted C_x and C_z as $C_{x'}$ and $C_{z'}$ in the *primed* coordinate system using Eqs. (48) and (49). We see that the fits to the data of differential cross sections (Fig. 41) P and Σ (Fig. 42) are fairly good. However, the fits to the data of C_x, C_z (Fig. 43) are very qualitative, in particular in the high-energy region, $W \gtrsim 1.8$ GeV.

We now present our fits to the very limited data of the $\gamma p \to K^0\Sigma^+$ reaction in Figs. 44 and 45. Clearly, our fits to the data of $d\sigma/d\Omega$, shown in Fig. 44, are qualitative only in the $W \gtrsim 1.9$ GeV region. However, we see in Fig. 45 that our fits to the data of P and Σ are reasonable.

VI. RESONANCE PARAMETERS

Once the model parameters are determined by the simultaneous fits to all of the considered data, as presented in Sec. V, we then apply the analytic continuation method of Refs. [8,9] to find the resonance pole positions and their

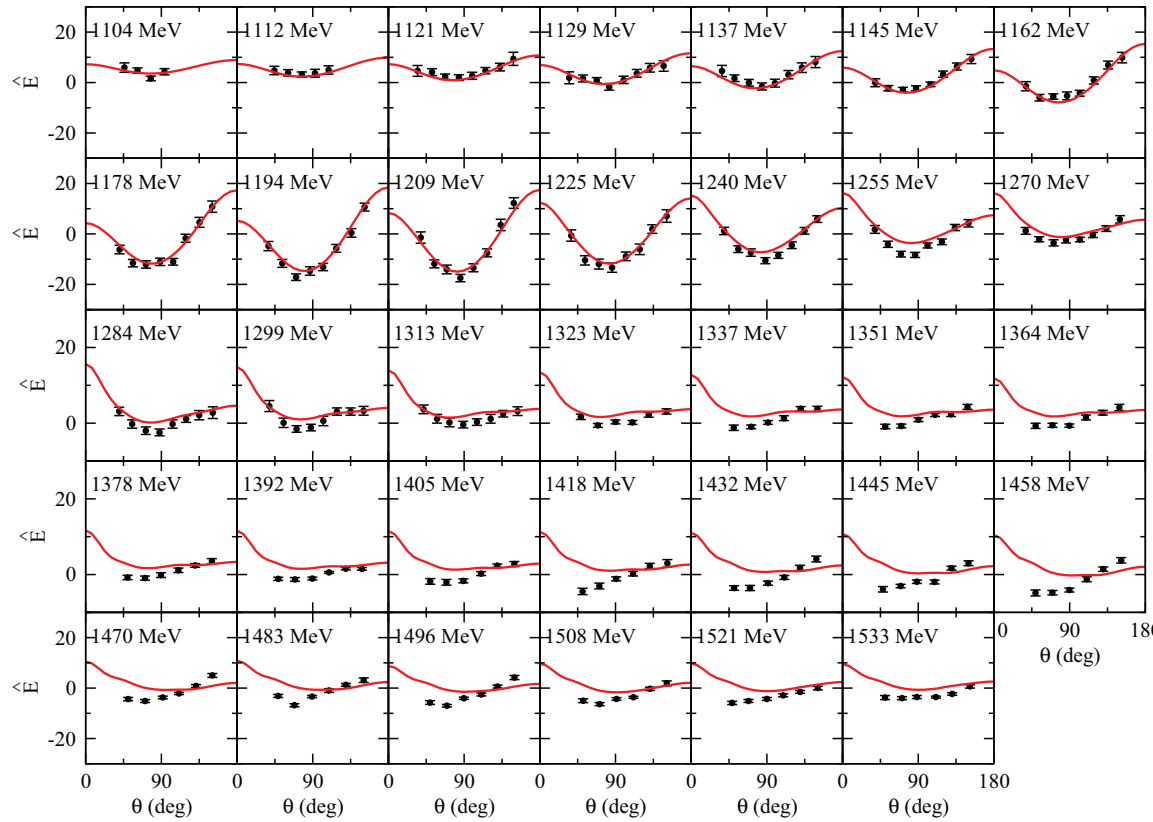

FIG. 22. (Color online) $\hat{E}$ of $\gamma p \to \pi^+ n$.

residues. We expect that the resonances with large widths [the widths are defined to be related to the resonance pole position M_R by $\Gamma^{\rm tot} = -2{\rm Im}(M_R)$] have less influence on the physical observables, and thus the extractions of these resonances from fitting the available reaction data, as done by all analysis groups, are more model dependent. As a result, the extracted information on those resonances is much less reliable. We therefore examine only the resonances with the width less than 400 MeV. Also, as already mentioned in Sec. IV, the resonances with ${\rm Re}(M_R) > 2$ GeV, found in F_{17}, G and H waves, are also not presented here. We will be able to present those high-mass resonances with confidence only after extending our analysis to higher energy regions and including ωN and $\pi\pi N$ production data.

As defined in Eqs. (32)–(42), we present our results for the resonance pole positions M_R and residues $R_{MB,\pi N}(M_R)$ for $MB = \pi N, \eta N, K\Lambda, K\Sigma$. Other components of the extracted residues do not correspond to the reaction data considered and are not presented. The elasticity η_e [Eq. (43)] and helicity amplitudes $A_{\lambda=1/2,3/2}$ [Eqs. (44) and (45)] are also presented. Our results are given and discussed in the following sections.

A. Resonance pole positions and residues

The N^* pole positions M_R extracted from our analysis are presented in Table VI and compared with those listed by Particle Data Group (PDG). The N^* states are specified by $J^P(L_{2I2J})$, where J is the spin, $P = \pm$ the parity, I the isospin, and L the orbital angular momentum of the associated πN partial wave. Here we list only the three- and four-star N^* of PDG because their values are rather stable in the past two decades and most of their widths are all less than 400 MeV that is the limit set in our search. We see that we agree well with PDG for the N^* resonances below 2 GeV except (a) we do not have a third state in $3/2^-(D_{13})$, (b) we do not have a third state in $3/2^+(P_{33})$, and (c) we have a second state in $3/2^-(D_{33})$. In our analysis, a resonance pole with $M_R = (1429, 147)$ MeV in $1/2^+(P_{11})$ is also found, which turns out to be a "shadow" of the first $1/2^+(P_{11})$ resonance with respect to the $\pi\Delta$ branch point. However, this pole is far from the physical region and thus is not listed. Such a shadow pole is also found in other analyses (e.g., Ref. [20]) as well as our early analyses [10,11]. In Table VI, we also see that the determined elasticities η_e are rather consistent with the values listed by PDG. However, some explanation may be required for the result that the elasticity for the 1st $3/2^+(P_{33})$ resonance exceeds 100%. The elasticity η_e is defined by Eq. (43), where $-2{\rm Im}(M_R)$ and $2|R_{\pi N,\pi N}|$ are interpreted as the total width and the partial width for the decay to the πN channel, respectively, evaluated at *the resonance pole position* in the complex energy plane. As is well known, the sum of the partial widths defined in this manner does not agree with the total width defined with the imaginary part of the resonance pole position.

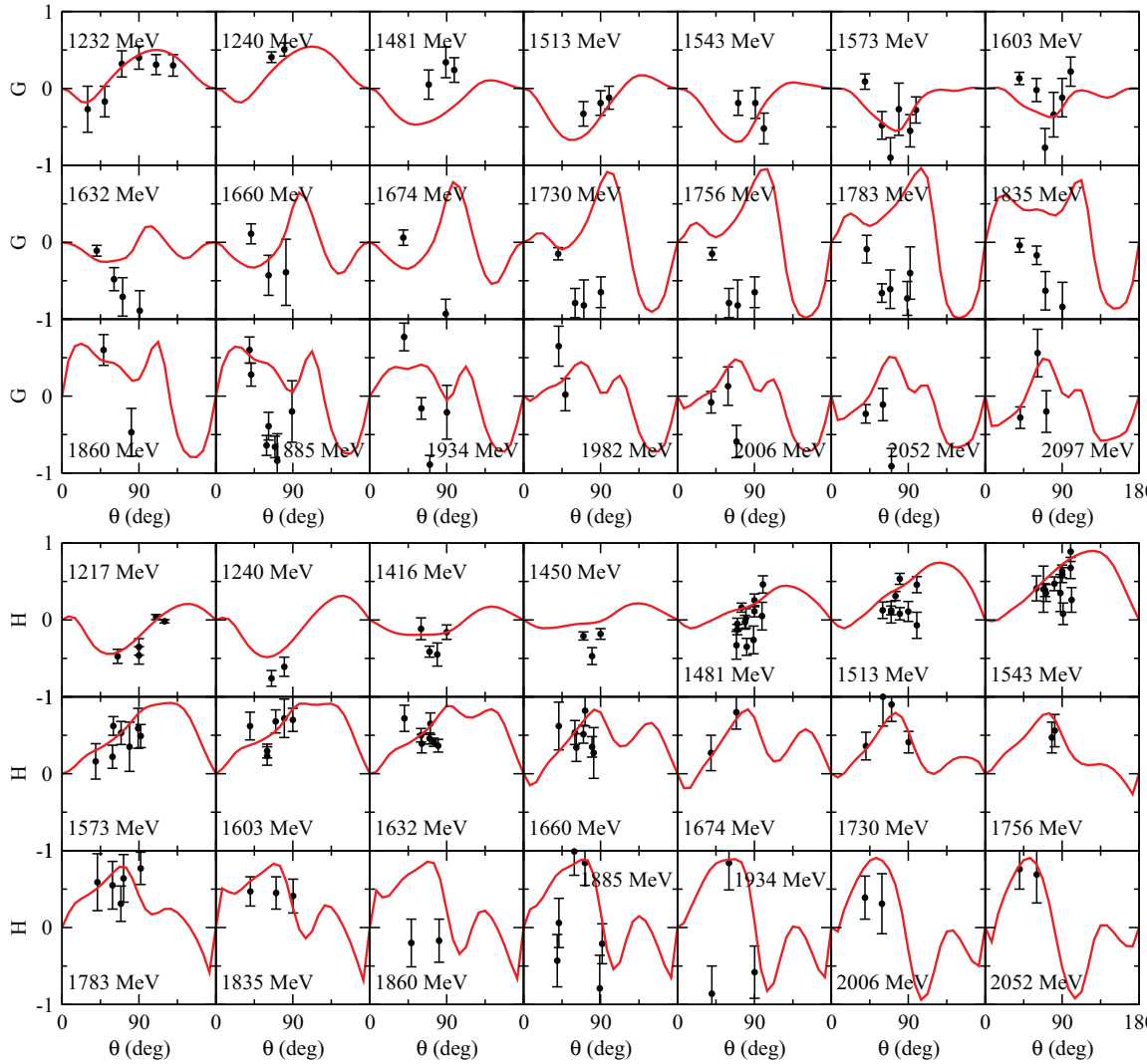

FIG. 23. (Color online) G and H of $\gamma p \to \pi^+ n$.

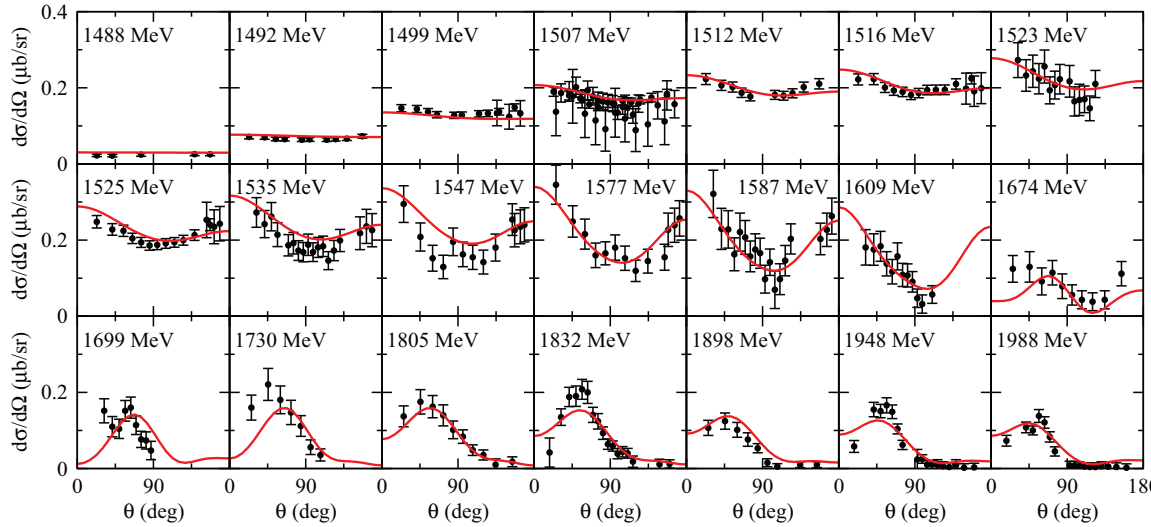

FIG. 24. (Color online) $d\sigma/d\Omega$ of $\pi^- p \to \eta n$.

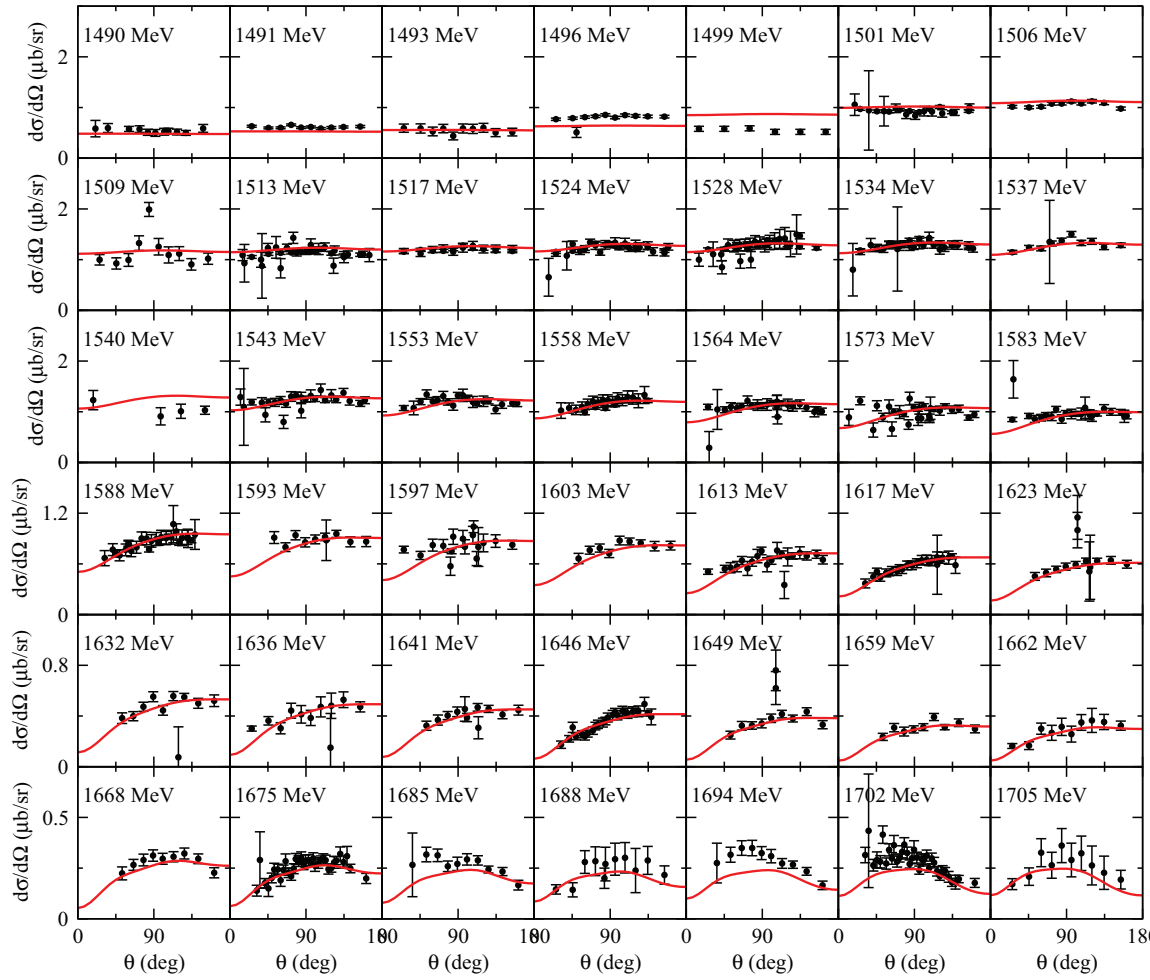

FIG. 25. (Color online) $d\sigma/d\Omega$ of $\gamma p \to \eta p$.

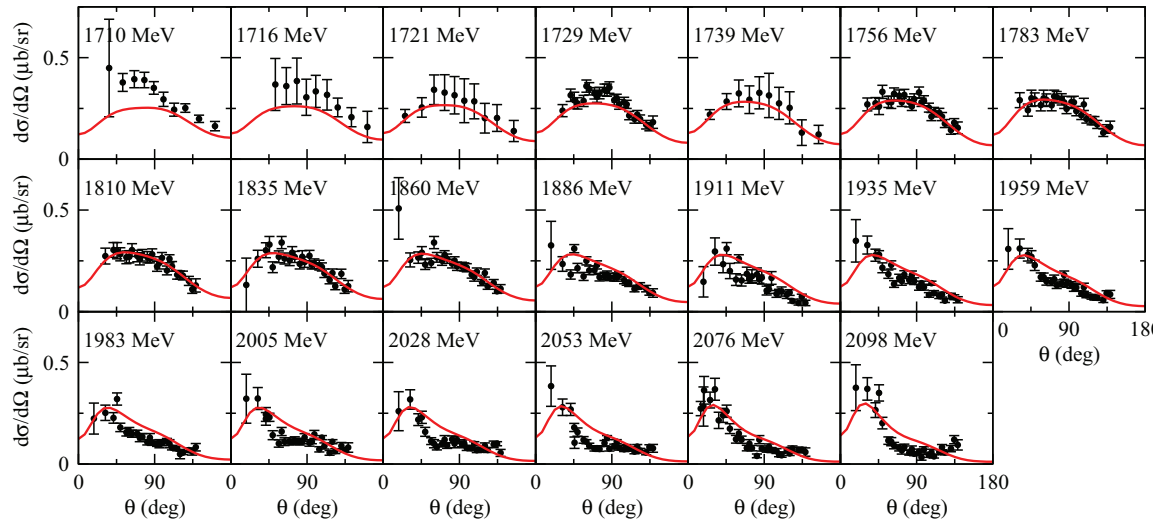

FIG. 26. (Color online) $d\sigma/d\Omega$ of $\gamma p \to \eta p$ (continued).

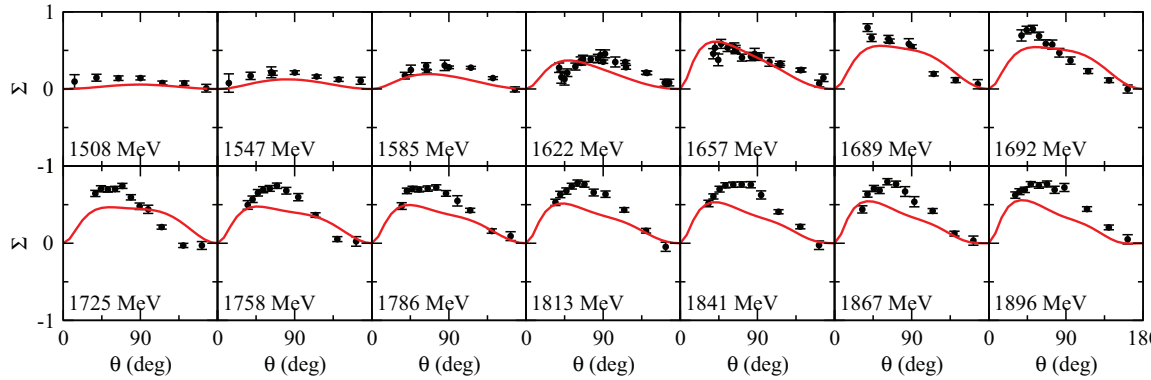

FIG. 27. (Color online) Σ of $\gamma p \to \eta p$.

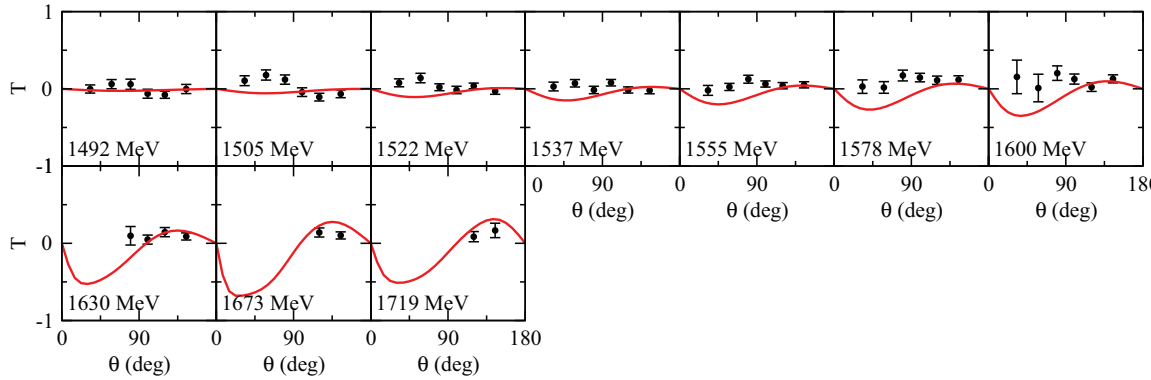

FIG. 28. (Color online) T of $\gamma p \to \eta p$.

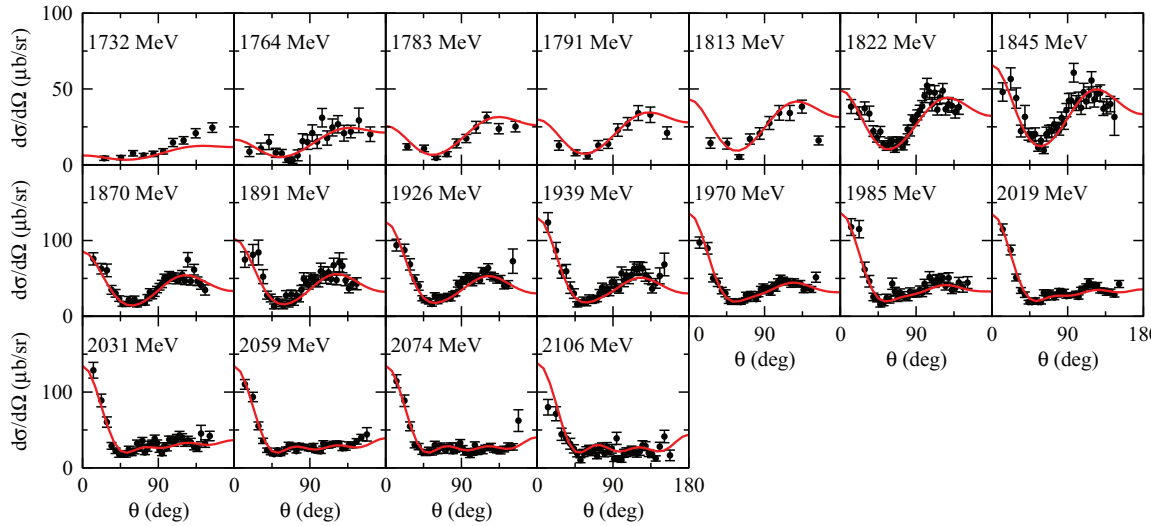

FIG. 29. (Color online) $d\sigma/d\Omega$ of $\pi^+ p \to K^+ \Sigma^+$.

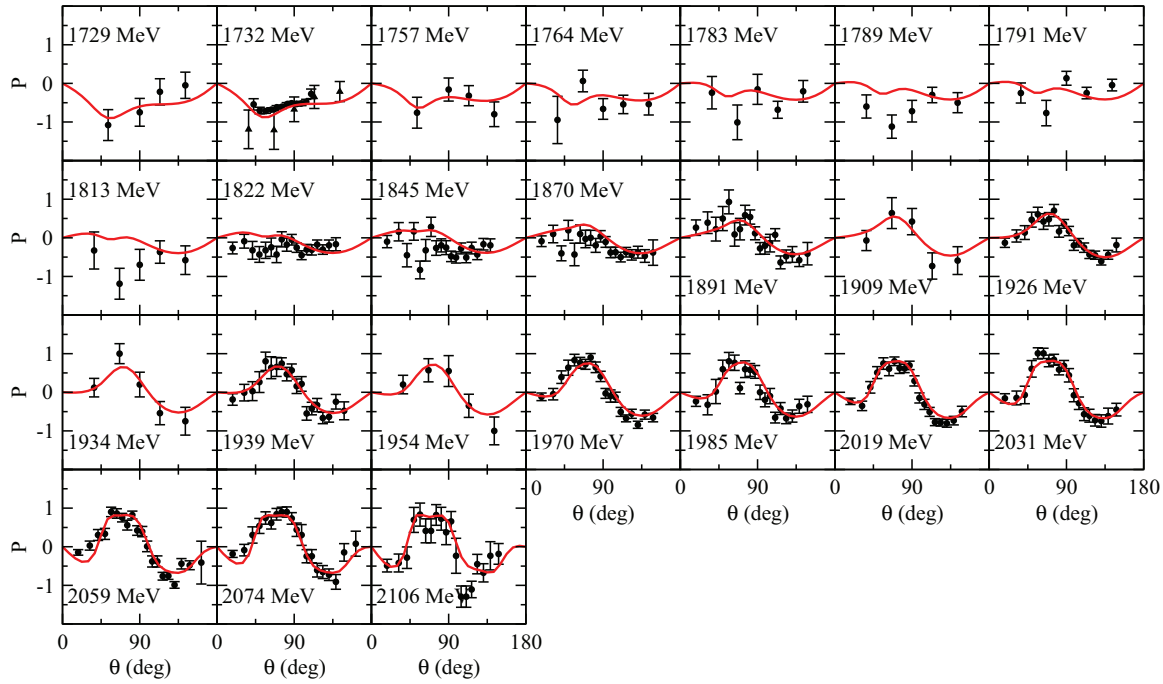

FIG. 30. (Color online) P of $\pi^+ p \to K^+\Sigma^+$.

In Figs. 46 and 47, we compare our (ANL-Osaka) values (AO, second column) of the N^* spectrum with those from PDG (PDG, first column) and the analyses by the Jülich [20] (J, third column) and the Bonn-Gatchina [23] (BG, fourth column) groups. In the figures only the resonances with the total widths less than 400 MeV are compared. It is noted, however, that some broad N^* resonances with $[\mathrm{Re}(M_R), -2\mathrm{Im}(M_R)] = (1787, 575)$ MeV in $1/2^+(P_{31})$, $(1727, 866)$ MeV in $3/2^+(P_{33})$, and $(1776, 646)$ MeV in $5/2^-(D_{35})$ have also been reported by the Jülich group, while $[\mathrm{Re}(M_R), -2\mathrm{Im}(M_R)] = (1660, 450)$ MeV in $3/2^+(P_{13})$, $(1770, 420)$ MeV in $3/2^-(D_{13})$, and $(1990, 450)$ MeV in $3/2^-(D_{33})$ have been reported by the Bonn-Gatchina group.

We see in Figs. 46 and 47 that the first N^* resonances from four results in each (J^P, I) state agree well, except (a) the $3/2^+(P_{13})$ from the Bonn-Gatchina analysis is about 200 MeV higher than the others, (b) the Jülich analysis does not have $1/2^+(P_{31})$, (c) only the Jülich analysis has $7/2^+(F_{17})$ below 2 GeV, and (d) the Jülich and Bonn-Gatchina analyses do not have $5/2^-(D_{35})$. For higher mass states, the number of states and their positions from four results do not agree well. Here we mention that the PDG values are mainly from the earlier results of πN elastic scattering data. The photoproduction data

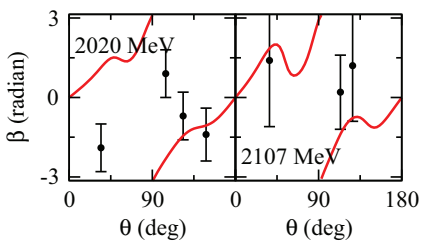

FIG. 31. (Color online) β of $\pi^+ p \to K^+\Sigma^+$.

of $\gamma p \to \pi N, \eta N, K\Lambda, K\Sigma$ have not been included in the Jülich analysis, while the data included in the AO and Bonn-Gatchina analyses are not too different. As discussed in the Introduction, the K-matrix model used in the Bonn-Gatchina analysis is very different from the DCC model used in the AO and Jülich analyses. In the Bonn-Gatchina analysis, like other K-matrix model analyses, the parameters in different partial waves are varied independently in the fits. However, the parameters of meson-exchange mechanisms in the AO and Jülich analyses can affect all partial waves and channels. Thus, the Bonn-Gatchina analysis is more flexible and efficient in fitting the data; in particular, in the area where the data have fluctuating structure with large uncertainties.

Thus, the differences between four results seen in Figs. 46 and 47 could be attributed to the differences in the employed analysis methods and the data included in the analysis. The much more divergent results for the second and third states could also be attributed to the fact that in the high $W \gtrsim 1.6$ GeV region, the available data are far from complete for determining the partial-wave amplitudes model independently. The difficulties in extracting the partial-wave amplitudes model independently from the data, even when they are complete, have been investigated recently in Ref. [44].

In Table VII, we list the extracted residues $R_{MB,\pi N}$ for $MB = \pi N, \eta N, K\Lambda, K\Sigma$. In Table VIII, we compare the extracted residues $R_{\pi N,\pi N}$ with those from the Bonn-Gatchina and Jülich analyses. Three analyses agree very well for the well-established $\Delta(1211)3/2^+(P_{33})$. For some states, three results agree qualitatively. However, the differences between three results can be very large for several states. This is perhaps attributable to the fact that the residues are more sensitive to the functional forms of the amplitudes which are very different between different

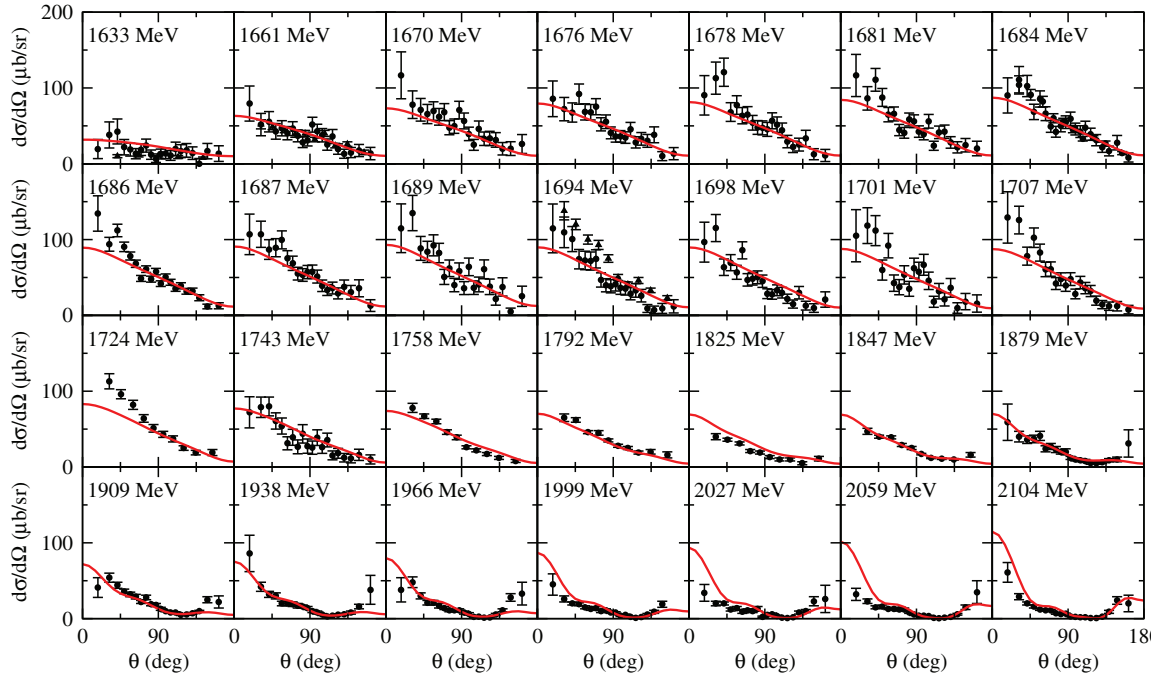

FIG. 32. (Color online) $d\sigma/d\Omega$ of $\pi^- p \to K^0\Lambda^0$.

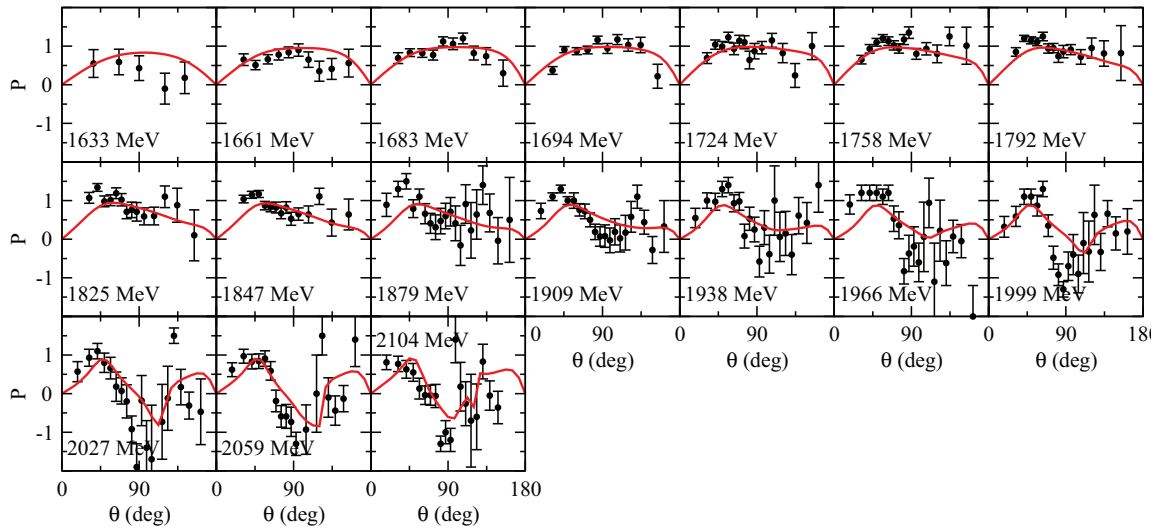

FIG. 33. (Color online) P of $\pi^- p \to K^0\Lambda^0$.

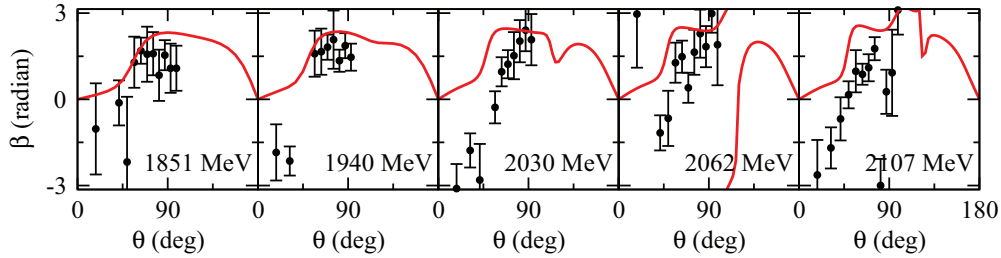

FIG. 34. (Color online) β of $\pi^- p \to K^0\Lambda^0$.

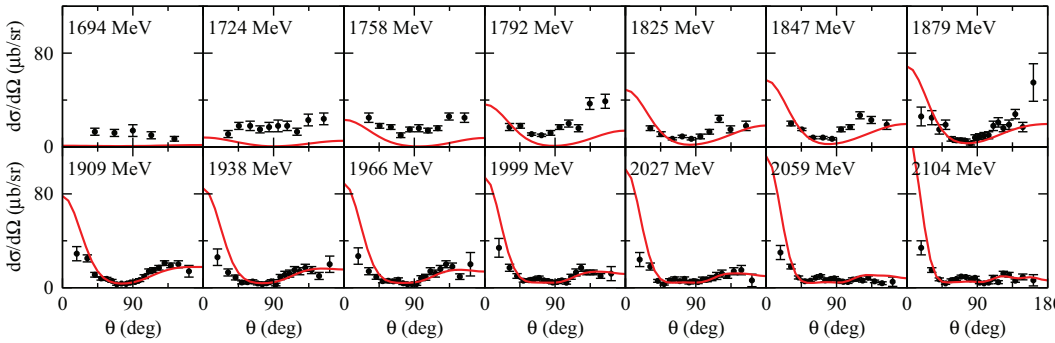

FIG. 35. (Color online) $d\sigma/d\Omega$ of $\pi^- p \to K^0\Sigma^0$.

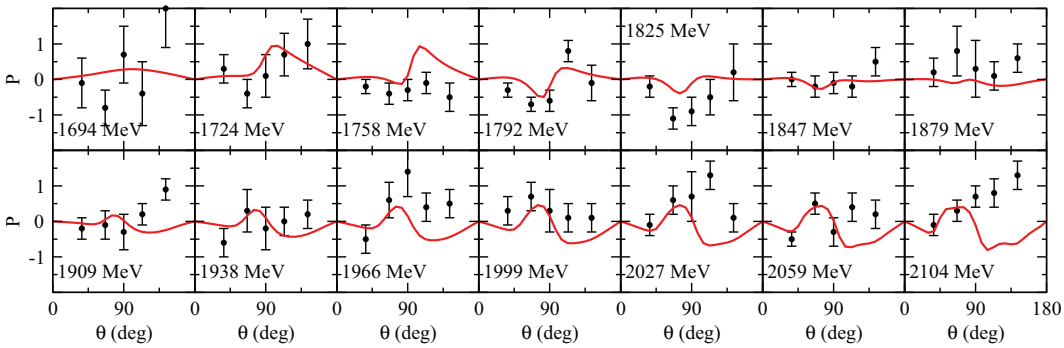

FIG. 36. (Color online) P of $\pi^- p \to K^0\Sigma^0$.

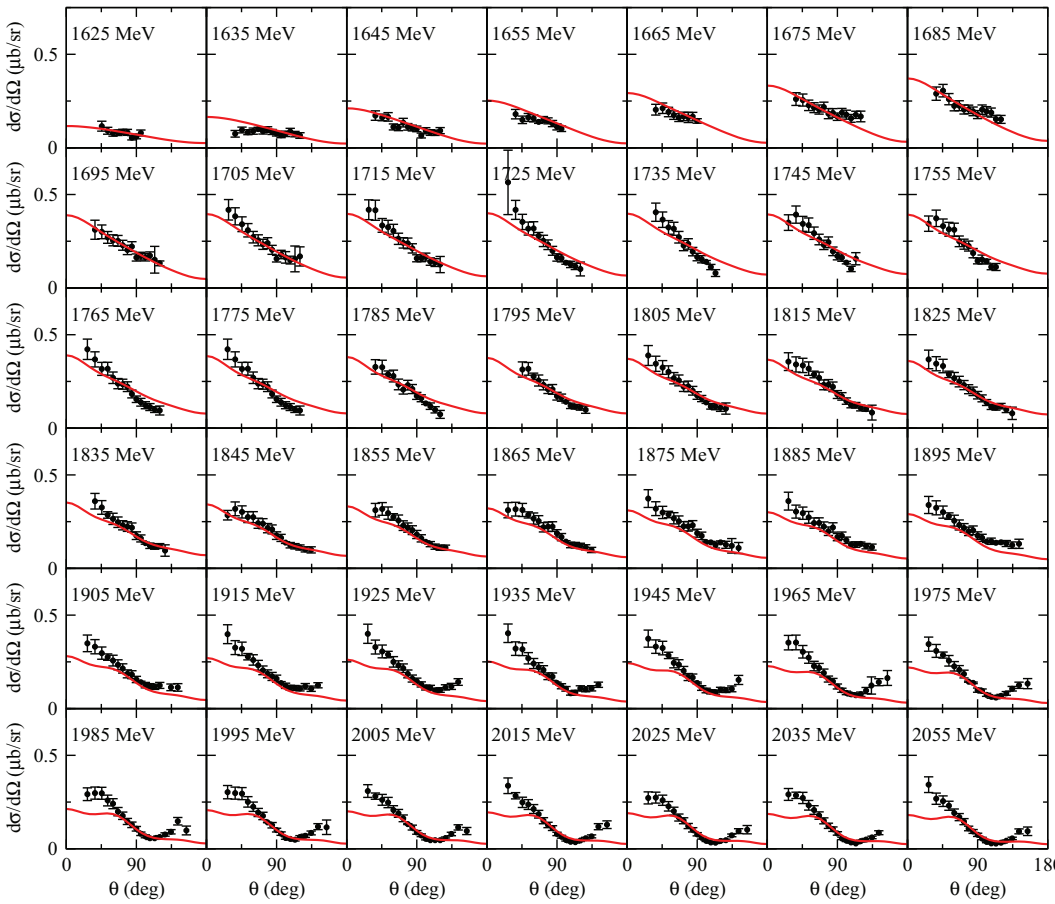

FIG. 37. (Color online) $d\sigma/d\Omega$ of $\gamma p \to K^+\Lambda$.

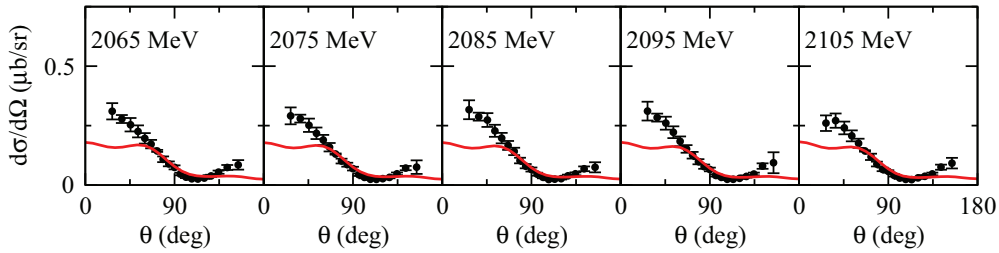

FIG. 38. (Color online) $d\sigma/d\Omega$ of $\gamma p \to K^+\Lambda$. (continued)

analyses. More detailed investigations of this issue are needed for advancing the field, but are beyond the scope of this paper.

B. $\gamma N \to N^*$ helicity amplitudes

To determine the $\gamma N \to N^*$ helicity amplitude, we first extract the residue $R_{\pi N,\gamma N}(M_R)$ of the $\gamma N \to \pi N$ amplitude at the resonance pole position M_R. By using Eq. (34) of the factorized form of $R_{M'B',MB}(M_R)$, the dressed vertex $\bar{\Gamma}_{\gamma N}(M_R)$ can be determined from the extracted $R_{\pi N,\gamma N}(M_R)$ and the $R_{\pi N,\pi N}(M_R)$ listed in Table VII. The $\gamma N \to N^*$ helicity amplitudes can then be calculated from the resulting $\bar{\Gamma}_{\gamma N}$ by using Eqs. (44)–(46).

Our results are listed in Table IX and are compared with those extracted by the Bonn-Gatchina group. We see that two results agree very well for the $\Delta(1211)$. For the N^* resonances with $L \leqslant 2$ and $\mathrm{Re}(M_R) < 1.7$ GeV, $N(1482)1/2^-(S_{11})$, $N(1656)1/2^-(S_{11})$, $N(1374)1/2^+(P_{11})$, $N(1500)3/2^-(D_{13})$, $N(1650)5/2^-(D_{15})$, $\Delta(1592)1/2^-(S_{31})$, and $\Delta(1872)7/2^+(F_{37})$, some qualitative agreements between the two analyses can be seen. However, it is difficult to compare the results for other resonance states. Here we note that the phase of $\gamma N \to N^*$ chosen by different analysis groups can be different, as discussed in Ref. [51]. This adds other complications in comparing the results listed in Table IX. Our choice of the phase has been given below Eq. (42). We do not compare our results with those from Refs. [52,53], because their results are from the Breit-Wigner parametrization, which cannot be related model independently to the residues at resonance pole, as discussed in Ref. [9].

VII. SUMMARY AND FUTURE DEVELOPMENTS

We have extended the DCC model developed in Refs. [1–11] to include the $K\Lambda$ and $K\Sigma$ channels and have completed a combined analysis of the data of $\pi N, \gamma N \to \pi N, \eta N, K\Lambda, K\Sigma$ reactions. The pole positions and residues of nucleon resonances with masses below 2 GeV and total widths less than 400 MeV have been extracted. From the extracted residues, we have determined the $N^* \to \gamma N, \pi N, \eta N, K\Lambda, K\Sigma$ transition amplitudes at the resonance positions. How this information can be related to the results from the hadron models and lattice QCD calculations is an important challenge in advancing our understanding of the structure of the nucleon and its excited states. While some progress in this direction has been made [15,54] for the $\Delta(1232) \to \gamma N$ transitions, much more work is needed.

The N^* masses extracted from our analysis, PDG, Jülich analysis, and Bonn-Gatchina analysis agree well only in the low-mass region. In the higher mass region the differences among four results are rather large. This could be mainly attributed to the fact that in the high $W \gtrsim 1.7$ GeV region, the available data of πN and γN reactions are far from complete to determine the partial-wave-amplitudes model independently. The difficulties in extracting the partial-wave-amplitudes model independently from the data, even when they are complete, have been investigated in Refs. [44,45,55,56]. Of course, the differences in the analysis methods and the data included in each analysis could also lead to large disagreements, as discussed in Sec. VI. It is necessary to clarify the situation.

The extracted residues of $\pi N \to \pi N$ partial-wave amplitudes are compared with Bonn-Gatchina analysis and Jülich analysis. Except for the well-established $\Delta(1232)$ resonance, the three analyses agree only qualitatively even for the cases that their pole positions are close. A similar situation is also found in comparing the extracted $N^* \to \gamma N$ helicity amplitudes with those from the Bonn-Gatchina analysis. This is perhaps attributable to the fact that the residues are more sensitive to the model or parametrization used in the analyses. It is necessary to clarify this issue for advancing the field.

To improve our analysis in the higher mass region, we need to include the data of $\pi N, \gamma N \to \pi\pi N$ reactions that dominate the πN and γN reaction cross sections at $W \gtrsim 1.6$ GeV. To proceed, we need detailed data for these two processes. For $\gamma N \to \pi\pi N$, the precise data of invariant mass distributions and some polarization observables are becoming available from facilities such as JLab, Mainz, Bonn, SPring-8, and ELPH at Tohoku University. For $\pi N \to \pi\pi N$, however, what is available is only the old data of the total cross sections with rather large uncertainties and very limited invariant mass distributions in the energy region above $W = 1.6$ GeV [6,24]. The situation can be improved greatly when the data from the new experiments on $\pi N \to \pi\pi N$ reactions at J-PARC [48] become available in the near future. To pin down the reaction mechanisms associated with the $\pi\Delta$, ρN, and σN channels, the Dalitz plot data of the $\pi\pi N$ distributions will be desirable. The importance of fitting the Dalitz plot data has been illustrated recently in Refs. [57,58] for the three-pion decays of heavy mesons. We also need to extend the analysis to include the ωN channel which has significant contributions to the πN and γN reaction cross sections at $W \gtrsim 1.7$ GeV. It will be useful if more extensive data of $\pi N \to \omega N$ can also be obtained at J-PARC.

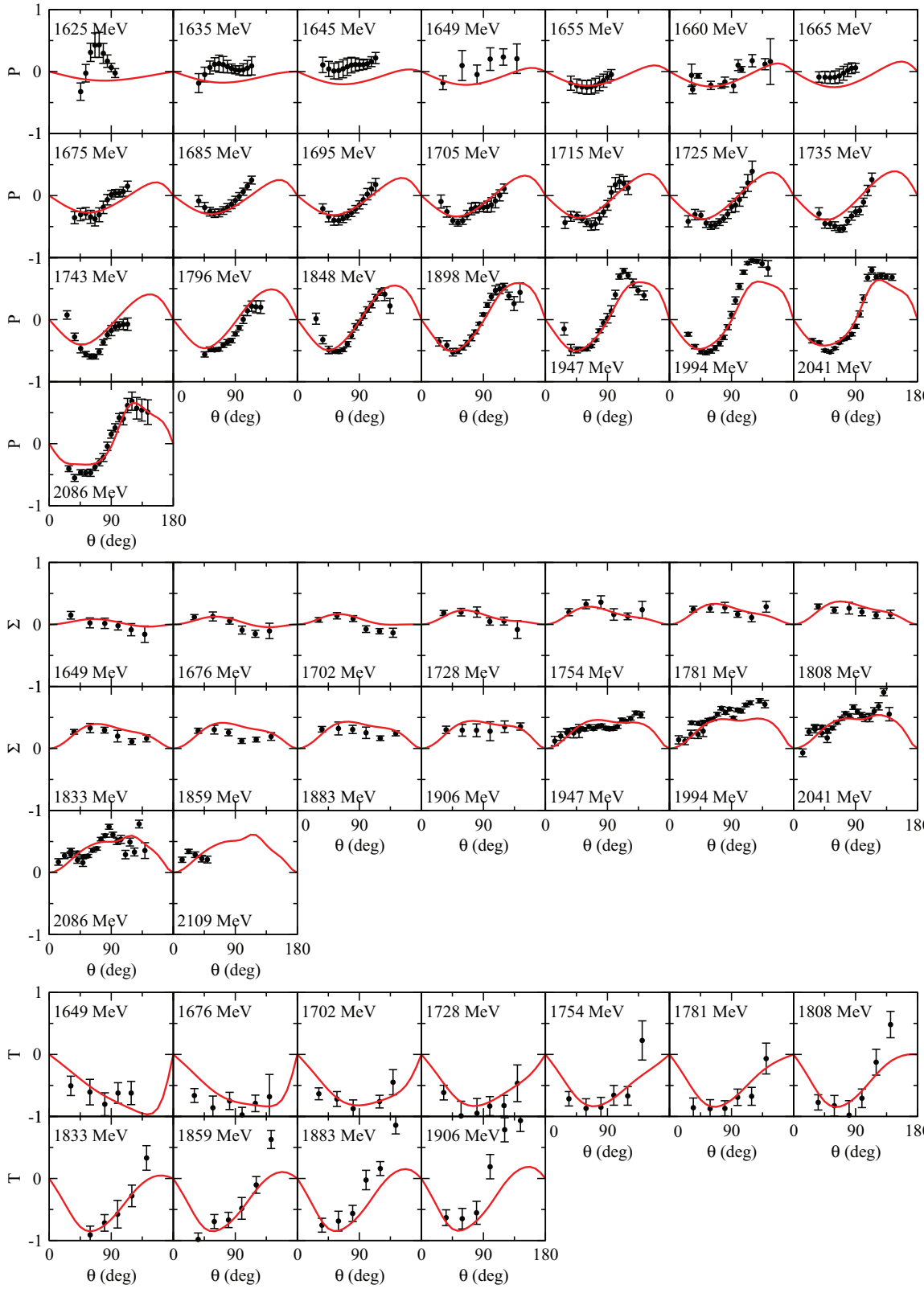

FIG. 39. (Color online) P, Σ, and T of $\gamma p \to K^+\Lambda$.

Our DCC model developed in this work can be readily applied to the electron- and neutrino-induced meson production reactions. The application to the electroproduction reactions, which corresponds to the extension of our early analysis of $p(e, e'\pi)N$ [4], is crucial for determining the Q^2 dependence of N-N^* electromagnetic transition form factors. This analysis

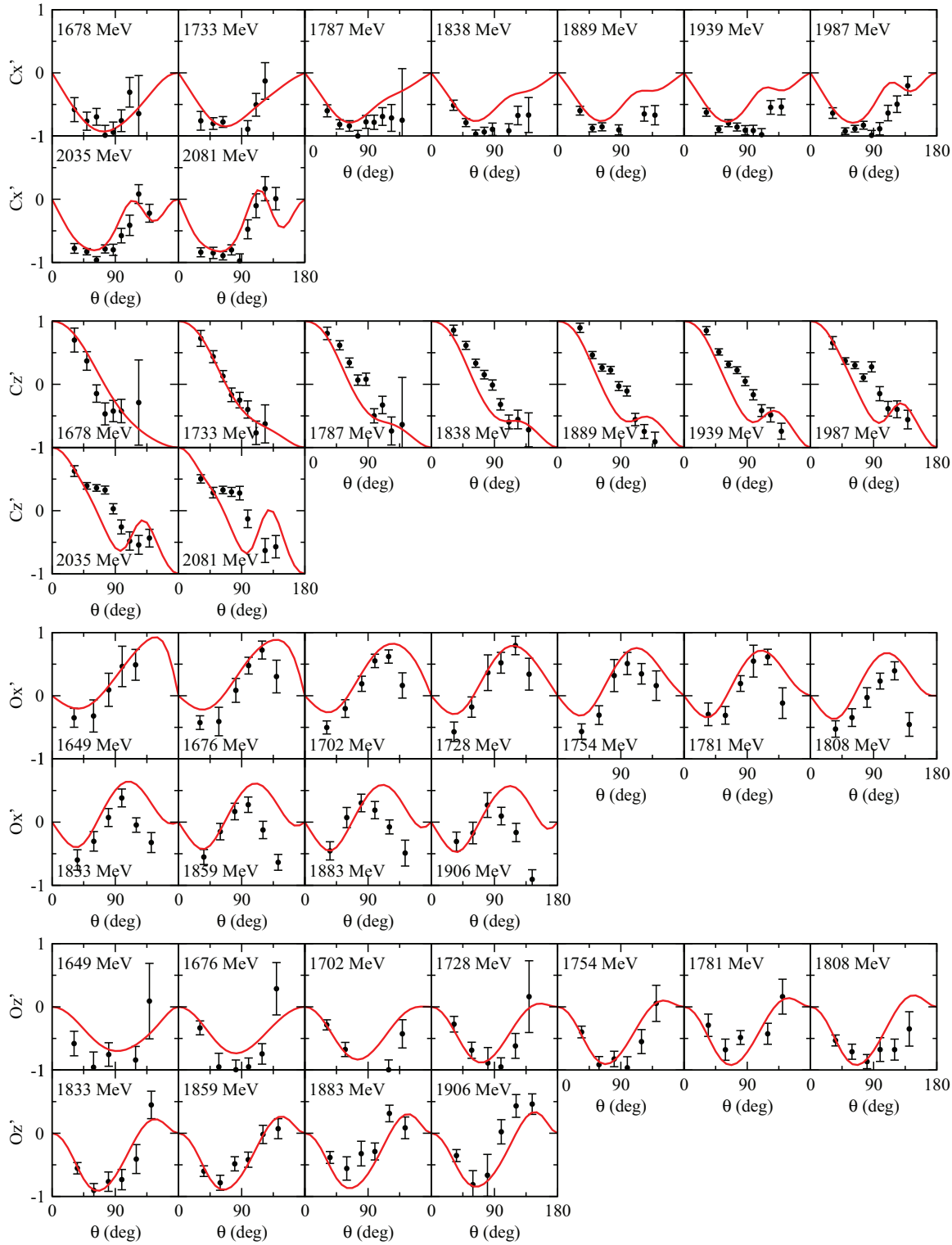

FIG. 40. (Color online) $C_{x'}$, $C_{z'}$, $O_{x'}$, and $O_{z'}$ of $\gamma p \to K^+\Lambda$.

is a key to understanding the quark-gluon substructure of the N^* states [59] and will be closely related to the N^* program at JLab after the 12-GeV upgrade [60]. Also, precise knowledge of the neutrino-nucleon/nucleus reactions in the GeV-energy region is expected to be very important for determining the leptonic CP-phase and neutrino-mass hierarchy from the neutrino-oscillation measurements through the accelerator and atmospheric experiments [61]. By following the procedure of Refs. [62,63], the DCC model presented in this work can be extended straightforwardly to describe the neutrino-induced reactions in the nucleon resonance region. A first attempt to study the neutrino-induced reactions within the current DCC

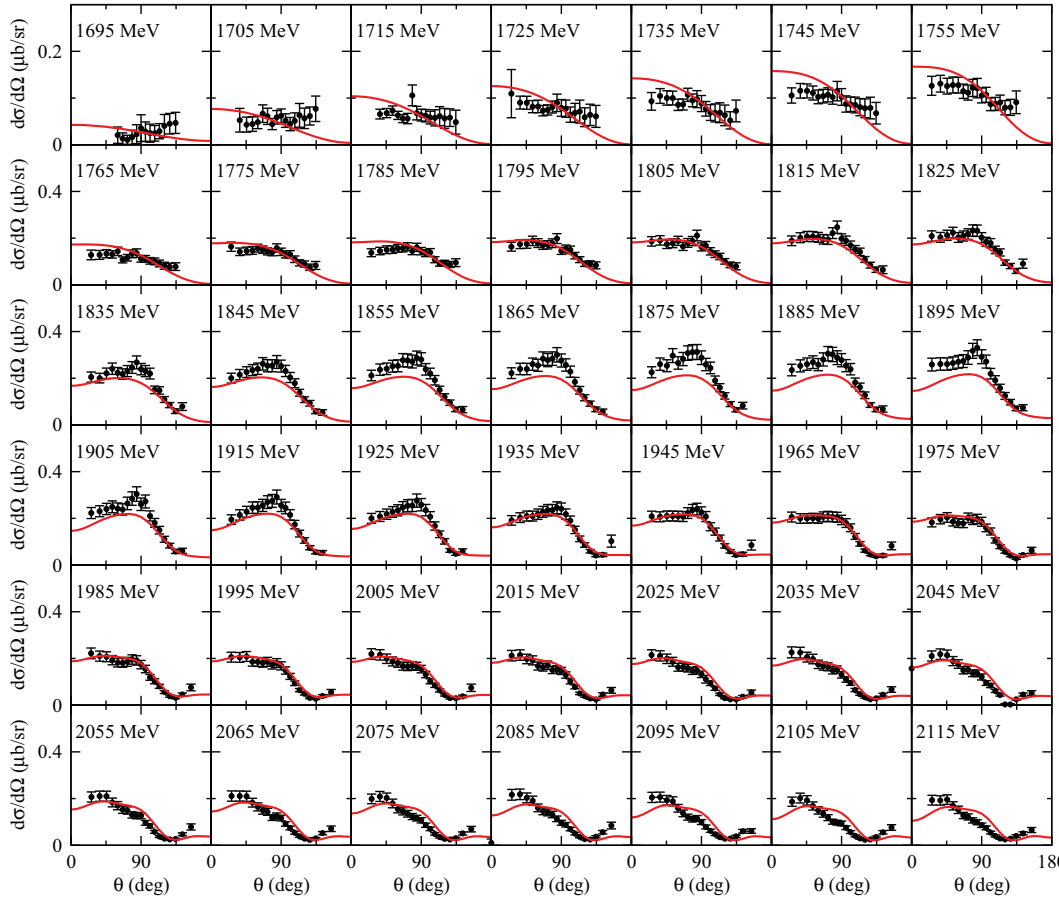

FIG. 41. (Color online) $d\sigma/d\Omega$ of $\gamma p \to K^+\Sigma^0$.

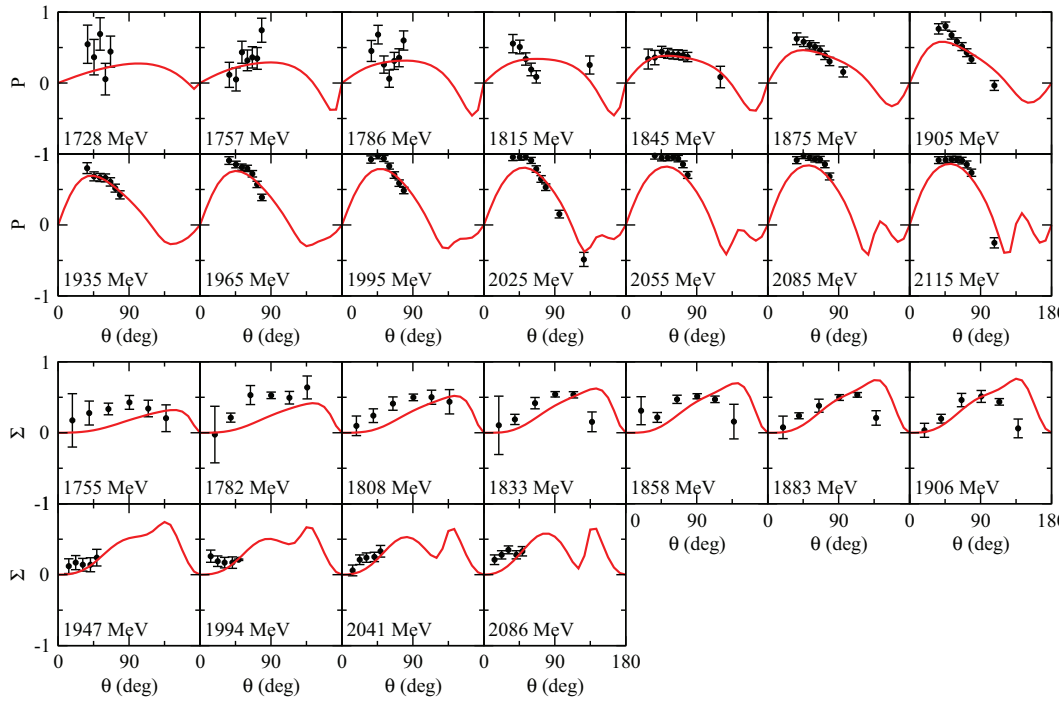

FIG. 42. (Color online) P and Σ of $\gamma p \to K^+\Sigma^0$.

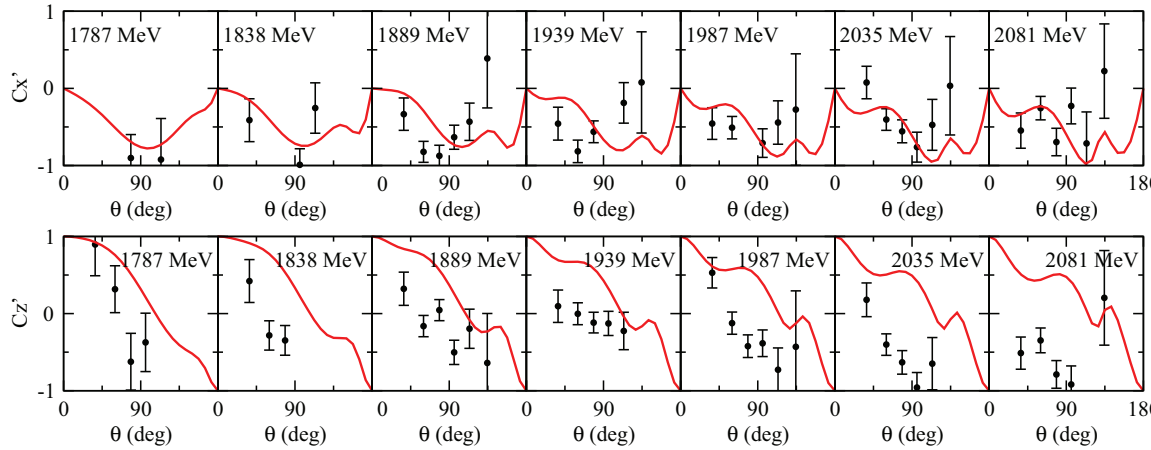

FIG. 43. (Color online) $C_{x'}$ and $C_{z'}$ of $\gamma p \to K^+\Sigma^0$.

model has been done in Ref. [64]. A further extensive study of the neutrino-induced reactions is ongoing and will be presented elsewhere.

ACKNOWLEDGMENTS

The authors thank J. Durand, B. Juliá-Díaz, A. Matsuyama, B. Saghai, L. C. Smith, N. Suzuki, and K. Tsushima for their collaborations at EBAC, and would also like to thank A. W. Thomas for his strong support and his many constructive discussions. We thank the support from JLab to the development of the first stage of this analysis as reported in Ref. [65]. This work was supported by the JSPS KAKENHI Grant No. 25800149 (H.K.) and No. 24540273 (T.S.), and by the U.S. Department of Energy, Office of Nuclear Physics Division, under Contract No. DE-AC02-06CH11357. H.K. acknowledges the support of the HPCI Strategic Program (Field 5 "The Origin of Matter and the Universe") of Ministry of Education, Culture, Sports, Science and Technology (MEXT) of Japan. S.X.N. is the Yukawa Fellow and his work is supported in part by Yukawa Memorial Foundation, the Yukawa International Program for Quark-hadron Sciences (YIPQS), and by Grants-in-Aid for the global COE program "The Next Generation of Physics, Spun from Universality and Emergence" from MEXT. This research used resources of the National Energy Research Scientific Computing Center, which is supported by the Office of Science of the U.S. Department of Energy under Contract No. DE-AC02-05CH11231, and resources provided on "Fusion," a 320-node computing cluster operated by the Laboratory Computing Resource Center at Argonne National Laboratory.

APPENDIX A: SELF-ENERGIES IN MESON-BARYON GREEN'S FUNCTIONS

In this appendix, we give an explicit expression of the self-energy $\Sigma_{MB}(k;W)$ appearing in the meson-baryon Green's function [Eq. (6)] for the unstable channels $MB = \pi\Delta, \rho N, \sigma N$.

As for the $\pi\Delta$ and ρN channels, the self-energies are explicitly given by

$$\Sigma_{\pi\Delta}(k;W) = \frac{m_\Delta}{E_\Delta(k)} \int_{C_3} q^2 dq \frac{M_{\pi N}(q)}{\left[M^2_{\pi N}(q)+k^2\right]^{1/2}} \times \frac{|f_{\Delta\to\pi N}(q)|^2}{W - E_\pi(k) - \left[M^2_{\pi N}(q)+k^2\right]^{1/2} + i\epsilon}, \tag{A1}$$

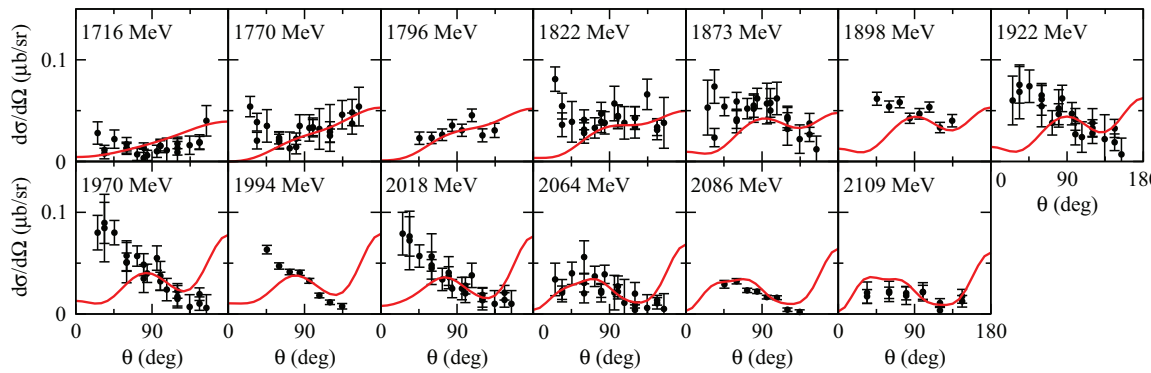

FIG. 44. (Color online) $d\sigma/d\Omega$ of $\gamma p \to K^0\Sigma^+$.

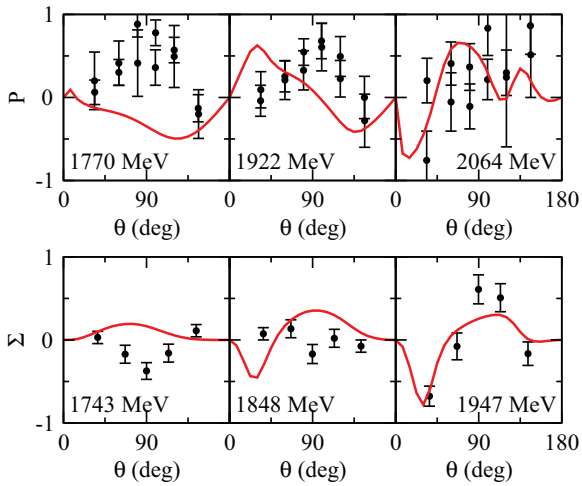

FIG. 45. (Color online) P and Σ of $\gamma p \to K^0\Sigma^+$.

$$\Sigma_{\rho N}(k;W) = \frac{m_\rho}{E_\rho(k)} \int_{C_3} q^2 dq \frac{M_{\pi\pi}(q)}{\left[M^2_{\pi\pi}(q)+k^2\right]^{1/2}} \times \frac{|f_{\rho\to\pi\pi}(q)|^2}{W - E_N(k) - \left[M^2_{\pi\pi}(q)+k^2\right]^{1/2} + i\epsilon}, \tag{A2}$$

where $m_\Delta = 1280\,\text{MeV}$, $m_\rho = 812\,\text{MeV}$, $M_{\pi N}(q) = E_\pi(q) + E_N(q)$, and $M_{\pi\pi}(q) = E_\pi(q) + E_\pi(q)$. The form factors $f_{\Delta\to\pi N}(q)$ and $f_{\rho\to\pi\pi}(q)$ are for describing the $\Delta \to \pi N$ and $\rho \to \pi\pi$ decays in the Δ and ρ rest frames, respectively. Those are parametrized as [2,66]

$$f_{\Delta\to\pi N}(q) = -i \frac{(0.98)}{[2(m_N+m_\pi)]^{1/2}} \left(\frac{q}{m_\pi}\right) \times \left(\frac{1}{1+[q/(358\text{MeV})]^2}\right)^2, \tag{A3}$$

$$f_{\rho\to\pi\pi}(q) = \frac{(0.6684)}{\sqrt{m_\pi}} \left(\frac{q}{(461\text{MeV})}\right) \times \left(\frac{1}{1+[q/(461\text{MeV})]^2}\right)^2. \tag{A4}$$

To construct the σ self-energy in the σN Green's function, $\Sigma_{\sigma N}(k;W)$, we first consider a $\pi\pi$ scattering model for the isospin $I = 0$ and s wave, described by the following separable potential in the $\pi\pi$ center-of-mass system:

$$v(p', p; E) = g(p') \frac{1}{E - m_\sigma + i\varepsilon} g(p) + h_0 h(p') h(p). \tag{A5}$$

Here p and p' are the magnitude of the initial and final momentum, E is the total scattering energy in the $\pi\pi$ system, and the form factors are parametrized as

$$g(p) = \frac{g_0}{\sqrt{m_\pi}} \frac{1}{1+(cp)^2}, \tag{A6}$$

$$h(p) = \frac{1}{m_\pi} \frac{1}{1+(dp)^2}. \tag{A7}$$

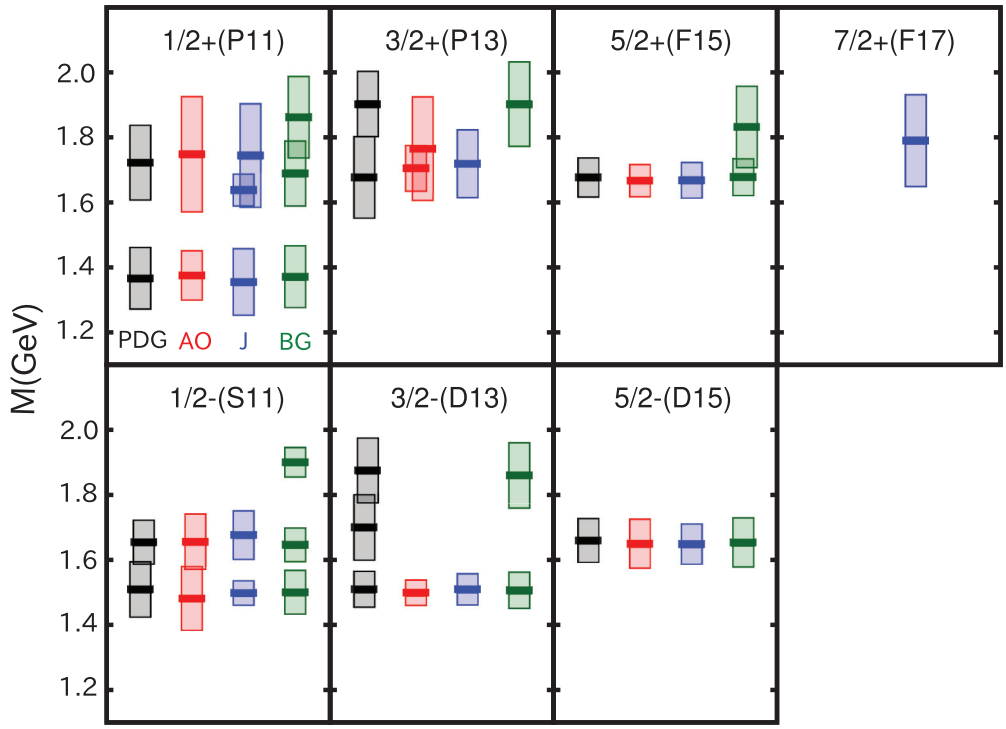

FIG. 46. (Color online) N^* spectrum with the isospin $I = 1/2$ determined by ANL-Osaka (AO) collaboration. For each N^* state, $\text{Re}(M_R)$ together with the $\text{Re}(M_R) \pm \text{Im}(M_R)$ band is plotted. The results are compared with four- and three-star states listed by the PDG [50], as well as the results from Jülich (J) (model A in Ref. [20]) and Bonn-Gatchina (BG) [23] groups. The spin and parity of states are denoted as J^P with $P = \pm$ and the associated πN partial wave.

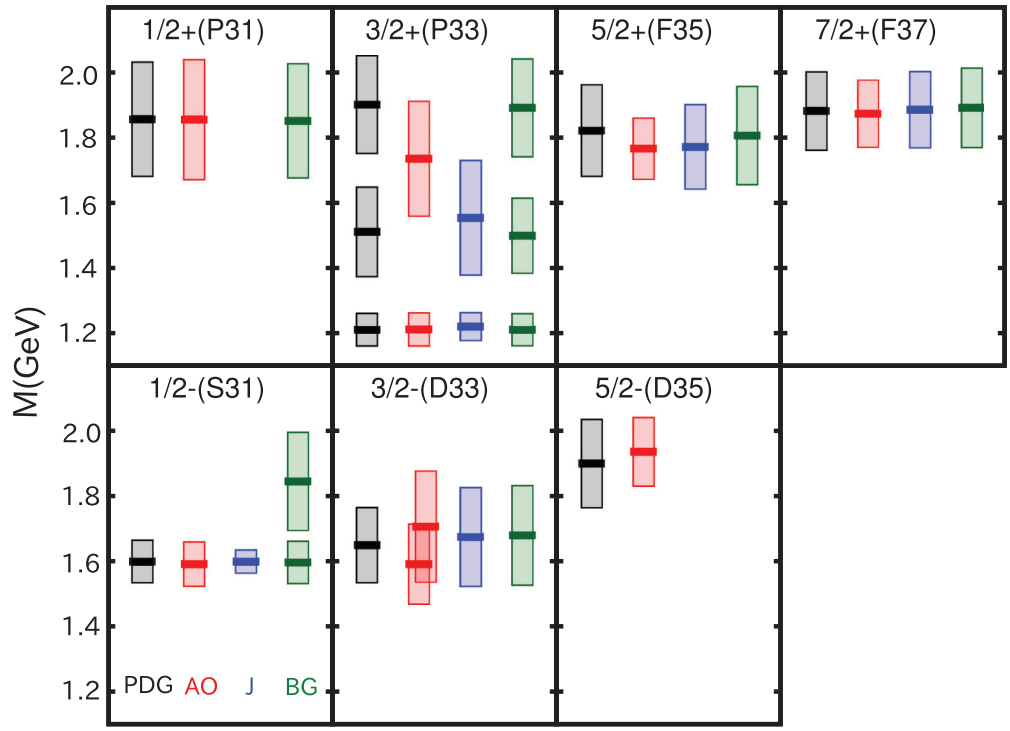

FIG. 47. (Color online) N^* spectrum with the isospin $I = 3/2$ determined by ANL-Osaka (AO) collaboration. For each N^* state, $\mathrm{Re}(M_R)$ together with the $\mathrm{Re}(M_R) \pm \mathrm{Im}(M_R)$ band is plotted. The results are compared with four- and three-star states listed by the PDG [50], as well as the results from Jülich (J) (model A in Ref. [20]) and Bonn-Gatchina (BG) [23] groups. The spin and parity of states are denoted as J^P with $P = \pm$ and the associated πN partial wave.

With this potential, one can solve the Lippmann-Schwinger equation to obtain the $\pi\pi$ scattering amplitude T. The solution is expressed as

$$T = t + t^R, \tag{A8}$$

where t is the "nonresonant" part of the amplitude given by

$$t(p', p; E) = h(p')\tau(E)h(p), \tag{A9}$$

$$\tau(E) = \frac{h_0}{1 - h_0\langle hG_{\pi\pi}h\rangle(E)}, \tag{A10}$$

$$\langle hG_{\pi\pi}h\rangle(E) = \int dqq^2 h(q)\frac{1}{E - M_{\pi\pi}(q) + i\varepsilon}h(q), \tag{A11}$$

while t_R the "resonant" part is given by

$$t^R(p', p; E) = \frac{\bar{\Gamma}_{\sigma\to\pi\pi}(p'; E)\bar{\Gamma}_{\pi\pi\to\sigma}(p; E)}{E - m_\sigma - \Sigma_\sigma(E)}. \tag{A12}$$

The σ self-energy $\Sigma_\sigma(E)$ and the dressed $\sigma \to \pi\pi$ vertex $\bar{\Gamma}_{\sigma\to\pi\pi}(p'; E)$ are then given by

$$\Sigma_\sigma(E) = \langle gG_{\pi\pi}g\rangle(E) + \tau(E)[\langle gG_{\pi\pi}h\rangle(E)]^2, \tag{A13}$$

$$\bar{\Gamma}_{\sigma\to\pi\pi}(p'; E) = g(p') + h(p')\tau(E)\langle hG_{\pi\pi}g\rangle(E), \tag{A14}$$

and $\bar{\Gamma}_{\pi\pi\to\sigma}(p; E) = \bar{\Gamma}_{\sigma\to\pi\pi}(p; E)$. The parameters in Eqs. (A5)–(A7) are determined by fitting the phase shift of the $I = 0$ and s-wave $\pi\pi$ scattering up to $E = 1$ GeV, and the resulting values are $m_\sigma^0 = 700.0$ MeV, $g_0 = 1.638$, $h_0 = 0.556$, $c = 1.02$ fm, and $d = 0.514$ fm.

With the above $\pi\pi$ model, the σ self-energy in the σN Green's function, $\Sigma_{\sigma N}(k; W)$ in Eq. (6), is obtained by

$$\Sigma_{\sigma N}(k; W) = \langle gG_{\pi\pi}g\rangle(k; W) + \tau(k; W)[\langle gG_{\pi\pi}h\rangle(k; W)]^2, \tag{A15}$$

with

$$\tau(k; W) = \frac{h_0}{1 - h_0\langle hG_{\pi\pi}h\rangle(k; W)}, \tag{A16}$$

$$\langle hG_{\pi\pi}h\rangle(k; W) = \int_{C_3} dqq^2 \frac{M_{\pi\pi}(q)}{\left[M_{\pi\pi}^2(q) + k^2\right]^{1/2}} \times \frac{h(q)^2}{W - E_N(k) - \left[M_{\pi\pi}^2(q) + k^2\right]^{1/2} + i\varepsilon}, \tag{A17}$$

$$\langle gG_{\pi\pi}g\rangle(k; W) = \frac{m_\sigma}{E_\sigma(k)}\int_{C_3} dqq^2 \frac{M_{\pi\pi}(q)}{\left[M_{\pi\pi}^2(q) + k^2\right]^{1/2}} \times \frac{g(q)^2}{W - E_N(k) - \left[M_{\pi\pi}^2(q) + k^2\right]^{1/2} + i\varepsilon}, \tag{A18}$$

$$\langle gG_{\pi\pi}h\rangle(k; W) = \sqrt{\frac{m_\sigma}{E_\sigma(k)}}\int_{C_3} dqq^2 \frac{M_{\pi\pi}(q)}{\left[M_{\pi\pi}^2(q) + k^2\right]^{1/2}} \times \frac{g(q)h(q)}{W - E_N(k) - \left[M_{\pi\pi}^2(q) + k^2\right]^{1/2} + i\varepsilon}. \tag{A19}$$

TABLE VI. N^* pole mass M_R and πN elasticity η_e extracted in this work. M_R is listed as [Re(M_R), −Im(M_R)] in units of MeV. As a reference, we also list the PDG values of the N^* states for which either four- or three-star status is assigned [50]. The N^* states for which the asterisk (*) is marked locate in the complex energy plane slightly off the closest sheet to the physical real energy axis, yet are still expected to visibly affect the physical observables.

	$J^P(L_{2I2J})$	M_R	M_R (PDG)	η_e (%)	η_e (PDG) (%)
N-baryons					
	$1/2^-(S_{11})$	(1482, 98)*	(1490–1530, 45–125)	64	35–55
		(1656, 85)	(1640–1670, 50–85)	62	50–90
	$1/2^+(P_{11})$	(1374, 76)	(1350–1380, 80–110)	48	55–75
		(1746, 177)	(1670–1770, 40–190)	11	5–20
	$3/2^+(P_{13})$	(1703, 70)	(1660–1690, 75–200)	11	9–14
		(1763, 159)	(1870–1930, 70–150)	18	∼10
	$3/2^-(D_{13})$	(1501, 39)	(1505–1515, 52–60)	67	55–65
		(1702, 141)*	(1650–1750, 50–150)	1	7–17
			(1800–1950, 75–125)		2–22
	$5/2^-(D_{15})$	(1650, 75)	(1655–1665, 62–75)	37	35–45
	$5/2^+(F_{15})$	(1665, 49)	(1665–1680, 55–68)	69	65–70
Δ-baryons					
	$1/2^-(S_{31})$	(1592, 68)	(1590–1610, 60–70)	29	20–30
		(1702, 193)*		10	
	$1/2^+(P_{31})$	(1854, 184)	(1830–1880, 100–250)	12	15–30
	$3/2^+(P_{33})$	(1211, 51)	(1209–1211, 49–51)	105	100
		(1734, 176)	(1460–1560, 100–175)	5	10–25
			(1850–1950, 100–200)		5–20
	$3/2^-(D_{33})$	(1592, 122)	(1620–1680, 80–150)	15	10–20
		(1707, 170)		7	
	$5/2^-(D_{35})$	(1936, 105)	(1840–1960, 88–180)	2	5–15
	$5/2^+(F_{35})$	(1765, 94)	(1805–1835, 132–150)	12	9–15
	$7/2^+(F_{37})$	(1872, 103)	(1870–1890, 110–130)	45	35–45

TABLE VII. Residues for $\pi N \to N^* \to MB$ amplitudes ($R_{MB,\pi N}$) at the N^* resonance pole position. The listed values of $R_{MB,\pi N}$ are in units of MeV. Each resonance is specified by its quantum numbers and the real part of the pole mass Re(M_R).

Particle $J^P(L_{2I2J})$	$R_{\pi N,\pi N}$		$R_{\eta N,\pi N}$		$R_{K\Lambda,\pi N}$		$R_{K\Sigma,\pi N}$	
	Re	Im	Re	Im	Re	Im	Re	Im
$N(1482)1/2^-(S_{11})$	45	−43	–	–	–	–	–	–
$N(1656)1/2^-(S_{11})$	18	−49	−31	−21	−2	−10	–	–
$N(1374)1/2^+(P_{11})$	13	−34	–	–	–	–	–	–
$N(1746)1/2^+(P_{11})$	20	1	9	−9	4	−10	2	12
$N(1703)3/2^+(P_{13})$	8	−0	1	−0	0	−0	0	0
$N(1763)3/2^+(P_{13})$	−8	−28	−1	0	0	−8	1	−5
$N(1500)3/2^-(D_{13})$	25	−5	−0	−1	–	–	–	–
$N(1702)3/2^-(D_{13})$	−0	2	−1	0	−1	1	−0	−1
$N(1650)5/2^-(D_{15})$	24	−15	−6	5	0	−0	–	–
$N(1665)5/2^+(F_{15})$	32	−12	−1	1	0	−0	–	–
$\Delta(1592)1/2^-(S_{31})$	−7	−18	–	–	–	–	–	–
$\Delta(1702)1/2^-(S_{31})$	8	18	–	–	–	–	13	−9
$\Delta(1854)1/2^+(P_{31})$	−12	−19	–	–	–	–	−18	−30
$\Delta(1211)3/2^+(P_{33})$	37	−39	–	–	–	–	–	–
$\Delta(1734)3/2^+(P_{33})$	−4	−7	–	–	–	–	−0	−1
$\Delta(1592)3/2^-(D_{33})$	8	−16	–	–	–	–	–	–
$\Delta(1707)3/2^+(D_{33})$	8	9	–	–	–	–	2	−3
$\Delta(1936)5/2^-(D_{35})$	2	−1	–	–	–	–	2	−3
$\Delta(1765)5/2^+(F_{35})$	5	−10	–	–	–	–	−1	−1
$\Delta(1872)7/2^+(F_{37})$	38	−27	–	–	–	–	0	−1

TABLE VIII. Comparison of residue $R_{\pi N,\pi N} = Re^{i\phi}$ of $\pi N \to \pi N$ amplitude between existing multichannel analyses.

Particle $J^P(L_{2I2J})$	ANL-Osaka		Bonn-Gatchina [23]		Jülich (model A) [20]	
	R	ϕ	R	ϕ	R	ϕ
$N(1482)1/2^-(S_{11})$	63	−44	31 ± 4	$-(29 \pm 5)$	16	−36
$N(1656)1/2^-(S_{11})$	53	−70	24 ± 3	$-(75 \pm 12)$	46	−42
$N(1374)1/2^+(P_{11})$	37	−69	48 ± 3	$-(78 \pm 4)$	58	−104
$N(1746)1/2^+(P_{11})$	20	3	6 ± 4	(120 ± 70)	4	−30
$N(1703)3/2^+(P_{13})$	8	−3	22 ± 8	$-(115 \pm 30)$	7	−73
$N(1763)3/2^+(P_{13})$	29	−106	–	–	–	–
$N(1500)3/2^-(D_{13})$	26	−11	36 ± 3	$-(14 \pm 3)$	32	−11
$N(1702)3/2^-(D_{13})$	2	104	50 ± 40	$-(100 \pm 40)$	–	–
$N(1650)5/2^-(D_{15})$	28	−31	28 ± 1	$-(26 \pm 4)$	24	−19
$N(1665)5/2^+(F_{15})$	34	−20	43 ± 4	$-(2 \pm 10)$	36	−24
$\Delta(1592)1/2^-(S_{31})$	20	−111	18 ± 2	$-(100 \pm 5)$	17	−106
$\Delta(1702)1/2^-(S_{31})$	19	65	10 ± 3	$-(125 \pm 20)$	–	–
$\Delta(1854)1/2^+(P_{31})$	23	−123	24 ± 6	$-(145 \pm 30)$	54	−140
$\Delta(1211)3/2^+(P_{33})$	53	−47	51.6 ± 0.6	$-(46 \pm 1)$	44	−35
$\Delta(1734)3/2^+(P_{33})$	8	−118	11 ± 6	$-(160 \pm 33)$	20	−158
$\Delta(1592)3/2^-(D_{33})$	18	−62	–	–	–	–
$\Delta(1707)3/2^-(D_{33})$	11	49	42 ± 7	$-(3 \pm 15)$	24	−9
$\Delta(1936)5/2^-(D_{35})$	2	−32	–	–	18	−159
$\Delta(1765)5/2^+(F_{35})$	11	−62	20 ± 2	$-(44 \pm 5)$	17	−59
$\Delta(1872)7/2^+(F_{37})$	46	−35	58 ± 2	$-(24 \pm 3)$	58	−25

The momentum integral path C_3 is appropriately deformed when we perform the analytic continuation of the scattering amplitudes. With the self-energies defined above, the branch points of the $\pi\Delta$, ρN, and σN Green's functions are those as listed in Table I. Although two branch points are found in the σN Green's function, the second one at $(1032.3 - i247.7) + m_N$ MeV hardly affects the resonance properties shown in this work because of the large imaginary part.

TABLE IX. Helicity amplitudes for $\gamma p \to N^*$. The values are presented in units of 10^{-3} GeV$^{-1/2}$. As a comparison, we also list those from Bonn-Gatchina group [23].

Particle $J^P(L_{2I2J})$	ANL-Osaka				Bonn-Gatchina [23]			
	$A_{3/2}$		$A_{1/2}$		$A_{3/2}$		$A_{1/2}$	
	Re	Im	Re	Im	Re	Im	Re	Im
$N(1482)1/2^-(S_{11})$	–	–	159	24	–	–	115.1	14.1
$N(1656)1/2^-(S_{11})$	–	–	29	−28	–	–	32.6	−5.2
$N(1374)1/2^+(P_{11})$	–	–	49	−10	–	–	−34.7	27.1
$N(1746)1/2^+(P_{11})$	–	–	−24	83	–	–	54.2	−9.6
$N(1703)3/2^+(P_{13})$	−70	8	234	8	63.4	135.9	110.0	0.0
$N(1763)3/2^+(P_{13})$	−44	1	126	−72	–	–	–	–
$N(1500)3/2^-(D_{13})$	−93	−11	38	2	131.9	4.6	−21.0	0.0
$N(1702)3/2^-(D_{13})$	−40	36	−11	−23	−37	0.0	3.8	43.8
$N(1650)5/2^-(D_{15})$	30	−13	5	−2	24.6	−8.5	23.1	−6.6
$N(1665)5/2^+(F_{15})$	−38	−2	53	−5	133.9	−4.7	−11.8	5.5
$\Delta(1592)1/2^-(S_{31})$	–	–	113	−2	–	–	51.4	−8.1
$\Delta(1702)1/2^-(S_{31})$	–	–	35	3	–	–	29.5	51.1
$\Delta(1854)1/2^+(P_{31})$	–	–	−51	9	–	–	17.6	14.8
$\Delta(1211)3/2^+(P_{33})$	−257	12	−129	34	−250.9	39.7	−123.9	42.6
$\Delta(1734)3/2^+(P_{33})$	−18	−135	−23	−68	−39.6	10.6	−34.1	40.6
$\Delta(1592)3/2^-(D_{33})$	−89	−76	−123	−38	–	–	–	–
$\Delta(1707)3/2^-(D_{33})$	32	−121	20	−56	120.2	120.2	109.3	130.2
$\Delta(1936)5/2^-(D_{35})$	34	−9	50	−19	–	–	–	–
$\Delta(1765)5/2^+(F_{35})$	0	−18	−1	−8	−50.0	0.0	23.0	−9.8
$\Delta(1872)7/2^+(F_{37})$	−76	−2	−61	10	−95.3	11.7	−71.5	8.8

APPENDIX B: MODEL LAGRANGIAN

In this appendix, we present a set of Lagrangians for deriving the meson-exchange potentials $v_{M'B',MB}$ and $v_{M'B',\gamma N}$. The details of the $Z^{(E)}_{M'B',MB}(k',k;W)$ term in Eq. (7) can be found in Ref. [1] and is not shown here.

It is necessary to define notations associated with isospin quantum numbers. For the isospin $I = 1/2$ hadrons, we use the following field operators:

$$N = \begin{pmatrix} p \\ n \end{pmatrix}, \tag{B1}$$

$$\Xi = \begin{pmatrix} \Xi^- \\ \Xi^0 \end{pmatrix}, \tag{B2}$$

$$K = \begin{pmatrix} K^+ \\ K^0 \end{pmatrix}, \tag{B3}$$

$$K_c = \begin{pmatrix} \bar{K}^0 \\ -K^- \end{pmatrix}. \tag{B4}$$

For the isovector ($I = 1$) pion field operator, we use the usual notations,

$$\vec{\pi} = (\pi^1, \pi^2, \pi^3), \tag{B5}$$

with the isospin triplet

$$\pi = \begin{pmatrix} \pi^+ \\ \pi^0 \\ \pi^- \end{pmatrix}, \tag{B6}$$

where

$$\pi^\pm = \mp\frac{1}{\sqrt{2}}(\pi^1 \pm i\pi^2), \tag{B7}$$

$$\pi^0 = \pi^3. \tag{B8}$$

The same definition is also applied to other $I = 1$ hadron operators. For Δ with $I = 3/2$, we define

$$\Delta = \begin{pmatrix} \Delta^{++} \\ \Delta^+ \\ \Delta^0 \\ \Delta^- \end{pmatrix}. \tag{B9}$$

For the doublet states, the isospin operator $\vec{\tau}$, with the spherical components $\tau^\pm = \mp(\tau_1 \pm i\tau_2)/\sqrt{2}$ and $\tau_0 = \tau_3$, is defined by the matrix elements

$$\langle s\, m_s|\tau_m|s\, m'_s\rangle = \langle s\, 1\, m'_s\, m|s\, m_s\rangle\langle s||\tau||s\rangle/\sqrt{2s+1}, \tag{B10}$$

where $\langle j_1\, j_2\, m_1\, m_2|J\, M\rangle$ is the usual Clebsch-Gordon coefficient, $m = \pm 1, 0$, and the reduced matrix element is $\langle\frac{1}{2}||\tau||\frac{1}{2}\rangle = \sqrt{6}$. The isospin operators $\vec{T}_\Delta$ for the $\Delta \to \Delta$ and $\vec{T}$ for the $N \to \Delta$ transitions are defined by

$$\langle j_\Delta m_s|T_{\Delta,m}|j_\Delta m'_s\rangle = \langle j_\Delta 1 m'_s m|j_\Delta m_s\rangle \times \langle j_\Delta||T_\Delta||j_\Delta\rangle/\sqrt{2j_\Delta+1}, \tag{B11}$$

$$\langle j m_s|T_m|j' m'_s\rangle = \langle j' 1 m'_s m|j m_s\rangle\langle j||T||j'\rangle/\sqrt{2j+1}, \tag{B12}$$

where $m = \pm 1, 0$ is the spherical component of $\vec{T}_\Delta$ and $\vec{T}$, $j_\Delta = 3/2$, j, $j' = 1/2$ or $3/2$, and the reduced matrix elements are

$$\left\langle\tfrac{3}{2}\middle||T_\Delta|\middle|\tfrac{3}{2}\right\rangle = \sqrt{15}, \tag{B13}$$

$$\left\langle\tfrac{3}{2}\middle||T|\middle|\tfrac{1}{2}\right\rangle = -\left\langle\tfrac{1}{2}\middle||T|\middle|\tfrac{3}{2}\right\rangle = 2. \tag{B14}$$

With the above definitions of isospin components, we list all Lagrangian used in our calculations. We follow the conventions of Bjoken and Drell [67] in defining the metric tensor $g_{\mu\nu}$ and the Dirac matrices γ_μ and γ_5. Also, we set $\epsilon^{0123} = +1$.

1. Hadronic interactions

a. PBB' interaction

The interaction Lagrangian between a pseudoscalar-octet meson (P) and spin-$\frac{1}{2}$ octet baryons (B, B') is given by

$$L_{PBB'} = -\frac{f_{PBB'}}{m_P}\bar{B}\gamma_\mu\gamma_5 B'\partial^\mu P \times L^{\rm iso}_{PBB'} + [\text{H.c. for } B \neq B']. \tag{B15}$$

Here $L^{\rm iso}_{PBB'}$ is the isospin structure of the interactions given by

$$L^{\rm iso}_{\pi NN} = (N^\dagger\vec{\tau}N)\cdot\vec{\pi}, \tag{B16}$$

$$L^{\rm iso}_{\pi\Xi\Xi} = (\Xi^\dagger\vec{\tau}\Xi)\cdot\vec{\pi}, \tag{B17}$$

$$L^{\rm iso}_{\pi\Lambda\Sigma} = \Lambda^\dagger(\vec{\Sigma}\cdot\vec{\pi}), \tag{B18}$$

$$L^{\rm iso}_{\pi\Sigma\Sigma} = i[\vec{\Sigma}^\dagger\times\vec{\Sigma}]\cdot\vec{\pi}, \tag{B19}$$

$$L^{\rm iso}_{K\Sigma N} = \vec{\Sigma}^\dagger\cdot(K^\dagger\vec{\tau}N), \tag{B20}$$

$$L^{\rm iso}_{K\Xi\Sigma} = (\Xi^\dagger\vec{\tau}K)\cdot\vec{\Sigma}, \tag{B21}$$

$$L^{\rm iso}_{K\Lambda N} = \Lambda^\dagger(K^\dagger N), \tag{B22}$$

$$L^{\rm iso}_{K\Xi\Lambda} = (\Xi^\dagger K_c)\Lambda, \tag{B23}$$

$$L^{\rm iso}_{\eta NN} = (N^\dagger N)\eta, \tag{B24}$$

$$L^{\rm iso}_{\eta\Xi\Xi} = (\Xi^\dagger\Xi)\eta, \tag{B25}$$

$$L^{\rm iso}_{\eta\Lambda\Lambda} = \Lambda^\dagger\Lambda\eta, \tag{B26}$$

$$L^{\rm iso}_{\eta\Sigma\Sigma} = (\vec{\Sigma}^\dagger\cdot\vec{\Sigma})\eta. \tag{B27}$$

The coupling constants of PBB' are fixed by the SU(3) relations and the πNN coupling constant:

$$g_{\pi\Xi\Xi} = (1-2\alpha)g_{\pi NN}, \tag{B28}$$

$$g_{\pi\Lambda\Sigma} = \frac{2}{\sqrt{3}}\alpha g_{\pi NN}, \tag{B29}$$

$$g_{\pi\Sigma\Sigma} = 2(-1+\alpha)g_{\pi NN}, \tag{B30}$$

$$g_{K\Sigma N} = (-1+2\alpha)g_{\pi NN}, \tag{B31}$$

$$g_{K\Xi\Sigma} = (-1)g_{\pi NN}, \tag{B32}$$

$$g_{K\Lambda N} = \frac{1}{\sqrt{3}}(-3+2\alpha)g_{\pi NN}, \tag{B33}$$

$$g_{K\Xi\Lambda} = \frac{1}{\sqrt{3}}(+3-4\alpha)g_{\pi NN}, \tag{B34}$$

$$g_{\eta NN} = \frac{1}{\sqrt{3}}(+3-4\alpha)g_{\pi NN}, \tag{B35}$$

$$g_{\eta\Lambda\Lambda} = \frac{1}{\sqrt{3}}(-2\alpha)g_{\pi NN}, \tag{B36}$$

$$g_{\eta\Sigma\Sigma} = \frac{1}{\sqrt{3}}(+2\alpha)g_{\pi NN}, \tag{B37}$$

where $g_{PBB'} = f_{PBB'}/m_P$, $\alpha = 0.635$, and $f_{\pi NN} = \sqrt{4\pi \times 0.08}$. In this work, however, we do not follow the SU(3) relations (B31) and (B35) for the ηNN and $K\Sigma N$ couplings, but vary $f_{\eta NN}$ and $f_{K\Sigma N}$ freely in the fit.

b. VBB' interaction

The interaction Lagrangian between a vector-octet meson (V) and spin-$\frac{1}{2}$ octet baryons (B, B') is given by

$$L_{VBB'} = +g_{VBB'}\bar{B}\left[\vec{\not{V}} - \frac{\kappa_{VBB'}}{m_B + m_{B'}}\sigma_{\mu\nu}(\partial^\nu \vec{V}^\mu)\right]B' \times L^{\rm iso}_{VBB'} + [\text{H.c. for } B \neq B']. \tag{B38}$$

The isospin structure of the interactions ($L^{\rm iso}_{VBB'}$) involving ρ, K^*, K_c^*, and ω_8 is given by the replacement of $\pi \to \rho$, $K \to K^*$, $K_c \to K_c^*$, and $\eta \to \omega_8$ in Eqs. (B16)–(B27). Here ω_8 is the eighth component of the octet representation of the vector mesons. Assuming the ideal mixing, it is related to the physical ω and ϕ mesons as

$$\omega_8 = \frac{1}{\sqrt{3}}\omega - \sqrt{\frac{2}{3}}\phi. \tag{B39}$$

In this work, only $g_{\rho NN}$, $\kappa_{\rho NN}$, $g_{\omega NN}$, and $\kappa_{\omega NN}$ are free parameters for VBB' coupling constants determined by the global fit. As for the other VBB' interactions, $g_{VBB'}$ is fixed by the value of $g_{\rho NN}$ and the corresponding SU(3) relations to Eqs. (B28)–(B37) with the replacement of $\pi \to \rho$, $K \to K^*$, $K_c \to K_c^*$, and $\eta \to \omega_8$, while $\kappa_{VBB'}$ is fixed with $\kappa_{VBB'}/(m_B + m_{B'}) \equiv \kappa_{\rho NN}/(2m_N)$.

c. SBB' interaction

The interaction Lagrangian between a scalar meson (S) and spin-$\frac{1}{2}$ octet baryons (B, B') used in this work is

$$L_{SBB'} = +g_{SBB'}\bar{B}B'S \times L^{\rm iso}_{SBB'} + [\text{H.c. for } B \neq B']. \tag{B40}$$

The isospin structure of the interactions ($L^{\rm iso}_{SBB'}$) is given by

$$L^{\rm iso}_{\sigma NN} = (N^\dagger N)\sigma, \tag{B41}$$

$$L^{\rm iso}_{f_0 NN} = (N^\dagger N)f_0, \tag{B42}$$

$$L^{\rm iso}_{\kappa\Lambda N} = \Lambda^\dagger(\kappa^\dagger N), \tag{B43}$$

$$L^{\rm iso}_{\kappa\Sigma N} = \vec{\Sigma}^\dagger \cdot (\kappa^\dagger \vec{\tau} N). \tag{B44}$$

Other SBB' interactions are not considered in this work.

d. ABB' interaction

As for the interaction between a axial-vector meson (A) and spin-$\frac{1}{2}$ octet baryons (B, B'), we consider only a_1NN interaction given by

$$L_{a_1 NN} = +g_{a_1 NN}\bar{N}\gamma^\mu\gamma_5\vec{\tau}N \cdot \vec{a}_{1\mu}. \tag{B45}$$

e. $PVBB'$ and $VVBB'$ interaction

The following contact terms are also included in the calculation:

$$L_{\rho\pi NN} = +\frac{f_{\pi NN}}{m_\pi}g_{\rho NN}\bar{N}\gamma_\mu\gamma_5\vec{\tau}N \cdot \left[\vec{\rho}^\mu \times \vec{\pi}\right], \tag{B46}$$

$$L_{\rho\rho NN} = -\frac{\kappa_\rho g^2_{\rho NN}}{8m_N}\bar{N}\sigma^{\mu\nu}\vec{\tau}N \cdot \left[\vec{\rho}_\mu \times \vec{\rho}_\nu\right]. \tag{B47}$$

Note that these contact terms are derived from applying $[\partial^\mu \to \partial^\mu - g_{\rho NN}\vec{\rho}^\mu \times]$ to $L_{\pi NN}$ and $L_{\rho NN}$, respectively. However, in this work we replace $f_{\pi NN}g_{\rho NN}$ $[\kappa_\rho g^2_{\rho NN}/8]$ in Eq. (B46) [Eq. (B47)] with a new parameter $c_{\rho\pi NN}$ $[c_{\rho\rho NN}]$ and vary the new parameter in the fit.

f. PBD interaction

The interaction Lagrangian involving a pseudoscalar-octet meson (P), a spin-$\frac{1}{2}$ octet baryon (B), and a spin-$\frac{3}{2}$ decuplet baryon (D) is given by

$$L_{PBD} = -\frac{f_{PBD}}{m_P}\bar{B}D^\mu\partial_\mu P \times L^{\rm iso}_{PBD} + [\text{H.c. for } B \neq B']. \tag{B48}$$

The isospin structure of the interactions ($L^{\rm iso}_{PBD}$) is given by

$$L^{\rm iso}_{\pi N\Delta} = (N^\dagger \vec{T}\Delta) \cdot \vec{\pi}, \tag{B49}$$

$$L^{\rm iso}_{\pi\Lambda\Sigma^*} = \Lambda^\dagger(\vec{\Sigma}^* \cdot \vec{\pi}), \tag{B50}$$

$$L^{\rm iso}_{\pi\Sigma\Sigma^*} = i[\vec{\Sigma}^\dagger \times \vec{\Sigma}^*] \cdot \vec{\pi}, \tag{B51}$$

$$L^{\rm iso}_{KN\Sigma^*} = (N^\dagger\vec{\tau}K) \cdot \vec{\Sigma}^*. \tag{B52}$$

g. VBD interaction

As for the interaction involving a vector-octet meson (V), a spin-$\frac{1}{2}$ octet baryon (B), and a spin-$\frac{3}{2}$ decuplet baryon (D), we consider only $\rho N\Delta$ interaction:

$$L_{\rho N\Delta} = -i\frac{f_{\rho N\Delta}}{m_\rho}\bar{\Delta}^\mu\gamma^\nu\gamma_5[\partial_\mu\vec{\rho}_\nu - \partial_\nu\vec{\rho}_\mu] \cdot \vec{T}N + \text{H.c.} \tag{B53}$$

h. PDD' interaction

As for the interaction between a pseudoscalar-octet meson (P) and spin-$\frac{3}{2}$ decuplet baryons (D, D'), we consider only the $\pi\Delta\Delta$ interaction:

$$L_{\pi\Delta\Delta} = +\frac{f_{\pi\Delta\Delta}}{m_\pi}\bar{\Delta}_\mu\gamma^\nu\gamma_5\vec{T}_\Delta\Delta^\mu \cdot \partial_\nu\vec{\pi}. \tag{B54}$$

i. VDD' interaction

As for the interaction between a vector-octet meson (V) and spin-$\frac{3}{2}$ decuplet baryons (D, D'), we consider only the $\rho\Delta\Delta$

interaction:

$$L_{\rho\Delta\Delta} = +g_{\rho\Delta\Delta}\bar{\Delta}_\alpha\left[\vec{\rho} - \frac{\kappa_{\rho\Delta\Delta}}{2m_\Delta}\sigma_{\mu\nu}(\partial^\nu\vec{\rho}^\mu)\right]\cdot\vec{T}_\Delta\Delta^\alpha. \quad \text{(B55)}$$

j. VPP' interaction

The interaction Lagrangian between a vector-octet meson (V) and pseudoscalar-octet mesons (P, P') used in this work is given by

$$L_{\rho\pi\pi} = +g_{\rho\pi\pi}[\vec{\pi}\times\partial_\mu\vec{\pi}]\cdot\vec{\rho}^\mu, \quad \text{(B56)}$$

$$L_{\rho KK} = +ig_{\rho KK}(K^\dagger\vec{\tau}\partial_\mu K)\cdot\vec{\rho}^\mu + \text{H.c.}, \quad \text{(B57)}$$

$$L_{K^*K\pi} = +ig_{K^*K\pi}[(K^{*\mu\dagger}\vec{\tau}K)\cdot\partial_\mu\vec{\pi} - (K^{*\mu\dagger}\vec{\tau}\partial_\mu K)\cdot\vec{\pi}] + \text{H.c.}, \quad \text{(B58)}$$

$$L_{\omega_8KK} = +ig_{\omega_8KK}[K^\dagger(\partial_\mu K) - (\partial_\mu K^\dagger)K]\omega_8^\mu, \quad \text{(B59)}$$

$$L_{K^*K\eta} = +ig_{K^*K\eta}K^{*\mu\dagger}[K(\partial_\mu\eta) - (\partial_\mu K)\eta] + \text{H.c.} \quad \text{(B60)}$$

In this work, the coupling constant $g_{VPP'}$ is fixed by the SU(3) relation,

$$g_{\rho KK} = \frac{1}{2}g_{\rho\pi\pi}, \quad \text{(B61)}$$

$$g_{K^*K\pi} = \frac{1}{2}g_{\rho\pi\pi}, \quad \text{(B62)}$$

$$g_{\omega KK} = \frac{1}{\sqrt{3}}g_{\omega_8KK} = \frac{1}{2}g_{\rho\pi\pi}, \quad \text{(B63)}$$

$$g_{\phi KK} = -\sqrt{\frac{2}{3}}g_{\omega_8KK} = -\frac{1}{\sqrt{2}}g_{\rho\pi\pi}, \quad \text{(B64)}$$

$$g_{K*K\eta} = \frac{\sqrt{3}}{2}g_{\rho\pi\pi}, \quad \text{(B65)}$$

so that only $g_{\rho\pi\pi}$ is a free parameter for the VPP' couplings.

k. SPP' interaction

The interaction Lagrangian between a scalar meson (S) and pseudoscalar-octet mesons (P, P') used in this work is given by

$$L_{\sigma\pi\pi} = -\frac{g_{\sigma\pi\pi}}{2m_\pi}(\partial^\mu\vec{\pi})\cdot(\partial_\mu\vec{\pi})\sigma + \frac{\tilde{g}_{\sigma\pi\pi}m_\pi^2}{2f_\pi}\vec{\pi}\cdot\vec{\pi}\sigma, \quad \text{(B66)}$$

$$L_{f_0\pi\pi} = -\frac{g_{f_0\pi\pi}}{2m_\pi}(\partial^\mu\vec{\pi})\cdot(\partial_\mu\vec{\pi})f_0, \quad \text{(B67)}$$

$$L_{\kappa K\pi} = -\frac{g_{\kappa K\pi}}{m_\pi}(\partial_\mu K^\dagger)\vec{\tau}\kappa\cdot(\partial^\mu\vec{\pi}) + \text{H.c.}, \quad \text{(B68)}$$

$$L_{\kappa K\eta} = -\frac{g_{\kappa K\eta}}{m_\eta}(\partial_\mu K^\dagger)\kappa(\partial^\mu\eta) + \text{H.c.} \quad \text{(B69)}$$

l. $VV'P$ interaction

As for the interaction between a pseudoscalar-octet meson (P) and vector-octet mesons (V, V'), in this work we consider only the $\omega\rho\pi$ interaction:

$$L_{\omega\rho\pi} = -\frac{g_{\omega\rho\pi}}{m_\omega}\epsilon_{\mu\alpha\lambda\nu}(\partial^\alpha\vec{\rho}^\mu)\cdot(\partial^\lambda\vec{\pi})\omega^\nu. \quad \text{(B70)}$$

2. Electromagnetic interactions

The electromagnetic interactions are obtained from the usual noninteracting Lagrangian and the above hadronic Lagrangian by using the minimum substitution $\partial_\mu \to \partial_\mu - ieA_\mu$. The resulting Lagrangians divided by $-e$ ($e = \sqrt{4\pi/137}$) are listed below.

a. $\gamma BB'$ interaction

The interaction Lagrangian between a photon and spin-$\frac{1}{2}$ octet baryons is given by

$$L_{\gamma BB'} = +\bar{B}\left[\hat{e}_{BB'}(Q^2)\,\not{A} - \frac{\hat{\kappa}_{BB'}(Q^2)}{2m_N}\sigma^{\mu\nu}(\partial_\nu A_\mu)\right]B' + [\text{H.c. for } B \neq B']. \quad \text{(B71)}$$

Here we have defined

$$\hat{e}_{NN} = \frac{F_{1S} + F_{1V}\tau^3}{2}, \quad \text{(B72)}$$

$$\hat{\kappa}_{NN} = \frac{F_{2S} + F_{2V}\tau^3}{2}, \quad \text{(B73)}$$

$$\hat{e}_{\Lambda\Lambda} = 0, \quad \text{(B74)}$$

$$\hat{\kappa}_{\Lambda\Lambda} = -0.61, \quad \text{(B75)}$$

$$\hat{e}_{\Sigma\Sigma} = T_\Sigma^3, \quad \text{(B76)}$$

$$\hat{\kappa}_{\Sigma\Sigma} = \kappa_s^\Sigma + \kappa_v^\Sigma T_\Sigma^3, \quad \text{(B77)}$$

$$\hat{e}_{\Lambda\Sigma} \sim (0, 0, 0), \quad \text{(B78)}$$

$$\hat{\kappa}_{\Lambda\Sigma} = (0, -1.61, 0). \quad \text{(B79)}$$

Here $F_{1S} = F_{1V} = 1$; $F_{2S} = \mu_p + \mu_n - 1 \sim -0.12$; $F_{2V} = \mu_p - \mu_n - 1 \sim 3.7$; $\kappa_s^\Sigma = 0.65$; $\kappa_v^\Sigma = 0.81$; and $T_\Sigma^3 = \text{diag}(1, 0, -1)$.

b. $\gamma PBB'$ and $\gamma VBB'$ interaction

The following four-point interactions are obtained by applying the minimum substitution $\partial_\mu \to \partial_\mu - ieA_\mu$ to the PBB' and VBB' interactions defined in Appendixes B 1 a and B 1 b:

$$L_{\gamma\pi NN} = +\frac{f_{\pi NN}}{m_\pi}[(\bar{N}\,\not{A}\gamma_5\vec{\tau}N)\times\vec{\pi}]_3, \quad \text{(B80)}$$

$$L_{\gamma KN\Lambda} = +i\frac{f_{KN\Lambda}}{m_K}[\bar{p}\,\not{A}\gamma_5 K^+\Lambda - \bar{\Lambda}\,\not{A}\gamma_5 K^- p], \quad \text{(B81)}$$

$$L_{\gamma KN\Sigma} = +i\frac{f_{KN\Sigma}}{m_K}[\bar{n}\,\not{A}\gamma_5 K^+\Sigma^{1+i2} + \bar{p}\,\not{A}\gamma_5 K^+\Sigma^3 - \bar{\Sigma}^{1-i2}\,\not{A}\gamma_5 K^- n - \bar{\Sigma}^3\,\not{A}\gamma_5 K^- p], \quad \text{(B82)}$$

$$L_{\gamma\rho NN} = +\frac{g_{\rho NN}\kappa_\rho}{2m_N}\left[\left(\bar{N}\frac{\vec{\tau}}{2}\sigma^{\nu\mu}N\right)\times\vec{\rho}_\nu\right]_3 A_\mu. \quad \text{(B83)}$$

Here the symbol $[\vec{A}\times\vec{B}]_3$ in the above equations means the third component of the outer product of the isospin vectors $\vec{A}$ and $\vec{B}$. In this work, we multiply the $\gamma\pi NN$, $\gamma KN\Lambda$, and $\gamma KN\Sigma$ interactions by additional phenomenological factors $c_{\gamma\pi NN}$, $c_{\gamma KN\Lambda}$, and $c_{\gamma KN\Sigma}$, respectively, and we treat those factors as parameters in the fit.

c. γBD interaction

The following Lagrangian is used for the interactions involving a photon (γ), spin-$\frac{1}{2}$ octet baryon (B), and a spin-$\frac{3}{2}$ decuplet baryon (D):

$$L_{\gamma N\Delta} = -i\bar{\Delta}^{\mu}\Gamma^{\mathrm{em},\Delta N}_{\mu\nu}T^{3}NA^{\nu} + \mathrm{H.c.}, \tag{B84}$$

$$L_{\gamma\Sigma\Sigma^{*}} = -i(\bar{\Sigma}^{*})^{\mu}\Gamma^{\mathrm{em},\Sigma^{*}\Sigma}_{\mu\nu}\Sigma A^{\nu} + \mathrm{H.c.} \tag{B85}$$

The matrix element of γBD vertex is explicitly given by

$$\begin{aligned}
&\langle D(p_D)|\Gamma^{\mathrm{em},DB}_{\mu\nu}|B(p_B)\rangle \\
&= \frac{m_D+m_B}{2m_B}\frac{1}{(m_D+m_B)^2-q^2} \\
&\quad\times\Bigg[\left(G^{DB}_{M}-G^{DB}_{E}\right)3\epsilon_{\mu\nu\alpha\beta}P^{\alpha}q^{\beta} \\
&\quad + G^{DB}_{E}i\gamma_5\frac{12}{(m_D-m_B)^2-q^2}\epsilon_{\mu\lambda\alpha\beta}P^{\alpha}q^{\beta}\epsilon^{\lambda}{}_{\nu\gamma\delta}p^{\gamma}_{D}q^{\delta} \\
&\quad + G^{DB}_{C}i\gamma_5\frac{6}{(m_D-m_B)^2-q^2}q_{\mu}(q^2P_{\nu}-q\cdot Pq_{\nu})\Bigg],
\end{aligned} \tag{B86}$$

with $P=(p_D+p_B)/2$ and $q=p_D-p_B$. Note that the index μ of $\Gamma^{\mathrm{em},DB}_{\mu\nu}$ contracts with the D field and ν with the photon field. The $\gamma N\Delta$ coupling strength $G^{\Delta N}_{M}=1.85$, $G^{\Delta N}_{E}=0.025$, and $G^{\Delta N}_{C}=-0.238$ are taken from the SL model [15]. However, for the $\gamma\Sigma\Sigma^{*}$ interactions, in this work we set $G^{(\Sigma^{*})^0\Sigma^0}_{E,C}=G^{(\Sigma^{*})^{\mp}\Sigma^{\pm}}_{E,C}=0$, and only $G^{(\Sigma^{*})^0\Sigma^0}_{M}$ and $G^{(\Sigma^{*})^{\pm}\Sigma^{\pm}}_{M}$ are treated as free parameters varied freely in the fit.

d. γPBD interaction

The following four-point interaction is given by applying the minimum substitution $\partial_{\mu}\to\partial_{\mu}-ieA_{\mu}$ to $L_{\pi N\Delta}$:

$$L_{\gamma\pi N\Delta} = +\frac{f_{\pi N\Delta}}{m_{\pi}}[(\bar{\Delta}^{\mu}\vec{T}N)\times\vec{\pi}]_3A_{\mu} + \mathrm{H.c.} \tag{B87}$$

e. $\gamma DD'$ interaction

As for the interaction involving a photon (γ) and spin-$\frac{3}{2}$ decuplet baryons (D, D'), we consider only the $\gamma\Delta\Delta$ interaction,

$$\begin{aligned}
L_{\gamma\Delta\Delta} = +\bar{\Delta}^{\eta}\left(T^{3}_{\Delta}+\tfrac{1}{2}\right)\big[&-\gamma_{\mu}g_{\eta\nu} \\
&+\left(g_{\mu\eta}\gamma_{\nu}+g_{\mu\nu}\gamma_{\eta}\right)+\tfrac{1}{3}\gamma_{\eta}\gamma_{\mu}\gamma_{\nu}\big]\Delta^{\nu}A^{\mu}.
\end{aligned} \tag{B88}$$

f. $\gamma PP'$ interaction

As for the interaction involving a photon (γ) and pseudoscalar octet mesons (P, P'), in this work only the following $\gamma\pi\pi$ and γKK interactions are considered:

$$L_{\gamma\pi\pi} = +[\vec{\pi}\times(\partial^{\mu}\vec{\pi})]_3A_{\mu}, \tag{B89}$$

$$L_{\gamma KK} = +i[K^{-}\partial^{\mu}K^{+}-(\partial^{\mu}K^{-})K^{+}]A_{\mu}. \tag{B90}$$

g. γVP interaction

The following Lagrangian is considered for interactions involving a photon (γ), a vector octet mesons (V), and a pseudoscalar octet mesons (P):

$$L_{\gamma\rho\pi} = +\frac{g_{\gamma\rho\pi}}{m_{\pi}}\epsilon_{\alpha\beta\gamma\delta}(\partial^{\alpha}A^{\beta})(\partial^{\gamma}\vec{\rho}^{\delta})\cdot\vec{\pi}, \tag{B91}$$

$$L_{\gamma\omega\pi} = +\frac{g_{\gamma\omega\pi}}{m_{\pi}}\epsilon_{\alpha\beta\gamma\delta}(\partial^{\alpha}A^{\beta})(\partial^{\gamma}\omega^{\delta})\pi^{3}, \tag{B92}$$

$$L_{\gamma\rho\eta} = +\frac{g_{\gamma\rho\eta}}{m_{\rho}}\epsilon_{\alpha\beta\gamma\delta}(\partial^{\alpha}A^{\beta})(\partial^{\gamma}\rho^{3\delta})\eta, \tag{B93}$$

$$L_{\gamma\omega\eta} = +\frac{g_{\gamma\omega\eta}}{m_{\omega}}\epsilon_{\alpha\beta\gamma\delta}(\partial^{\alpha}A^{\beta})(\partial^{\gamma}\omega^{\delta})\eta, \tag{B94}$$

$$\begin{aligned}
L_{\gamma K^{*}K} = &+\frac{g^{0}_{\gamma K^{*}K}}{m_K}\epsilon_{\alpha\beta\gamma\delta}[\bar{K}^{0}(\partial^{\gamma}K^{*0,\delta}) \\
&+K^{0}(\partial^{\gamma}\bar{K}^{*0,\delta})]\partial^{\alpha}A^{\beta} \\
&+\frac{g^{c}_{\gamma K^{*}K}}{m_K}\epsilon_{\alpha\beta\gamma\delta}[K^{+}(\partial^{\gamma}K^{*-,\delta}) \\
&+K^{-}(\partial^{\gamma}K^{*+,\delta})]\partial^{\alpha}A^{\beta}.
\end{aligned} \tag{B95, B96}$$

In this work, we treat $g_{\gamma\rho\pi}$, $g_{\gamma\omega\pi}$, $g_{\gamma\rho\eta}$, and $g_{\gamma\omega\eta}$ as free parameters in the fit, while we use the fixed values for $\gamma K^{*}K$ couplings, i.e., $g^{0}_{\gamma K^{*}K}/m_K=-0.388\ \mathrm{GeV}^{-1}$ and $g^{c}_{\gamma K^{*}K}=0.254\ \mathrm{GeV}^{-1}$ [68].

h. $\gamma VPP'$ interaction

The following four-point interaction is given by applying the minimum substitution $\partial_{\mu}\to\partial_{\mu}-ieA_{\mu}$ to $L_{\rho\pi\pi}$:

$$L_{\gamma\rho\pi\pi} = -g_{\rho\pi\pi}[(\vec{\rho}^{\mu}\times\vec{\pi})\times\vec{\pi}]_3A_{\mu}. \tag{B97}$$

i. γAP interaction

As for the interaction involving a photon (γ), an axial-vector meson (A), and a pseudoscalar meson (P), in this paper only the $\gamma a_1\pi$ interaction is considered:

$$\begin{aligned}
L_{\gamma a_1\pi} = &+\frac{1}{m_{a_1}}(\partial^{\mu}A^{\nu}-\partial^{\nu}A^{\mu}) \\
&\times\{2[(\partial_{\mu}\vec{\pi})\times\vec{a}_{1\nu}]_3-2[(\partial_{\nu}\vec{\pi})\times\vec{a}_{1\mu}]_3 \\
&+[\vec{\pi}\times(\partial_{\mu}\vec{a}_{1\nu}-\partial_{\nu}\vec{a}_{1\mu})]_3\}.
\end{aligned} \tag{B98}$$

j. $\gamma VV'$ interaction

As for the interaction involving a photon (γ) and vector octet mesons (V, V'), in this paper only the $\gamma\rho\rho$ interaction is considered:

$$L_{\gamma\rho\rho} = +[(\partial^{\mu}\vec{\rho}^{\nu}-\partial^{\nu}\vec{\rho}^{\mu})\times\vec{\rho}_{\nu}]_3A_{\mu}. \tag{B99}$$

APPENDIX C: MATRIX ELEMENTS OF MESON-BARYON POTENTIALS

It is convenient to get the partial-wave matrix elements of the meson-exchange potential $v_{M'B',MB}$ by first evaluating $v_{M'B',MB}$ in helicity representation and then transforming them into the usual $|(LS)JT\rangle$ representation with J, T, L, and S denoting the total angular momentum, isospin, orbital angular momentum, and spin quantum numbers, respectively. For each meson-baryon (MB) state, we use $k(p)$ to denote the

momentum of $M(B)$. In the center-of-mass frame, we thus have $\vec{p} = -\vec{k}$. Following the Jacob-Wick formulation [69], the partial-wave matrix elements of $v_{M'B',MB}$ can be written as

$$\begin{aligned} & v^{JT}_{L'S'M'B',LSMB}(k', k, W) \\ &= \sum_{\lambda'_M \lambda'_B \lambda_M \lambda_B} \frac{\sqrt{(2L+1)(2L'+1)}}{2J+1} \\ &\quad \times \langle j'_M j'_B \lambda'_M - \lambda'_B | S' S'_z \rangle \langle L' S' 0 S'_z | J S'_z \rangle \\ &\quad \times \langle j_M j_B \lambda_M - \lambda_B | S S_z \rangle \langle L S 0 S_z | J S_z \rangle \\ &\quad \times \langle J, k' \lambda'_M - \lambda'_B | v_{M'B',MB} | J, k \lambda_M - \lambda_B \rangle, \end{aligned} \tag{C1}$$

where j_M and j_B are the spins of the meson and baryon, respectively, and λ_M and λ_B are their helicities, and

$$\begin{aligned} & \langle J, k' \lambda'_M - \lambda'_B | v_{M'B',MB} | J, k \lambda_M - \lambda_B \rangle \\ &= 2\pi \int_{-1}^{+1} d(\cos\theta) d^J_{\lambda_M - \lambda_B, \lambda'_M - \lambda'_B}(\theta) \\ &\quad \times \langle M'(\vec{k}', s'_M \lambda'_M) B'(-\vec{k}', s'_B, -\lambda'_B) | \\ &\quad \times v_{M'B',MB} | M(\vec{k}, s_M \lambda_M) B(-\vec{k}, s_B, -\lambda_B) \rangle. \end{aligned} \tag{C2}$$

Here we have chosen the coordinates such that

$$\vec{k}' = (k' \sin\theta, 0, k' \cos\theta), \tag{C3}$$

$$\vec{k} = (0, 0, k), \tag{C4}$$

and the helicity eigenstates are defined by

$$\hat{k} \cdot \vec{s}_M | M(\vec{k}, s_M \lambda_M) \rangle = \lambda_M | M(\vec{k}, s_M \lambda_M) \rangle, \tag{C5}$$

$$[-\hat{k} \cdot \vec{s}_B] | B(-\vec{k}, s_B \lambda_B) \rangle = \lambda_B | B(-\vec{k}, s_B \lambda_B) \rangle. \tag{C6}$$

Note the "−" sign in Eq. (C6).

TABLE X. Label n for $\bar{V}(n)$ in Eq. (C7).

Channel	πN	ηN	σN	ρN	$\pi\Delta$	$K\Lambda$	$K\Sigma$
πN	1	2	4	7	11	16	19
ηN		3	5	8	12	17	20
σN			6	9	13	–	–
ρN				10	14	–	–
$\pi\Delta$					15	–	–
$K\Lambda$						18	21
$K\Sigma$							22

To evaluate the matrix elements in the right-hand side of Eq. (C2), we define (suppressing the helicity and isospin indices)

$$\begin{aligned} & \langle k'(j), p' | v_{M'B',MB} | k(i), p \rangle \\ &= \frac{1}{(2\pi)^3} \sqrt{\frac{m'_B}{E_{B'}(p')}} \frac{1}{\sqrt{2E_{M'}(k')}} \sqrt{\frac{m_B}{E_B(p)}} \frac{1}{\sqrt{2E_M(k)}} \\ &\quad \times \bar{u}_{B'}(\vec{p}') \bar{V}(n) u_B(\vec{p}). \end{aligned} \tag{C7}$$

Here the label n indicates the considered $MB \to M'B'$ transition as specified in Table X; i, j are the isospin indices of the mesons. We also use the notation $q = k' - k$ or $q = p - p'$ in this Appendix. The expressions of each term in $\bar{V}(n)$ are given in the following sections.

1. $\pi(k, i) + N(p) \to \pi(k', j) + N(p')$

$$\bar{V}(1) = \bar{V}^1_a + \bar{V}^1_b + \bar{V}^1_c + \bar{V}^1_d + \bar{V}^1_e + \bar{V}^1_f, \tag{C8}$$

with

$$\bar{V}^1_a = \left(\frac{f_{\pi NN}}{m_\pi}\right)^2 \not{k}' \gamma_5 \tau^j S_N(p+k) \not{k} \gamma_5 \tau^i, \tag{C9}$$

$$\bar{V}^1_b = \left(\frac{f_{\pi NN}}{m_\pi}\right)^2 \not{k} \gamma_5 \tau^i S_N(p-k') \not{k}' \gamma_5 \tau^j, \tag{C10}$$

$$\bar{V}^1_c = \left(\frac{f_{\pi N\Delta}}{m_\pi}\right)^2 k_\alpha (T^\dagger)^i S^{\alpha\beta}_\Delta(p-k') k'_\beta T^j, \tag{C11}$$

$$\begin{aligned} \bar{V}^1_d = & -C_{V1} \frac{g_{\rho NN} g_{\rho\pi\pi}}{m^2_\rho} \left[(\not{k} + \not{k}') + C_{V2} \frac{\kappa_\rho}{4m_N} \{ (\not{k} + \not{k}') \not{q} - \not{q} (\not{k} + \not{k}') \} \right] i\epsilon_{jil} \frac{\tau^l}{2} \\ & + g_{\rho NN} g_{\rho\pi\pi} \frac{q^2}{m^2_\rho (q^2 - m^2_\rho)} \left[(\not{k} + \not{k}') + \frac{\kappa_\rho}{4m_N} \{ (\not{k} + \not{k}') \not{q} - \not{q} (\not{k} + \not{k}') \} \right] i\epsilon_{jil} \frac{\tau^l}{2}, \end{aligned} \tag{C12}$$

$$\bar{V}^1_e = + C_S \frac{k \cdot k'}{m_\pi} \delta_{ij} - \left(g_{\sigma NN} g_{\sigma\pi\pi} \frac{q^2}{m^2_\sigma (q^2 - m^2_\sigma)} + g_{f_0 NN} g_{f_0\pi\pi} \frac{q^2}{m^2_{f_0} (q^2 - m^2_{f_0})} \right) \frac{k \cdot k'}{m_\pi} \delta_{ij}, \tag{C13}$$

$$\bar{V}^1_f = - \frac{g_{\sigma NN} \tilde{g}_{\sigma\pi\pi} m^2_\pi}{f_\pi} \frac{1}{q^2 - m^2_\sigma} \delta_{ij}. \tag{C14}$$

Here one can see that parameters C_{V1}, C_{V2}, and C_S, which are somewhat unusual and require some explanation, appear in the meson-exchange potentials $\bar{V}^1_d$ and $\bar{V}^1_e$. Let us explain this by taking ρ-meson-exchange potential $\bar{V}^1_d$ as an example. It is first noticed that if one takes $C_{V1} = C_{V2} = 1$, $\bar{V}^1_d$ reduces to the familiar ρ-meson exchange $\pi N \to \pi N$ potential derived

from $L_{\rho\pi\pi}$ and $L_{\rho NN}$. In effective theories, the propagator of heavy mesons M is expanded as

$$\frac{1}{q^2 - m_M^2} = -\frac{1}{m_M^2} + \mathcal{O}\left(\frac{q^2}{m_M^4}\right), \tag{C15}$$

and the effect of the heavy-particle exchanges is absorbed into contact terms of the effective theories. We have taken into account contributions of higher excited ρ meson states phenomenologically by making C_{V1} and C_{V2} as free parameters that can be different from $C_{V1} = 1$ and $C_{V2} = 1$, respectively. Furthermore, we attach different cutoff factors for the first and second terms of $\bar{V}_d^1$. A similar prescription has been applied also to the scalar-meson-exchange potential $\bar{V}_e^1$. In addition, in this work we include a phenomenological contact potential $\bar{V}^1 = c_{S31}$ in getting a good fit to S_{31} partial wave. We do not need this for other partial waves.

2. $\pi(k, i) + N(p) \to \eta(k') + N(p')$

$$\bar{V}(2) = \bar{V}_a^2 + \bar{V}_b^2, \tag{C16}$$

with

$$\bar{V}_a^2 = \frac{f_{\pi NN} f_{\eta NN}}{m_\pi m_\eta} \not{k}' \gamma_5 S_N(p + k) \not{k} \gamma_5 \tau^i, \tag{C17}$$

$$\bar{V}_b^2 = \frac{f_{\pi NN} f_{\eta NN}}{m_\pi m_\eta} \not{k} \gamma_5 \tau^i S_N(p - k') \not{k}' \gamma_5. \tag{C18}$$

3. $\eta(k) + N(p) \to \eta(k') + N(p')$

$$\bar{V}(3) = \bar{V}_a^3 + \bar{V}_b^3, \tag{C19}$$

with

$$\bar{V}_a^3 = \left(\frac{f_{\eta NN}}{m_\eta}\right)^2 \not{k}' \gamma_5 S_N(p + k) \not{k} \gamma_5, \tag{C20}$$

$$\bar{V}_b^3 = \left(\frac{f_{\eta NN}}{m_\eta}\right)^2 \not{k} \gamma_5 S_N(p - k') \not{k}' \gamma_5. \tag{C21}$$

4. $\pi(k, i) + N(p) \to \sigma(k') + N(p')$

$$\bar{V}(4) = \bar{V}_a^4 + \bar{V}_b^4 + \bar{V}_c^4, \tag{C22}$$

with

$$\bar{V}_a^4 = i g_{\sigma NN} \frac{f_{\pi NN}}{m_\pi} S_N(p + k) \not{k} \gamma_5 \tau^i, \tag{C23}$$

$$\bar{V}_b^4 = i g_{\sigma NN} \frac{f_{\pi NN}}{m_\pi} \not{k} \gamma_5 S_N(p - k') \tau^i, \tag{C24}$$

$$\bar{V}_c^4 = i \frac{f_{\pi NN} g_{\sigma\pi\pi}}{m_\pi^2} \not{q} \gamma_5 \tau^i \frac{q \cdot k}{q^2 - m_\pi^2}. \tag{C25}$$

5. $\eta(k) + N(p) \to \sigma(k') + N(p')$

$$\bar{V}(5) = \bar{V}_a^5 + \bar{V}_b^5, \tag{C26}$$

with

$$\bar{V}_a^5 = i g_{\sigma NN} \frac{f_{\eta NN}}{m_\eta} S_N(p + k) \not{k} \gamma_5, \tag{C27}$$

$$\bar{V}_b^5 = i g_{\sigma NN} \frac{f_{\eta NN}}{m_\eta} \not{k} \gamma_5 S_N(p - k'). \tag{C28}$$

6. $\sigma(k) + N(p) \to \sigma(k') + N(p')$

$$\bar{V}(6) = \bar{V}_a^6 + \bar{V}_b^6, \tag{C29}$$

with

$$\bar{V}_a^6 = g_{\sigma NN}^2 S_N(p + k), \tag{C30}$$

$$\bar{V}_b^6 = g_{\sigma NN}^2 S_N(p - k'). \tag{C31}$$

7. $\pi(k, i) + N(p) \to \rho'(k', j) + N(p')$

$$\bar{V}(7) = \bar{V}_a^7 + \bar{V}_b^7 + \bar{V}_c^7 + \bar{V}_d^7 + \bar{V}_e^7, \tag{C32}$$

with

$$\bar{V}_a^7 = i \frac{f_{\pi NN}}{m_\pi} g_{\rho NN} \Gamma_{\rho'} S_N(p + k) \not{k} \gamma_5 \tau^i, \tag{C33}$$

$$\bar{V}_b^7 = i \frac{f_{\pi NN}}{m_\pi} g_{\rho NN} \not{k} \gamma_5 \tau^i S_N(p - k') \Gamma_{\rho'}, \tag{C34}$$

$$\bar{V}_c^7 = \frac{f_{\pi NN}}{m_\pi} g_{\rho\pi\pi} \epsilon_{ijl} \tau^l \frac{(q - k) \cdot \epsilon_{\rho'}^* \not{q} \gamma_5}{q^2 - m_\pi^2}, \tag{C35}$$

$$\bar{V}_d^7 = -\frac{f_{\pi NN}}{m_\pi} g_{\rho NN} \not{\epsilon}_{\rho'}^* \gamma_5 \epsilon_{jil} \tau^l, \tag{C36}$$

$$\bar{V}_e^7 = \frac{g_{\omega NN} g_{\omega\pi\rho}}{m_\omega} \delta_{ij} \frac{\epsilon_{\alpha\beta\gamma\delta} \epsilon_{\rho'}^{*\alpha} k'^\beta k^\gamma}{q^2 - m_\omega^2} \times \left[\gamma^\delta + \frac{\kappa_\omega}{4m_N}(\gamma^\delta \not{q} - \not{q} \gamma^\delta)\right], \tag{C37}$$

where

$$\Gamma_{\rho'} = \frac{\tau^j}{2}\left[\not{\epsilon}_{\rho'}^* + \frac{\kappa_\rho}{4m_N}(\not{\epsilon}_{\rho'}^* \not{k}' - \not{k}' \not{\epsilon}_{\rho'}^*)\right]. \tag{C38}$$

8. $\eta(k) + N(p) \to \rho'(k', j) + N(p')$

$$\bar{V}(8) = \bar{V}_a^8 + \bar{V}_b^8, \tag{C39}$$

with

$$\bar{V}_a^8 = i \frac{f_{\eta NN}}{m_\eta} g_{\rho NN} \Gamma_{\rho'} S_N(p + k) \not{k} \gamma_5, \tag{C40}$$

$$\bar{V}_b^8 = i \frac{f_{\eta NN}}{m_\eta} g_{\rho NN} \not{k} \gamma_5 S_N(p - k') \Gamma_{\rho'}. \tag{C41}$$

9. $\sigma(k) + N(p) \to \rho'(k', j) + N(p')$

$$\bar{V}(9) = \bar{V}_a^9 + \bar{V}_b^9, \tag{C42}$$

with

$$\bar{V}_a^9 = g_{\rho NN} g_{\sigma NN} \Gamma_{\rho'} S_N(p+k), \tag{C43}$$

$$\bar{V}_b^9 = g_{\rho NN} g_{\sigma NN} S_N(p-k') \Gamma_{\rho'}. \tag{C44}$$

10. $\rho(k, i) + N(p) \to \rho'(k', j) + N(p')$

$$\bar{V}(10) = \bar{V}_a^{10} + \bar{V}_b^{10} + \bar{V}_c^{10}, \tag{C45}$$

with

$$\bar{V}_a^{10} + \bar{V}_b^{10} = g_{\rho NN}^2 [\Gamma_{\rho'} S_N(p+k) \Gamma_\rho + \Gamma_\rho S_N(p-k') \Gamma_{\rho'}], \tag{C46}$$

where

$$\Gamma_\rho = \frac{\tau^i}{2} \left[\not{\epsilon}_\rho - \frac{\kappa_\rho}{4m_N} (\not{\epsilon}_\rho \not{k} - \not{k} \not{\epsilon}_\rho) \right] \tag{C47}$$

and

$$\bar{V}_c^{10} = i \frac{\kappa_\rho g_{\rho NN}^2}{8m_N} [\not{\epsilon}_\rho \not{\epsilon}_{\rho'}^* - \not{\epsilon}_{\rho'}^* \not{\epsilon}_\rho] \epsilon_{ijl} \tau^l. \tag{C48}$$

11. $\pi(k, i) + N(p) \to \pi(k', j) + \Delta(p')$

$$\bar{V}(11) = \bar{V}_a^{11} + \bar{V}_b^{11} + \bar{V}_c^{11} + \bar{V}_d^{11} + \bar{V}_e^{11}, \tag{C49}$$

with

$$\bar{V}_a^{11} = \frac{f_{\pi NN} f_{\pi N\Delta}}{m_\pi^2} T^j \epsilon_\Delta^* \cdot k' S_N(p+k) \not{k} \gamma_5 \tau^i, \tag{C50}$$

$$\bar{V}_b^{11} = \frac{f_{\pi NN} f_{\pi N\Delta}}{m_\pi^2} T^i \epsilon_\Delta^* \cdot k S_N(p-k') \not{k}' \gamma_5 \tau^j, \tag{C51}$$

$$\bar{V}_c^{11} = i \frac{f_{\rho N\Delta} f_{\rho\pi\pi}}{m_\rho} \frac{\epsilon_{jil} T^l}{q^2 - m_\rho^2} \times [\epsilon_\Delta^* \cdot q (\not{k} + \not{k}') \gamma_5 - \epsilon_\Delta^* \cdot (k + k') \not{q} \gamma_5], \tag{C52}$$

$$\bar{V}_d^{11} = -\frac{f_{\pi\Delta\Delta} f_{\pi N\Delta}}{m_\pi^2} [\epsilon_\Delta^*]_\mu \not{k}' \gamma_5 T_\Delta^j S_\Delta^{\mu\nu}(p'+k') T^i k_\nu, \tag{C53}$$

$$\bar{V}_e^{11} = -\frac{f_{\pi\Delta\Delta} f_{\pi N\Delta}}{m_\pi^2} [\epsilon_\Delta^*]_\mu \not{k} \gamma_5 T_\Delta^i S_\Delta^{\mu\nu}(p-k') T^j k'_\nu. \tag{C54}$$

12. $\eta(k) + N(p) \to \pi(k', j) + \Delta(p')$

$$\bar{V}(12) = \frac{f_{\eta NN} f_{\eta N\Delta}}{m_\pi m_\eta} T^j \epsilon_\Delta^* \cdot k' S_N(p+k) \not{k} \gamma_5. \tag{C55}$$

13. $\sigma(k) + N(p) \to \pi(k', j) + \Delta(p')$

$$\bar{V}(13) = -i g_{\sigma NN} \frac{f_{\pi N\Delta}}{m_\pi} T^j \epsilon_\Delta^* \cdot k' S_N(p+k). \tag{C56}$$

14. $\rho(k, i) + N(p) \to \pi(k', j) + \Delta(p')$

$$\bar{V}(14) = \bar{V}_a^{14} + \bar{V}_b^{14} + \bar{V}_c^{14} + \bar{V}_d^{14}, \tag{C57}$$

with

$$\bar{V}_a^{14} = -i \frac{f_{\pi N\Delta} g_{\rho NN}}{m_\pi} T^j \epsilon_\Delta^* \cdot k' S_N(p+k) \Gamma_\rho, \tag{C58}$$

$$\bar{V}_b^{14} = i \frac{f_{\pi NN} f_{\rho N\Delta}}{m_\pi m_\rho} T^i [\epsilon_\Delta^* \cdot k \not{\epsilon}_\rho \gamma_5 - \epsilon_\Delta^* \cdot \epsilon_\rho \not{k} \gamma_5] \times S_N(p-k') \not{k}' \gamma_5 \tau^j, \tag{C59}$$

$$\bar{V}_c^{14} = -i \frac{f_{\pi\Delta\Delta} f_{\rho N\Delta}}{m_\pi m_\rho} [\epsilon_\Delta^*]_\alpha \not{k}' \gamma_5 T_\Delta^j S_\Delta^{\alpha\beta}(p'+k') \times [k_\beta \not{\epsilon}_\rho \gamma_5 - [\epsilon_\rho]_\beta \not{k} \gamma_5] T^i, \tag{C60}$$

$$\bar{V}_d^{14} = -i \frac{g_{\rho\Delta\Delta} f_{\pi N\Delta}}{m_\pi} [\epsilon_\Delta^*]_\alpha \left[\not{\epsilon}_\rho - \frac{\kappa_{\rho\Delta\Delta}}{4m_\Delta} (\not{\epsilon}_\rho \not{k} - \not{k} \not{\epsilon}_\rho) \right] \times T_\Delta^i S_\Delta^{\alpha\beta}(p-k') T^j k'_\beta. \tag{C61}$$

15. $\pi(k, i) + \Delta(p) \to \pi(k', j) + \Delta'(p')$

$$\bar{V}(15) = \bar{V}_a^{15} + \bar{V}_b^{15} + \bar{V}_c^{15} + \bar{V}_d^{15}, \tag{C62}$$

with

$$\bar{V}_a^{15} = \left(\frac{f_{\pi N\Delta}}{m_\pi} \right)^2 \epsilon_{\Delta'}^* \cdot k' T^j S_N(p+k) \epsilon_\Delta \cdot k (T^i)^\dagger, \tag{C63}$$

$$\bar{V}_b^{15} = \left(\frac{f_{\pi\Delta\Delta}}{m_\pi} \right)^2 \not{k}' \gamma_5 T_\Delta^j [\epsilon_{\Delta'}^*]_\mu S_\Delta^{\mu\nu}(p+k) [\epsilon_\Delta]_\nu \not{k} \gamma_5 T_\Delta^i, \tag{C64}$$

$$\bar{V}_c^{15} = \left(\frac{f_{\pi\Delta\Delta}}{m_\pi} \right)^2 \not{k} \gamma_5 T_\Delta^i [\epsilon_{\Delta'}^*]_\mu S_\Delta^{\mu\nu}(p-k') [\epsilon_\Delta]_\nu \not{k}' \gamma_5 T_\Delta^j, \tag{C65}$$

$$\bar{V}_d^{15} = i g_{\rho\Delta\Delta} g_{\rho\pi\pi} \frac{\epsilon_{jil} T_\Delta^l}{q^2 - m_\rho^2} \times \left[(\not{k} + \not{k}') + \frac{\kappa_{\rho\Delta\Delta}}{4m_\Delta} ((\not{k} + \not{k}') \not{q} - \not{q} (\not{k} + \not{k}')) \right] \epsilon_{\Delta'}^* \cdot \epsilon_\Delta. \tag{C66}$$

16. $\pi(k, i) + N(p) \to K(k') + \Lambda(p')$

$$\bar{V}(16) = \bar{V}_a^{16} + \bar{V}_b^{16} + \bar{V}_c^{16} + \bar{V}_d^{16} + \bar{V}_e^{16}, \tag{C67}$$

with

$$\bar{V}_a^{16} = \frac{f_{K\Lambda N} f_{\pi NN}}{m_K m_\pi} \not{k}' \gamma_5 S_N(p+k) \not{k} \gamma_5 \tau^i, \tag{C68}$$

$$\bar{V}_b^{16} = \frac{f_{\pi\Lambda\Sigma} f_{K\Sigma N}}{m_K m_\pi} \not{k} \gamma_5 S_\Sigma(p-k') \not{k}' \gamma_5 \tau^i, \tag{C69}$$

$$\bar{V}_c^{16} = \frac{f_{\pi\Lambda\Sigma^*} f_{KN\Sigma^*}}{m_K m_\pi} k_\alpha S^{\alpha\beta}_{\Sigma^*}(p-k') k'_\beta \tau^i, \tag{C70}$$

$$\bar{V}_d^{16} = -g_{K^*N\Lambda} g_{K^*K\pi} \frac{-g_{\mu\rho} + q_\mu q_\rho / m_{K^*}^2}{q^2 - m_{K^*}^2} \times \left(\gamma^\mu - i \frac{\kappa_{K^*N\Lambda}}{m_N + m_\Lambda} \sigma^{\mu\nu} q_\nu \right) (k+k')^\rho \tau^i, \tag{C71}$$

$$\bar{V}_e^{16} = -\frac{g_{\kappa\Lambda N} g_{\kappa K\pi}}{m_\pi} \frac{k \cdot k'}{q^2 - m_\kappa^2} \tau^i. \tag{C72}$$

17. $\eta(k) + N(p) \to K(k') + \Lambda(p')$

$$\bar{V}(17) = \bar{V}_a^{17} + \bar{V}_b^{17} + \bar{V}_c^{17} + \bar{V}_d^{17}, \tag{C73}$$

with

$$\bar{V}_a^{17} = \frac{f_{K\Lambda N} f_{\eta NN}}{m_K m_\eta} \not{k}' \gamma_5 S_N(p+k) \not{k} \gamma_5, \tag{C74}$$

$$\bar{V}_b^{17} = \frac{f_{\eta\Lambda\Lambda} f_{K\Lambda N}}{m_K m_\eta} \not{k} \gamma_5 S_\Lambda(p-k') \not{k}' \gamma_5, \tag{C75}$$

$$\bar{V}_c^{17} = -g_{K^*N\Lambda} g_{K^*K\eta} \frac{-g_{\mu\rho} + q_\mu q_\rho / m_{K^*}^2}{q^2 - m_{K^*}^2} \times \left(\gamma^\mu - i \frac{\kappa_{K^*N\Lambda}}{m_N + m_\Lambda} \sigma^{\mu\nu} q_\nu \right) (k+k')^\rho, \tag{C76}$$

$$\bar{V}_d^{17} = -\frac{g_{\kappa\Lambda N} g_{\kappa K\eta}}{m_\pi} \frac{k \cdot k'}{q^2 - m_\kappa^2}. \tag{C77}$$

18. $K(k) + \Lambda(p) \to K(k') + \Lambda(p')$

$$\bar{V}(18) = \bar{V}_a^{18} + \bar{V}_b^{18} + \bar{V}_c^{18} + \bar{V}_d^{18}, \tag{C78}$$

with

$$\bar{V}_a^{18} = \left(\frac{f_{K\Lambda N}}{m_K} \right)^2 \not{k}' \gamma_5 S_N(p+k) \not{k} \gamma_5, \tag{C79}$$

$$\bar{V}_b^{18} = \left(\frac{f_{K\Xi\Lambda}}{m_K} \right)^2 \not{k} \gamma_5 S_\Xi(p-k') \not{k}' \gamma_5, \tag{C80}$$

$$\bar{V}_c^{18} = -g_{\omega\Lambda\Lambda} g_{\omega KK} \frac{-g_{\mu\rho} + q_\mu q_\rho / m_\omega^2}{q^2 - m_\omega^2} \times \left(\gamma^\mu - i \frac{\kappa_{\omega\Lambda\Lambda}}{2m_\Lambda} \sigma^{\mu\nu} q_\nu \right) (k+k')^\rho, \tag{C81}$$

$$\bar{V}_d^{18} = -g_{\phi\Lambda\Lambda} g_{\phi KK} \frac{-g_{\mu\rho} + q_\mu q_\rho / m_\phi^2}{q^2 - m_\phi^2} \times \left(\gamma^\mu - i \frac{\kappa_{\phi\Lambda\Lambda}}{2m_\Lambda} \sigma^{\mu\nu} q_\nu \right) (k+k')^\rho. \tag{C82}$$

19. $\pi(k, i) + N(p) \to K(k') + \Sigma(p', j)$

$$\bar{V}(19) = \bar{V}_a^{19} + \bar{V}_b^{19} + \bar{V}_c^{19} + \bar{V}_d^{19} + \bar{V}_e^{19} + \bar{V}_f^{19}, \tag{C83}$$

with

$$\bar{V}_a^{19} = \frac{f_{K\Sigma N} f_{\pi NN}}{m_K m_\pi} \not{k}' \gamma_5 \tau^j S_N(p+k) \not{k} \gamma_5 \tau^i, \tag{C84}$$

$$\bar{V}_b^{19} = \frac{f_{\pi\Lambda\Sigma} f_{K\Lambda N}}{m_K m_\pi} \not{k} \gamma_5 S_\Lambda(p-k') \not{k}' \gamma_5 \delta^{ij}, \tag{C85}$$

$$\bar{V}_c^{19} = \frac{f_{\pi\Sigma\Sigma} f_{K\Sigma N}}{m_K m_\pi} \not{k} \gamma_5 S_\Sigma(p-k') \not{k}' \gamma_5 i \epsilon^{ijk} \tau_k, \tag{C86}$$

$$\bar{V}_d^{19} = \frac{f_{\pi\Sigma\Sigma^*} f_{KN\Sigma^*}}{m_K m_\pi} k_\alpha S^{\alpha\beta}_{\Sigma^*}(p-k') k'_\beta i \epsilon^{ijk} \tau_k, \tag{C87}$$

$$\bar{V}_e^{19} = -g_{K^*N\Sigma} g_{K^*K\pi} \frac{-g_{\mu\rho} + q_\mu q_\rho / m_{K^*}^2}{q^2 - m_{K^*}^2} \times \left(\gamma^\mu - i \frac{\kappa_{K^*N\Sigma}}{m_N + m_\Sigma} \sigma^{\mu\nu} q_\nu \right) (k+k')^\rho \tau^i \tau^j, \tag{C88}$$

$$\bar{V}_f^{19} = -\frac{g_{\kappa\Sigma N} g_{\kappa K\pi}}{m_\pi} \frac{k \cdot k'}{q^2 - m_\kappa^2} \tau^i \tau^j. \tag{C89}$$

20. $\eta(k) + N(p) \to K(k') + \Sigma(p', j)$

$$\bar{V}(20) = \bar{V}_a^{20} + \bar{V}_b^{20} + \bar{V}_c^{20} + \bar{V}_d^{20}, \tag{C90}$$

with

$$\bar{V}_a^{20} = \frac{f_{K\Sigma N} f_{\eta NN}}{m_K m_\eta} \not{k}' \gamma_5 S_N(p+k) \not{k} \gamma_5 \tau^j, \tag{C91}$$

$$\bar{V}_b^{20} = \frac{f_{\eta\Sigma\Sigma} f_{K\Sigma N}}{m_K m_\eta} \not{k} \gamma_5 S_\Sigma(p-k') \not{k}' \gamma_5 \tau^j, \tag{C92}$$

$$\bar{V}_c^{20} = -g_{K^*N\Sigma} g_{K^*K\eta} \frac{-g_{\mu\rho} + q_\mu q_\rho / m_{K^*}^2}{q^2 - m_{K^*}^2} \times \left(\gamma^\mu - i \frac{\kappa_{K^*N\Sigma}}{m_N + m_\Sigma} \sigma^{\mu\nu} q_\nu \right) (k+k')^\rho \tau^j, \tag{C93}$$

$$\bar{V}_d^{20} = -\frac{g_{\kappa\Sigma N} g_{\kappa K\eta}}{m_\pi} \frac{k \cdot k'}{q^2 - m_\kappa^2} \tau^j. \tag{C94}$$

21. $K(k) + \Sigma(p, i) \to K(k') + \Lambda(p')$

$$\bar{V}(21) = \bar{V}_a^{21} + \bar{V}_b^{21} + \bar{V}_c^{21}, \tag{C95}$$

with

$$\bar{V}_a^{21} = \frac{f_{K\Lambda N} f_{K\Sigma N}}{m_K^2} \not{k}' \gamma_5 S_N(p+k) \not{k} \gamma_5 \tau^i, \tag{C96}$$

$$\bar{V}_b^{21} = \frac{f_{K\Xi\Sigma} f_{K\Xi\Lambda}}{m_K^2} \not{k} \gamma_5 \tau^i S_\Xi(p-k') \not{k}' \gamma_5, \tag{C97}$$

$$\bar{V}_e^{21} = -g_{\rho\Sigma\Lambda} g_{\rho KK} \frac{-g_{\mu\rho} + q_\mu q_\rho / m_\rho^2}{q^2 - m_\rho^2} \times \left(\gamma^\mu - i \frac{\kappa_{\rho\Sigma\Lambda}}{m_\Sigma + m_\Lambda} \sigma^{\mu\nu} q_\nu \right) (k+k')^\rho \tau_i. \tag{C98}$$

22. $K(k) + \Sigma(p, i) \to K(k') + \Sigma(p', j)$

$$\bar{V}(22) = \bar{V}_a^{22} + \bar{V}_b^{22} + \bar{V}_c^{22} + \bar{V}_d^{22} + \bar{V}_e^{22}, \tag{C99}$$

with

$$\bar{V}_a^{22} = \left(\frac{f_{K\Sigma N}}{m_K}\right)^2 \not{k}'\gamma_5\tau^j S_N(p+k)\ \not{k}\gamma_5\tau^i, \tag{C100}$$

$$\bar{V}_b^{22} = \left(\frac{f_{K\Xi\Sigma}}{m_K}\right)^2 \not{k}\gamma_5\tau^i S_\Xi(p-k')\ \not{k}'\gamma_5\tau^j, \tag{C101}$$

$$\bar{V}_c^{22} = -g_{\omega\Sigma\Sigma}g_{\omega KK}\frac{-g_{\mu\rho} + q_\mu q_\rho/m_\omega^2}{q^2 - m_\omega^2} \times \left(\gamma^\mu - i\frac{\kappa_{\omega\Sigma\Sigma}}{2m_\Sigma}\sigma^{\mu\nu}q_\nu\right)(k+k')^\rho\delta^{ij}, \tag{C102}$$

$$\bar{V}_d^{22} = -g_{\phi\Sigma\Sigma}g_{\phi KK}\frac{-g_{\mu\rho} + q_\mu q_\rho/m_\phi^2}{q^2 - m_\phi^2} \times \left(\gamma^\mu - i\frac{\kappa_{\phi\Sigma\Sigma}}{2m_\Sigma}\sigma^{\mu\nu}q_\nu\right)(k+k')^\rho\delta^{ij}, \tag{C103}$$

$$\bar{V}_e^{22} = -g_{\rho\Sigma\Sigma}g_{\rho KK}\frac{-g_{\mu\rho} + q_\mu q_\rho/m_\rho^2}{q^2 - m_\rho^2} \times \left(\gamma^\mu - i\frac{\kappa_{\rho\Sigma\Sigma}}{2m_\Sigma}\sigma^{\mu\nu}q_\nu\right)(k+k')^\rho i\epsilon^{jik}\tau_k. \tag{C104}$$

The baryon propagators for the spin-$\frac{1}{2}$ octet baryon B and the spin-$\frac{3}{2}$ decuplet baryon D appearing in Eqs. (C8)–(C104) are given by

$$S_B(p) = \frac{1}{\not{p} - m_B}, \tag{C105}$$

$$S_D^{\mu\nu}(p) = \frac{1}{3(\not{p} - m_D)}\left[2\left(-g^{\mu\nu} + \frac{p^\mu p^\nu}{m_D^2}\right) + \frac{\gamma^\mu\gamma^\nu - \gamma^\nu\gamma^\mu}{2} - \frac{p^\mu\gamma^\nu - p^\nu\gamma^\mu}{m_D}\right]. \tag{C106}$$

Equation (C106) is the simplest choice of many possible definitions of the spin-$\frac{3}{2}$ propagator. It is part of our phenomenology for this rather complex coupled-channels calculations.

Although the expressions (C8)–(C104) look like the usual Feynman amplitudes, the unitary transformation method [15,35–37] defines definite procedures in evaluating the time component of each propagator. For each propagator, the vertex interactions associated with its ends define either a "virtual" process or a "real" process. The real process is the process that can occur in free space such as $\Delta \to \pi N$. The virtual processes, such as the $\pi N \to N$, $\pi\Delta \to \Delta$, and $\pi\Delta \to N$ transitions, are not allowed by the energy-momentum conservation. The consequences of the unitary transformation is the following. When both vertex interactions are "virtual," the propagator is the average of the propagators calculated with two different momenta specified by the initial and final external momenta. For example, the propagator of $\bar{V}_a^1$ of Eq. (C9), which corresponds to the s channel $\pi(k) + N(p) \to N \to \pi(k') + N(p')$, should be evaluated by

$$\begin{aligned} &S_N(p+k) \\ &\to \frac{1}{2}[S_N(p+k) + S_N(p'+k')] \\ &= \frac{1}{2}\left\{\frac{[E_N(p) + E_\pi(k)]\gamma^0 - \vec{\gamma}\cdot(\vec{p}+\vec{k}) + m_N}{[E_N(p) + E_\pi(k)]^2 - (\vec{p}+\vec{k})^2 - m_N^2}\right. \\ &\quad \left. + \frac{[E_N(p') + E_\pi(k')]\gamma^0 - \vec{\gamma}\cdot(\vec{p}'+\vec{k}') + m_N}{[E_N(p') + E_\pi(k')]^2 - (\vec{p}'+\vec{k}')^2 - m_N^2}\right\}. \end{aligned} \tag{C107}$$

One sees clearly that the denominators of the above expression are independent of the collision energy E of scattering equation and finite in the all real momentum region. This is the essence of the unitary transformation method in deriving the interactions from Lagrangian. When only one of the vertex interactions is "real," the propagator is evaluated by using the momenta associated with the "virtual" vertex. For example, the propagator of $\bar{V}_d^{11}$ of Eq. (C53), which corresponds to the s channel $\pi(k) + N(p) \to \Delta \to \pi(k') + \Delta(p')$, is $S_\Delta^{\mu\nu}(p'+k')$, but neither $S_\Delta^{\mu\nu}(p+k)$ nor $[S_\Delta^{\mu\nu}(p'+k') + S_\Delta^{\mu\nu}(p+k)]/2$. We note that there is no propagator in Eqs. (C8)–(C104), which is attached by two real processes such as $\pi N \to \Delta \to \pi N$. Such real processes are included in the resonant term $t^R_{MB,M'B'}$ of Eq. (3).

APPENDIX D: MATRIX ELEMENTS OF $\gamma N \to MB$ TRANSITIONS

To include the final meson-baryon interactions in the photoproduction, it is only necessary to perform the partial-wave decomposition of the final MB state. We thus introduce the following helicity-LSJ mixed representation

$$\begin{aligned} v^{JT}_{L'S'M'B',\lambda_\gamma\lambda_N}(k',q) = \sum_{\lambda'_M\lambda'_B}\sqrt{\frac{(2L'+1)}{2J+1}}\langle j'_M j'_B\lambda'_M(-\lambda'_B)|S'S'_z\rangle \\ \times\langle L'S'0S'_z|JS'_z\rangle\langle J,k'\lambda'_M(-\lambda'_B)| \\ \times v_{M'B',\gamma N}|J,q\lambda_\gamma(-\lambda_N)\rangle, \end{aligned} \tag{D1}$$

where $\langle J,k'\lambda'_M(-\lambda'_B)|v_{M'B',\gamma N}|J,q\lambda_\gamma(-\lambda_N)\rangle$ can be evaluated using the same expression as Eq. (C2) but replacing $v_{M'B',MB}$ with $v_{M'B',\gamma N}$. To evaluate these quantities with our normalizations of states, we define for a photon four-momentum $q = (\omega, \vec{q})$

$$\begin{aligned} &\langle(k'j), p'|v_{M'B',\gamma N}|q, p\rangle \\ &= \frac{1}{\sqrt{2q_0}}\langle(k'j), p'|\sum_n J^\mu(n)\epsilon_\mu|q, p\rangle \\ &= \frac{1}{(2\pi)^3}\sum_n\sqrt{\frac{m_{B'}}{E_{B'}(k')}}\sqrt{\frac{1}{2E_{M'}(k')}} \\ &\quad\times\bar{u}_{B'}(\vec{p}')eI(n)u_N(\vec{p})\sqrt{\frac{m_N}{E_N(q)}}\frac{1}{\sqrt{2q_0}}, \end{aligned} \tag{D2}$$

where ϵ_μ is the photon polarization vector, and n denotes a given considered process

$$I(n) = \epsilon\cdot\bar{j}(n). \tag{D3}$$

Here $\bar{j}(n)$ can be constructed by using the Feynman rules. The resulting expressions for each of $\gamma N \to \pi N, \eta N, \sigma N, \rho N, \pi\Delta, K\Lambda, K\Sigma$ are listed below.

1. $\gamma(q) + N(p) \to \pi(k', j) + N(p')$

$$I(1) = I_a^1 + I_b^1 + I_c^1 + I_d^1 + I_e^1 + I_f^1 + I_g^1 + I_h^1, \quad \text{(D4)}$$

with

$$I_a^1 = +i\frac{f_{\pi NN}}{m_\pi}\ \not{k}'\gamma_5\tau^j \frac{1}{\not{p}' + \not{k}' - m_N}\Gamma_N, \quad \text{(D5)}$$

$$I_b^1 = +i\frac{f_{\pi NN}}{m_\pi}\Gamma_N \frac{1}{\not{p} - \not{k}' - m_N}\ \not{k}'\gamma_5\tau^j, \quad \text{(D6)}$$

$$I_c^1 = -\frac{f_{\pi N\Delta}}{m_\pi}\Gamma_\nu^{\text{em},\Delta\dagger} S_\Delta^{\nu\mu}(p-k')k'_\mu T^j, \quad \text{(D7)}$$

$$I_d^1 = +\frac{f_{\pi NN}}{m_\pi}\epsilon_{ij3}\tau^i\ \not{\epsilon}_\gamma\gamma_5, \quad \text{(D8)}$$

$$I_e^1 = -\frac{f_{\pi NN}}{m_\pi}\frac{\tilde{\not{k}}\gamma_5}{\tilde{k}^2 - m_\pi^2}\epsilon_{ij3}\tau^i(\tilde{k}+k')\cdot\epsilon_\gamma, \quad \text{(D9)}$$

$$I_f^1 = -\frac{g_{\rho NN}g_{\rho\pi\gamma}}{m_\pi}\frac{\tau^j}{2}\left[\gamma^\delta + \frac{\kappa_\rho}{4m_N}(\gamma^\delta\ \tilde{\not{k}} - \tilde{\not{k}}\gamma^\delta)\right] \times \epsilon_{\alpha\beta\eta\delta}\tilde{k}^\eta q^\alpha \epsilon_\gamma^\beta \frac{1}{\tilde{k}^2 - m_\rho^2}, \quad \text{(D10)}$$

$$I_g^1 = -\frac{g_{\omega NN}g_{\omega\pi\gamma}}{m_\pi}\left[\gamma^\delta + \frac{\kappa_\omega}{4m_N}(\gamma^\delta\ \tilde{\not{k}} - \tilde{\not{k}}\gamma^\delta)\right] \times \epsilon_{\alpha\beta\eta\delta}\tilde{k}^\eta q^\alpha \epsilon_\gamma^\beta \delta_{j3}\frac{1}{\tilde{k}^2 - m_\omega^2}. \quad \text{(D11)}$$

In the above equations, we introduced $\tilde{k} = p - p'$, $\Gamma_N = \hat{e}_N\ \not{\epsilon}_\gamma - (\hat{\kappa}_{NN}/4m_N)[\not{\epsilon}_\gamma\ \not{q} - \not{q}\ \not{\epsilon}_\gamma]$, and $\Gamma_\mu^{\text{em},\Delta} = \Gamma_{\mu\nu}^{\text{em},\Delta}\epsilon_\gamma^\nu$.

2. $\gamma(q) + N(p) \to \eta(k') + N(p')$

$$I(2) = I_a^2 + I_b^2 + I_c^2, \quad \text{(D12)}$$

with

$$I_a^2 = +i\frac{f_{\eta NN}}{m_\eta}\ \not{k}'\gamma_5 \frac{1}{\not{p}' + \not{k}' - m_N}\Gamma_N, \quad \text{(D13)}$$

$$I_b^2 = +i\frac{f_{\eta NN}}{m_\eta}\Gamma_N \frac{1}{\not{p} - \not{k}' - m_N}\ \not{k}'\gamma_5, \quad \text{(D14)}$$

$$I_c^2 = -\frac{g_{\rho NN}g_{\rho\eta\gamma}}{m_\rho}\frac{\tau^3}{2}\left[\gamma^\nu + \frac{\kappa_\rho}{4m_N}(\gamma^\nu\ \tilde{\not{k}} - \tilde{\not{k}}\gamma^\nu)\right] \times \epsilon_{\mu\nu\alpha\beta}\tilde{k}^\mu q^\alpha \epsilon_\gamma^\beta \frac{1}{\tilde{k}^2 - m_\rho^2}. \quad \text{(D15)}$$

3. $\gamma(q) + N(p) \to \sigma(k') + N(p')$

$$I(3) = I_a^3 + I_b^3, \quad \text{(D16)}$$

with

$$I_a^3 = -g_{\sigma NN}\frac{1}{\not{p}' + \not{k}' - m_N}\Gamma_N, \quad \text{(D17)}$$

$$I_b^3 = -g_{\sigma NN}\Gamma_N \frac{1}{\not{p} - \not{k}' - m_N}. \quad \text{(D18)}$$

4. $\gamma(q) + N(p) \to \rho'(k', j) + N(p')$

$$I(4) = I_a^4 + I_b^4 + I_c^4 + I_d^4 + I_e^4 + I_f^4 + I_g^4, \quad \text{(D19)}$$

with

$$I_a^4 = -g_{\rho NN}\Gamma_{\rho'}\frac{1}{\not{p}' + \not{k}' - m_N}\Gamma_N, \quad \text{(D20)}$$

$$I_b^4 = -g_{\rho NN}\Gamma_N \frac{1}{\not{p} - \not{k}' - m_N}\Gamma_{\rho'}, \quad \text{(D21)}$$

$$I_c^4 = +\frac{f_{\rho N\Delta}}{m_\rho}(k'_\mu\ \not{\epsilon}_{\rho'}{}^* - \not{k}'\epsilon^*_{\rho'\mu})\gamma_5 T^{\dagger j} S_\Delta^{\mu\nu}(p'+k')\Gamma_\nu^{\text{em},\Delta}, \quad \text{(D22)}$$

$$I_d^4 = -\frac{f_{\rho N\Delta}}{m_\rho}\left[\Gamma_\mu^{\text{em},\Delta}\right]^\dagger S_\Delta^{\mu\nu}(p-k')T^j(k'_\nu\ \not{\epsilon}_\rho{}^* - \not{k}'\epsilon^*_{\rho'\nu})\gamma_5, \quad \text{(D23)}$$

$$I_e^4 = +i\frac{g_{\rho NN}\kappa_\rho}{8m_N}\epsilon_{ij3}\tau_i(\not{\epsilon}_{\rho'}{}^*\ \not{\epsilon}_\gamma - \not{\epsilon}_\gamma\ \not{\epsilon}_{\rho'}{}^*), \quad \text{(D24)}$$

$$I_f^4 = -i\frac{g_{\rho NN}}{2}\left[\gamma_\mu + \frac{\kappa_\rho}{2m_N}(\gamma_\mu\ \tilde{\not{k}} - \tilde{\not{k}}\gamma_\mu)\right]\left[\epsilon_{\rho'}^{\mu*}(\tilde{k}+k')\cdot\epsilon_\gamma - (\tilde{k}\cdot\epsilon^*_{\rho'})\epsilon_\gamma^\mu - (\epsilon_\gamma\cdot\epsilon^*_{\rho'})k'^\mu\right]\frac{\epsilon_{ij3}\tau^i}{\tilde{k}^2 - m_\rho^2}, \quad \text{(D25)}$$

$$I_g^4 = +i\frac{f_{\pi NN}g_{\rho\pi\gamma}}{m_\pi^2}\tau^j\ \tilde{\not{k}}\gamma_5\epsilon_{\alpha\beta\eta\delta}k'^\eta\epsilon_{\rho'}^{\delta*}q^\alpha\epsilon_\gamma^\beta\frac{1}{\tilde{k}^2 - m_\pi^2}. \quad \text{(D26)}$$

5. $\gamma(q) + N(p) \to \pi(k', j) + \Delta(p')$

$$I(5) = I_a^5 + I_b^5 + I_c^5 + I_d^5 + I_e^5 + I_f^5 + I_g^5, \quad \text{(D27)}$$

with

$$I_a^5 = +i\frac{f_{\pi N\Delta}}{m_\pi}\epsilon_\Delta^*\cdot k' T^j S_N(p'+k')\Gamma_N, \quad \text{(D28)}$$

$$I_b^5 = +i\frac{f_{\pi N\Delta}}{m_\pi}\Gamma_\nu^{\text{em},\Delta}\epsilon_\Delta^{\nu*}S_N(p-k')\ \not{k}'\gamma_5\tau^j, \quad \text{(D29)}$$

$$I_c^5 = -\frac{f_{\pi\Delta\Delta}}{m_\pi}\epsilon^*_{\Delta\mu}\ \not{k}'\gamma_5 T_\Delta^j S_\Delta^{\mu\nu}(p'+k')\Gamma_\nu^{\text{em},\Delta}, \quad \text{(D30)}$$

$$I_d^5 = +i\frac{f_{\pi N\Delta}}{m_\pi}\epsilon^*_{\Delta_\eta}\left(\frac{1}{2} + T_\Delta^3\right) \times \left[-g^{\eta\mu}\ \not{\epsilon}_\gamma + (\epsilon_\gamma)^\eta\gamma^\mu\right]S^\Delta_{\mu\nu}(p-k')k'^\nu T^j, \quad \text{(D31)}$$

$$I_e^5 = +\frac{f_{\pi N\Delta}}{m_\pi}\epsilon_{ij3}T^i\epsilon_\gamma\cdot\epsilon_\Delta^*, \quad \text{(D32)}$$

$$I_g^5 = -\frac{f_{\pi N\Delta}}{m_\pi}\epsilon_{ij3}T^i\left[V_g^5 + Z_g^5\right], \quad \text{(D33)}$$

$$I_g^5 = -\frac{f_{\rho N\Delta}}{m_\rho}\frac{g_{\rho\pi\gamma}}{m_\pi}T^j\frac{1}{\tilde{k}^2 - m_\rho^2} \times \left[\tilde{k}\cdot\epsilon_\Delta^*\gamma^\mu - \tilde{\not{k}}\epsilon_\Delta^{*\mu}\right]\gamma_5\epsilon_{\alpha\beta\eta\mu}q^\alpha\epsilon_\gamma^\beta\tilde{k}^\eta, \quad \text{(D34)}$$

where the pion pole term I_g^5 consists of energy-independent interaction V_g^5 and energy-dependent interaction Z_g^5 given as

$$V_g^5 = \frac{1}{2E_\pi(k'-q)} \frac{\epsilon_\Delta^* \cdot k_1 (k_1+k') \cdot \epsilon_\gamma}{E_N(q) - E_\Delta(k') - E_\pi(k'-q)} + \epsilon_\Delta^{0*} \epsilon_\gamma^0, \tag{D35}$$

$$Z_g^5 = \frac{1}{2E_\pi(k'-q)} \frac{\epsilon_\Delta^* \cdot k_2 (k_2+k') \cdot \epsilon_\gamma}{E - E_N(q) - E_\pi(k') - E_\pi(k'-q) + i\epsilon}, \tag{D36}$$

with $k_1 = (E_\pi(k'-q), \vec{k}'-\vec{q})$ and $k_2 = (-E_\pi(k'-q), \vec{k}'-\vec{q})$. The on-shell matrix element of $V_g^5 + Z_g^5$ is given as

$$V^5 + Z^5 = \epsilon_\Delta^* \cdot \tilde{k} (\tilde{k}+k') \cdot \epsilon_\gamma \frac{1}{\tilde{k}^2 - m_\pi^2}. \tag{D37}$$

6. $\gamma(q) + N(p) \to K(k') + \Lambda(p')$

$$\begin{aligned} I(6) &= I_a^6(1/2) + I_b^6 + I_c^6 + I_d^6 + I_e^6 + g^c_{K^*K\gamma} I_f^6 \\ \text{for} \quad \gamma p &\to \Lambda K^+, \end{aligned} \tag{D38}$$

$$\begin{aligned} &= I_a^6(-1/2) + I_b^6 - I_c^6 + g^0_{K^*K\gamma} I_f^6 \\ \text{for} \quad \gamma n &\to \Lambda K^0, \end{aligned} \tag{D39}$$

with

$$I_a^6(t_N) = +i \frac{f_{KN\Lambda}}{m_K} \not{k}' \gamma_5 S_N(p'+k') \Gamma_N(t_N), \tag{D40}$$

$$I_b^6 = +i \frac{f_{KN\Lambda}}{m_K} \Gamma_\Lambda S_\Lambda(p-k') \not{k}' \gamma_5, \tag{D41}$$

$$I_c^6 = +i \frac{f_{KN\Sigma}}{m_K} \Gamma_{\Lambda\Sigma} S_\Sigma(p-k') \not{k}' \gamma_5, \tag{D42}$$

$$I_d^6 = -i \frac{f_{KN\Lambda}}{m_K} \not{\epsilon}_\gamma \gamma_5, \tag{D43}$$

$$I_e^6 = +i \frac{f_{KN\Lambda}}{m_K} \frac{\tilde{\not{k}} \gamma_5}{\tilde{k}^2 - m_K^2} (\tilde{k}+k') \cdot \epsilon_\gamma, \tag{D44}$$

$$I_f^6 = -\frac{g_{K^*N\Lambda}}{m_K} \left[\gamma^\delta + \frac{\kappa_{K^*N\Lambda}}{2(m_N+m_\Lambda)} (\gamma^\delta \tilde{\not{k}} - \tilde{\not{k}} \gamma^\delta) \right] \times \epsilon_{\alpha\beta\eta\delta} \tilde{k}^\eta q^\alpha \epsilon_\gamma^\beta \frac{1}{\tilde{k}^2 - m_{K^*}^2}, \tag{D45}$$

where $t_N = +(-)1/2$ for the proton (neutron).

7. $\gamma(q) + N(p) \to K(k') + \Sigma(p')$

$$\begin{aligned} I(7) &= I_a^7(1/2) + I_b^7 + I_c^7 + I_d^7 + I_e^7 + g^c_{K^*K\gamma} I_f^7 \\ &\quad + I_g^7(0) \quad \text{for} \quad \gamma p \to \Sigma^0 K^+, \end{aligned} \tag{D46}$$

$$\begin{aligned} &= -\sqrt{2}\big[I_a^7(1/2) + I_c^7 + g^0_{K^*K\gamma} I_f^7 \\ &\quad + I_g^7(+1) \big] \quad \text{for} \quad \gamma p \to \Sigma^+ K^0, \end{aligned} \tag{D47}$$

$$\begin{aligned} &= \sqrt{2}\big[I_a^7(-1/2) + I_c^7 + I_d^7 + I_e^7 + g^c_{K^*K\gamma} I_f^7 \\ &\quad + I_g^7(-1) \big] \quad \text{for} \quad \gamma n \to \Sigma^- K^+, \end{aligned} \tag{D48}$$

$$\begin{aligned} &= -I_a^7(-1/2) + I_b^7 - I_c^7 - g^0_{K^*K\gamma} I_f^7 \\ &\quad - I_g^7(0) \quad \text{for} \quad \gamma n \to \Sigma^0 K^0, \end{aligned} \tag{D49}$$

with

$$I_a^7(t_N) = +i \frac{f_{KN\Sigma}}{m_K} \not{k}' \gamma_5 S_N(p'+k') \Gamma_N(t_N), \tag{D50}$$

$$I_b^7 = +i \frac{f_{KN\Lambda}}{m_K} \Gamma_{\Sigma\Lambda} S_\Lambda(p-k') \not{k}' \gamma_5, \tag{D51}$$

$$I_c^7 = +i \frac{f_{KN\Sigma}}{m_K} \Gamma_\Sigma S_\Sigma(p-k') \not{k}' \gamma_5, \tag{D52}$$

$$I_d^7 = -i \frac{f_{K\Lambda\Sigma}}{m_K} \not{\epsilon}_\gamma \gamma_5, \tag{D53}$$

$$I_e^7 = +i \frac{f_{K\Lambda\Sigma}}{m_K} \frac{\tilde{\not{k}} \gamma_5}{\tilde{k}^2 - m_K^2} (\tilde{k}+k') \cdot \epsilon_\gamma, \tag{D54}$$

$$I_f^7 = -\frac{g_{K^*N\Sigma}}{m_K} \left[\gamma^\delta + \frac{\kappa_{K^*N\Lambda}}{2(m_N+m_\Lambda)} (\gamma^\delta \tilde{\not{k}} - \tilde{\not{k}} \gamma^\delta) \right] \times \epsilon_{\alpha\beta\eta\delta} \tilde{k}^\eta q^\alpha \epsilon_\gamma^\beta \frac{1}{\tilde{k}^2 - m_{K^*}^2}, \tag{D55}$$

$$I_g^7(t_\Sigma) = -\frac{f_{KN\Sigma^*}}{m_K} \big[\Gamma_\nu^{\text{em},\Sigma^*\Sigma}(t_\Sigma) \big]^\dagger S_{\Sigma^*}^{\nu\mu}(p-k') k'_\mu, \tag{D56}$$

where $\Gamma_\nu^{\text{em},\Sigma^*\Sigma}(t_\Sigma)$ is the matrix element defined in Eq. (B86), which contains $G_{M,E,C}^{(\Sigma^*)^0\Sigma^0}$ for $t_\Sigma = 0$ and $G_{M,E,C}^{(\Sigma^*)^\pm\Sigma^\pm}$ for $t_\Sigma = \pm 1$.

The isospin projections for the matrix elements are given as

$$j_{1/2p} = \frac{1}{\sqrt{3}} \langle K^+\Sigma^0 | j | p \rangle - \frac{\sqrt{2}}{\sqrt{3}} \langle K^0\Sigma^+ | j | p \rangle, \tag{D57}$$

$$j_{3/2p} = \frac{\sqrt{2}}{\sqrt{3}} \langle K^+\Sigma^0 | j | p \rangle + \frac{1}{\sqrt{3}} \langle K^0\Sigma^+ | j | p \rangle, \tag{D58}$$

TABLE XI. Masses appearing in the meson-exchange potentials. All the masses are kept constant during the fit except for the σ and κ masses, m_σ and m_κ.

Mass	(MeV)
m_N	938.5
m_Λ	1115.7
m_Σ	1193.2
m_Ξ	1318.1
m_Δ	1236.0
m_{Σ^*}	1385.0
m_π	138.5
m_η	547.5
m_K	495.7
m_ρ	769.0
m_{K^*}	893.9
m_ω	782.6
m_ϕ	1019.5
m_{f_0}	974.1
m_{a_1}	1260.0
m_σ	326.2
m_κ	803.6

TABLE XII. Fitted values of coupling constants associated with the meson-exchange potentials. Here only the coupling constants varied and adjusted in the fit are listed. The values of fixed coupling constants can be found in Appendix B.

Couplings		Couplings	
$f_{\eta NN}$	0.050	$f_{KN\Sigma}$	−0.140
$g_{\rho NN}$	4.724	$g_{\kappa\Lambda N}$	2.674
$\kappa_{\rho NN}$	1.177	$g_{\kappa\Sigma N}$	11.823
$g_{\omega NN}$	5.483	$f_{\pi\Lambda\Sigma^*}$	23.060
$\kappa_{\omega NN}$	0.944	$f_{KN\Sigma^*}$	0.039
$g_{\sigma NN}$	13.453	$f_{\pi\Sigma\Sigma^*}$	87.891
$f_{\pi N\Delta}$	1.256	$g_{\kappa K\pi}$	0.094
$g_{\rho N\Delta}$	8.260	$g_{\kappa K\eta}$	−0.147
$f_{\pi\Delta\Delta}$	0.415		
$g_{\rho\Delta\Delta}$	7.576	$f_{KN\Sigma^*} \times G_M^{(\Sigma^*)^0\Sigma^0}$	−0.286
$\kappa_{\rho\Delta\Delta}$	4.799	$f_{KN\Sigma^*} \times G_M^{(\Sigma^*)^+\Sigma^+}$	−0.156
g_{a_1NN}	8.247	$f_{KN\Sigma^*} \times G_M^{(\Sigma^*)^-\Sigma^-}$	−2.648
$g_{f_0NN} \times g_{f_0\pi\pi}$	182.490	$c_{\gamma\pi NN}$	0.896
$c_{\pi\rho NN}$	6.910	$c_{\gamma KN\Lambda}$	−0.003
$c_{\rho\rho NN}$	−1.052	$c_{\gamma KN\Sigma}$	0.001
C_{V1}	0.786	$g_{\gamma\rho\pi}$	0.128
C_{V2}	1.531	$g_{\gamma\omega\pi}$	0.211
$C_S \times m_\sigma^2$	1.683	$g_{\gamma\rho\eta}$	1.150
c_{S31}	−0.152	$g_{\gamma\omega\eta}$	0.237
$g_{\rho\pi\pi}$	6.938		
$g_{\sigma\pi\pi}$	1.173		
$\tilde{g}_{\sigma\pi\pi}$	−3.015		
$g_{\omega\pi\rho}$	4.486		

TABLE XIII. Fitted values of cutoff parameters associated with the meson-exchange potentials.

Cutoffs	(MeV)	Cutoffs	(MeV)
$\Lambda_{\pi NN}$	656	$\Lambda_{\pi\Lambda\Sigma}$	674
$\Lambda_{\eta NN}$	494	$\Lambda_{\pi\Sigma\Sigma}$	1716
$\Lambda_{\rho NN}$	920	$\Lambda_{KN\Sigma}$	1142
$\Lambda_{\omega NN}$	768	$\Lambda_{KN\Lambda}$	500
$\Lambda_{\sigma NN}$	1209	$\Lambda_{K\Xi\Lambda}$	538
Λ_{f_0NN}	680	$\Lambda_{K\Xi\Sigma}$	619
Λ_{a_1NN}	658	$\Lambda_{\eta\Lambda\Lambda}$	880
$\Lambda_{\pi N\Delta}$	709	$\Lambda_{\eta\Sigma\Sigma}$	1676
$\Lambda_{\rho N\Delta}$	1611	$\Lambda_{\rho\Lambda\Sigma}$	1699
$\Lambda_{\pi\Delta\Delta}$	703	$\Lambda_{\rho\Sigma\Sigma}$	1066
$\Lambda_{\rho\Delta\Delta}$	755	$\Lambda_{K^*N\Sigma}$	536
Λ_V	1296	$\Lambda_{K^*N\Lambda}$	1492
Λ_S	1147	$\Lambda_{\omega\Lambda\Lambda}$	672
Λ_{S31}	646	$\Lambda_{\omega\Sigma\Sigma}$	601
$\Lambda_{\rho\pi\pi}$	868	$\Lambda_{\phi\Lambda\Lambda}$	587
$\Lambda_{\sigma\pi\pi}$	1242	$\Lambda_{\phi\Sigma\Sigma}$	1089
$\Lambda'_{\sigma\pi\pi}$	1986	$\Lambda_{\kappa N\Lambda}$	1381
$\Lambda_{f_0\pi\pi}$	1268	$\Lambda_{\kappa N\Sigma}$	800
$\Lambda_{\omega\pi\rho}$	620	$\Lambda_{\pi\Lambda\Sigma^*}$	1582
$\Lambda^{\rm em}_{\pi NN}$	527	$\Lambda_{KN\Sigma^*}$	722
$\Lambda_{\gamma\pi NN}$	883	$\Lambda_{\pi\Sigma\Sigma^*}$	814
		$\Lambda_{\rho KK}$	1600
		$\Lambda_{K^*K\pi}$	1455
		$\Lambda_{\omega KK}$	500
		$\Lambda_{\phi KK}$	500
		$\Lambda_{K^*K\eta}$	500
		$\Lambda_{\kappa K\pi}$	1131
		$\Lambda_{\kappa K\eta}$	1490

TABLE XIV. Fitted values of bare mass $M^0_{N^*}$ of the N^* states.

L_{2I2J}	$M^0_{N^*}$ (MeV)
S_{11} (1)	2400
S_{11} (2)	2878
P_{11} (1)	2210
P_{11} (2)	2440
P_{13} (1)	2087
P_{13} (2)	2901
D_{13} (1)	2480
D_{13} (2)	3926
D_{15} (1)	2058
D_{15} (2)	3258
F_{15}	2292
F_{17}	2629
G_{17}	2785
G_{19}	2733
H_{19}	2967
S_{31}	2100
P_{31} (1)	2374
P_{31} (2)	3287
P_{33} (1)	1600
P_{33} (2)	2397
D_{33} (1)	2403
D_{33} (2)	2564
D_{35} (1)	2231
D_{35} (2)	3700
F_{35} (1)	3131
F_{35} (2)	3710
F_{37} (1)	2076
F_{37} (2)	2698
G_{37}	3218
G_{39}	3541
H_{39}	3400

$$j_{1/2n} = \frac{\sqrt{2}}{\sqrt{3}}\langle K^+\Sigma^-|j|n\rangle - \frac{1}{\sqrt{3}}\langle K^0\Sigma^0|j|n\rangle, \quad \text{(D59)}$$

$$j_{3/2n} = \frac{1}{\sqrt{3}}\langle K^+\Sigma^-|j|n\rangle + \frac{\sqrt{2}}{\sqrt{3}}\langle K^0\Sigma^0|j|n\rangle. \quad \text{(D60)}$$

APPENDIX E: MODEL PARAMETERS

In this appendix, we list the model parameters determined by our global fits to the data of pion- and photon-induced πN, ηN, $K\Lambda$, and $K\Sigma$ reactions in Tables XI–XVI.

Here it will be worthwhile to mention that the bare N^* masses (Table XIV) resulting from the current analysis are larger than those in our early analysis [2] in general. This increase of the value of the bare masses is mainly attributable to the KY channels newly included in this analysis. The coupling of a resonance to a meson-baryon channel produces an attractive (repulsive) mass shift for the resonance which locates in the complex energy plane below (above) the threshold energy of the meson-baryon channel. Therefore, as a general tendency, the value of the bare mass becomes larger when we include a new channel whose threshold energy is higher than the resulting resonance masses.

TABLE XV. Fitted values of cutoffs and coupling constants of the bare $N^* \to MB$ vertices ($MB = \pi N, \eta N, \pi\Delta, \sigma N, \rho N, K\Lambda, K\Sigma$). The corresponding ($LS$) quantum numbers of each MB state are shown in Table II. The cutoff Λ_{N^*} is listed in units of MeV.

L_{2I2J}	Λ_{N^*}	$C_{MB(LS),N^*}$									
		πN	ηN	$(\pi\Delta)_1$	$(\pi\Delta)_2$	σN	$(\rho N)_1$	$(\rho N)_2$	$(\rho N)_3$	$K\Lambda$	$K\Sigma$
S_{11} (1)	2000	12.412	6.374	−0.021	–	0.621	0.457	−0.117	–	2.324	0.352
S_{11} (2)	750	−3.562	7.234	1.124	–	−8.903	5.207	−5.024	–	−0.371	4.968
P_{11} (1)	1179	2.809	1.286	0.743	–	0.293	3.209	−0.600	–	1.124	0.441
P_{11} (2)	517	12.312	−0.479	9.266	–	9.984	12.498	3.210	–	4.545	2.500
P_{13} (1)	518	7.139	−0.248	8.003	−0.929	−2.089	1.341	0.833	1.487	1.237	0.820
P_{13} (2)	1170	1.426	0.089	−4.735	0.147	−0.707	−0.931	−0.300	−0.069	0.543	0.406
D_{13} (1)	1519	0.178	0.125	4.563	−0.040	0.658	0.126	−9.865	−0.230	0.157	−0.063
D_{13} (2)	1614	0.254	0.234	2.063	0.164	0.333	−0.392	1.554	−0.417	0.154	−0.134
D_{15} (1)	613	1.006	−0.475	−2.414	0.001	−0.772	−0.808	1.749	0.215	0.011	−0.065
D_{15} (2)	1286	0.309	−0.004	−0.523	−0.001	−0.084	0.283	−0.182	0.011	0.000	0.086
F_{15}	1003	0.145	−0.010	0.836	−0.178	0.567	−0.161	1.463	−0.005	0.007	−0.017
F_{17}	1028	0.004	0.007	−0.141	0.004	−0.005	0.064	0.025	−0.002	0.046	0.030
G_{17}	1191	0.008	0.001	−0.385	−0.009	0.055	−0.004	−0.436	0.001	0.001	0.003
G_{19}	874	0.013	0.000	−0.081	0.000	−0.000	−0.017	0.019	−0.000	−0.009	0.012
H_{19}	1110	0.002	0.000	−0.043	−0.002	0.010	−0.001	−0.127	0.000	−0.000	0.001
S_{31}	657	0.000	–	−3.829	–	–	−20.000	1.355	–	–	−1.927
P_{31} (1)	725	1.205	–	7.353	–	–	4.252	0.476	–	–	2.386
P_{31} (2)	2000	1.651	–	1.691	–	–	0.607	0.653	–	–	1.259
P_{33} (1)	878	1.038	–	−2.662	0.183	–	0.544	6.000	0.033	–	−0.005
P_{33} (2)	739	10.069	–	5.907	0.308	–	1.621	5.346	0.246	–	0.063
D_{33} (1)	1086	0.512	–	13.498	−0.060	–	−0.272	−8.482	0.963	–	0.193
D_{33} (2)	629	0.144	–	−1.599	−0.260	–	0.933	3.901	−2.794	–	−0.523
D_{35} (1)	641	0.573	–	−0.527	0.029	–	0.917	−0.312	0.213	–	0.490
D_{35} (2)	1098	0.602	–	−0.268	−0.004	–	−0.606	0.543	−0.008	–	−0.201
F_{35} (1)	1026	0.032	–	3.181	−0.284	–	0.114	3.558	0.088	–	0.083
F_{35} (2)	1631	0.048	–	2.872	0.001	–	−0.001	−0.233	−0.005	–	0.006
F_{37} (1)	778	0.216	–	0.308	0.004	–	0.019	−0.072	0.002	–	0.026
F_{37} (2)	903	0.145	–	0.208	−0.001	–	0.131	0.110	−0.000	–	−0.052
G_{37}	1203	0.006	–	−0.384	−0.016	–	0.002	0.480	0.002	–	0.002
G_{39}	874	0.022	–	−0.108	0.000	–	0.004	−0.003	0.000	–	−0.003
H_{39}	973	0.001	–	−0.086	−0.010	–	0.001	0.167	0.001	–	0.004

TABLE XVI. Fitted values of model parameters associated with the bare $\gamma N \to N^*$ helicity amplitudes defined in Eqs. (19)–(25). In the last column, fixed values of M_{N^*} that are used for computing q_R in Eq. (19) are presented. The helicity amplitudes $\tilde{A}_{1/2}$ and $\tilde{A}_{3/2}$ shown in the third and the fourth columns, respectively, are $A_{1/2}$ and $A_{3/2}$ calculated at $q = m_\pi$, where $\tilde{M}^{N^*}_{l\pm}$ and $\tilde{E}^{N^*}_{l\pm}$ are obtained with the use of the relations in Eqs. (20)–(23). As for the first bare P_{33} state [$P_{33}(1)$], we list the value of $x_{A_{1/2}}$ and $x_{A_{3/2}}$ in the columns of $\tilde{A}^{N^*}_{1/2}$ and $\tilde{A}^{N^*}_{3/2}$, respectively.

L_{2I2J}	$\Lambda^{\text{e.m.}}_{N^*}$ (MeV)	$\tilde{A}^{N^*}_{1/2}$ (10^{-3} GeV$^{-1/2}$)	$\tilde{A}^{N^*}_{3/2}$ (10^{-3} GeV$^{-1/2}$)	M_{N^*} (MeV)
S_{11} (1)	634	78.79	–	1535
S_{11} (2)	1595	−2.92	–	1650
P_{11} (1)	1035	−1.83	–	1440
P_{11} (2)	1558	56.60	–	1710
P_{13} (1)	1208	3.07	1.67	1720
P_{13} (2)	510	258.77	−22.46	1900
D_{13} (1)	538	27.24	−59.49	1520
D_{13} (2)	986	−7.53	4.00	1700
D_{15} (1)	655	0.62	7.40	1675
D_{15} (2)	1099	5.39	5.03	2200
F_{15}	569	7.22	−10.18	1680
F_{17}	870	0.35	0.12	1990

TABLE XVI. (*Continued*.)

L_{2I2J}	$\Lambda_{N^*}^{\text{e.m.}}$ (MeV)	$\tilde{A}_{1/2}^{N^*}$ (10^{-3} GeV$^{-1/2}$)	$\tilde{A}_{3/2}^{N^*}$ (10^{-3} GeV$^{-1/2}$)	M_{N^*} (MeV)
G_{17}	510	4.71	−5.89	2190
G_{19}	505	−3.05	−5.09	2250
H_{19}	1589	0.03	0.03	2220
S_{31}	500	−291.50	–	1620
P_{31} (1)	1599	6.49	–	1750
P_{31} (2)	1600	4.04	–	1910
P_{33} (1)	–	1.10	1.36	1238
P_{33} (2)	1670	−32.08	−59.12	1600
D_{33} (1)	1615	−11.53	−18.14	1700
D_{33} (2)	1374	−6.31	−44.47	1940
D_{35} (1)	826	8.41	8.40	1935
D_{35} (2)	594	−1.97	−30.00	1935
F_{35} (1)	1601	1.08	1.84	1905
F_{35} (2)	1306	−1.01	−1.81	2000
F_{37} (1)	1562	−0.49	−0.55	1950
F_{37} (2)	703	−5.36	−8.43	2390
G_{37}	500	12.07	10.74	2200
G_{39}	803	0.75	1.39	2400
H_{39}	518	−2.34	−1.67	2300

[1] A. Matsuyama, T. Sato, and T.-S. H. Lee, Phys. Rep. **439**, 193 (2007).

[2] B. Juliá-Díaz, T.-S. H. Lee, A. Matsuyama, and T. Sato, Phys. Rev. C **76**, 065201 (2007).

[3] B. Juliá-Díaz, T.-S. H. Lee, A. Matsuyama, T. Sato, and L. C. Smith, Phys. Rev. C **77**, 045205 (2008).

[4] B. Juliá-Díaz, H. Kamano, T.-S. H. Lee, A. Matsuyama, T. Sato, and N. Suzuki, Phys. Rev. C **80**, 025207 (2009).

[5] J. Durand, B. Juliá-Díaz, T.-S. H. Lee, B. Saghai, and T. Sato, Phys. Rev. C **78**, 025204 (2008).

[6] H. Kamano, B. Juliá-Díaz, T.-S. H. Lee, A. Matsuyama, and T. Sato, Phys. Rev. C **79**, 025206 (2009).

[7] H. Kamano, B. Juliá-Díaz, T.-S. H. Lee, A. Matsuyama, and T. Sato, Phys. Rev. C **80**, 065203 (2009).

[8] N. Suzuki, T. Sato, and T.-S. H. Lee, Phys. Rev. C **79**, 025205 (2009).

[9] N. Suzuki, T. Sato, and T.-S. H. Lee, Phys. Rev. C **82**, 045206 (2010).

[10] N. Suzuki, B. Juliá-Díaz, H. Kamano, T.-S. H. Lee, A. Matsuyama, and T. Sato, Phys. Rev. Lett. **104**, 042302 (2010).

[11] H. Kamano, S. X. Nakamura, and T.-S. H. Lee, and T. Sato, Phys. Rev. C **81**, 065207 (2010).

[12] B. C. Pearce and B. K. Jennings, Nucl. Phys. A **528**, 655 (1991).

[13] C. C. Lee, S. N. Yang, and T.-S. H. Lee, J. Phys. G **17**, L131 (1991); C. T. Hung, S. N. Yang, and T.-S. H. Lee, Phys. Rev. C **64**, 034309 (2001).

[14] F. Gross and Y. Surya, Phys. Rev. C **47**, 703 (1993).

[15] T. Sato and T.-S. H. Lee, Phys. Rev. C **54**, 2660 (1996); **63**, 055201 (2001); B. Juliá-Díaz, T.-S. H. Lee, T. Sato, and L. C. Smith, *ibid.* **75**, 015205 (2007).

[16] Y. Elmessiri and M. G. Fuda, Phys. Rev. C **60**, 044001 (1999); M. G. Fuda and H. Alharbi, *ibid.* **68**, 064002 (2003).

[17] V. Pascalutsa and J. A. Tjon, Phys. Rev. C **61**, 054003 (2000); G. L. Caia, L. E. Wright, and V. Pascalutsa, *ibid.* **72**, 035203 (2005).

[18] W.-T. Chiang, F. Tabakin, T.-S. H. Lee, and B. Saghai, Phys. Lett. B **517**, 101 (2001); B. Juliá-Díaz, B. Saghai, T.-S. H. Lee, and F. Tabakin, Phys. Rev. C **73**, 055204 (2006).

[19] A. M. Gasparyan, J. Haidenbauer, C. Hanhart, and J. Speth, Phys. Rev. C **68**, 045207 (2003); M. Döring, C. Hanhart, F. Huang, S. Krewald, and U.-G. Meißner, Nucl. Phys. A **829**, 170 (2009); M. Döring, C. Hanhart, F. Huang, S. Krewald, U.-G. Meißner, and D. Rönchen, *ibid.* **851**, 58 (2011); F. Huang, M. Döring, H. Haberzettl, J. Haidenbauer, C. Hanhart, S. Krewald, U.-G. Meißner, and K. Nakayama, Phys. Rev. C **85**, 054003 (2012).

[20] D. Rönchen, M. Döring, F. Huang, H. Haberzettl, J. Haidenbauer, C. Hanhart, S. Krewald, U.-G. Meißner, and K. Nakayama, Eur. Phys. J. A **49**, 44 (2013).

[21] R. A. Arndt, J. M. Ford, and L. D. Roper, Phys. Rev. D **32**, 1085 (1985); R. A. Arndt, W. J. Briscoe, I. I. Strakovsky, and R. L. Workman, Phys. Rev. C **74**, 045205 (2006), and references therein.

[22] A. V. Anisovich, A. V. Sarantsev, O. Bartholomy, E. Klempt, V. A. Nikonov, and U. Thoma, Eur. Phys. J. A **25**, 427 (2005); A. V. Sarantsev *et al.*, Phys. Lett. B **659**, 94 (2008); A. V. Anisovich, E. Klempt, V. Kuznetsov, V. A. Nikonov, M. V. Polyakov, A. V. Sarantsev, and U. Thoma, *ibid.* **719**, 89 (2013); A. V. Anisovich, R. Beck, E. Klempt, V. A. Nikonov, A. V. Sarantsev, and U. Thoma, Eur. Phys. J. A **48**, 88 (2012); A. V. Anisovich, E. Klempt, V. A. Nikonov, A. V. Sarantsev, H. Schmieden, and U. Thoma, Phys. Lett. B **711**, 162 (2012); A. V. Anisovich, E. Klempt, V. A. Nikonov, A. V. Sarantsev, and U. Thoma, *ibid.* **711**, 167 (2012); Eur. Phys. J. A **47**, 153 (2011); **47**, 27 (2011); A. V. Anisovich, E. Klempt, V. A. Nikonov, M. A. Matveev, A. V. Sarantsev, and U. Thoma, *ibid.* **44**, 203 (2010).

[23] A. V. Anisovich, R. Beck, E. Klempt, V. A. Nikonov, A. V. Sarantsev, and U. Thoma, Eur. Phys. J. A **48**, 15 (2012), and references therein.

[24] D. M. Manley, R. A. Arndt, Y. Goradia, and V. L. Teplitz, Phys. Rev. D **30**, 904 (1984); D. M. Manley and E. M. Saleski, *ibid.* **45**, 4002 (1992).

[25] D. Drechsel, O. Hanstein, S. S. Kamalov, and L. Tiator, Nucl. Phys. A **645**, 145 (1999); S. S. Kamalov, S. N. Yang, D. Drechsel, O. Hanstein, and L. Tiator, Phys. Rev. C **64**, 032201(R) (2001).

[26] I. G. Aznauryan, Phys. Rev. C **68**, 065204 (2003).

[27] V. I. Mokeev, V. D. Burkert, T.-S. H. Lee, L. Elouadrhiri, G. V. Fedotov, and B. S. Ishkhanov, Phys. Rev. C **80**, 045212 (2009).

[28] T. Feuster and U. Mosel, Phys. Rev. C **58**, 457 (1998); **59**, 460 (1999); V. Shklyar, H. Lenske, U. Mosel, and G. Penner, *ibid.* **71**, 055206 (2005).

[29] A. Usov and O. Scholten, Phys. Rev. C **72**, 025205 (2005).

[30] R. E. Cutkosky, C. P. Forsyth, R. E. Hendrick, and R. L. Kelly, Phys. Rev. D **20**, 2839 (1979); R. E. Cutkosky and S. Wang, *ibid.* **42**, 235 (1990).

[31] M. Batinic, I. Slaus, A. Svarc, and B. M. K. Nefkens, Phys. Rev. C **51**, 2310 (1995); M. Batinic, I. Dadic, I. Slaus, A. Svarc, B. M. K. Nefkens, and T.-S. H. Lee, Phys. Scr. **58**, 15 (1998); S. Ceci, A. Svarc, and B. Zauner, Phys. Rev. Lett. **97**, 062002 (2006).

[32] T. P. Vrana, S. A. Dytman, and T.-S. H. Lee, Phys. Rep. **328**, 181 (2000).

[33] C. D. Roberts, I. C. Cloët, L. Chang, and H. L. L. Roberts, AIP Conf. Proc. **1432**, 309 (2012).

[34] H. Feshbach, *Theoretical Nuclear Physics, Nuclear Reactions* (Wiley, New York, 1992).

[35] M. Kobayashi, T. Sato, and H. Ohtsubo, Prog. Theor. Phys. **98**, 927 (1997).

[36] B. Juliá-Díaz, H. Kamano, T.-S. H. Lee, A. Matsuyama, T. Sato, and N. Suzuki, Chin. J. Phys. **47**, 142 (2009).

[37] T. Sato and T.-S. H. Lee, J. Phys. G **36**, 073001 (2009).

[38] A. Bohm, *Quantum Mechanics: Foundations and Applications* (Springer-Verlag, New York, 1993).

[39] R. H. Dalitz and R. G. Moorhouse, Proc. R. Soc. London A **318**, 279 (1970); A. J. F. Siegert, Phys. Rev. **56**, 750 (1939).

[40] CNS Data Analysis Center, George Washington University University, http://gwdac.phys.gwu.edu

[41] G. Hohler, F. Kaiser, R. Koch, and E. Pietarinen, *Handbook of Pion Nucleon Scattering, Physics Data* (FIZ-Karlsruhe, Berlin, 1979), Vol. 12; G. Höhler, *Pion-nucleon Scattering* (Springer-Verlag, Berlin, 1983), Vol. I/92; G. Hoehler and A. Schulte, πN Newsl. **7**, 94 (1992); G. Hoehler, *ibid.* **9**, 1 (1993).

[42] R. E. Cutkosky, R. E. Hendrick, J. W. Alcock, Y. A. Chao, R. G. Lipes, J. C. Sandusky, and R. L. Kelly, Phys. Rev. D **20**, 2804 (1979); R. L. Kelly and R. E. Cutkosky, *ibid.* **20**, 2782 (1979).

[43] A. Thiel *et al.* (CBELSA/TAPS Collaboration), Phys. Rev. Lett. **109**, 102001 (2012).

[44] A. M. Sandorfi, S. Hoblit, H. Kamano, and T.-S. H. Lee, J. Phys. G **38**, 053001 (2011).

[45] W.-T. Chiang and F. Tabakin, Phys. Rev. C **55**, 2054 (1997).

[46] A. M. Sandorfi, B. Dey, A. Sarantsev, L. Tiator, and R. Workman, AIP Conf. Proc. **1432**, 219 (2012); see arXiv:1108.5411v2 for the updated version.

[47] J. Ahrens *et al.* (GDH and A2 Collaboration), Phys. Rev. Lett. **88**, 232002 (2002); Eur. Phys. J. A **21**, 323 (2004); Phys. Rev. C **74**, 045204 (2006).

[48] K. Hicks and H. Sako *et al.*, Proposal for Measurements of $\pi N \to \pi\pi N$ and $\pi N \to KY$ at J-PARC (J-PARC P45), http://j-parc.jp/researcher/Hadron/en/pac_1207/pdf/P45_2012-3.pdf.

[49] A. Sandorfi, J. Phys.: Conf. Ser. **424**, 012001 (2013).

[50] J. Beringer *et al.* (Particle Data Group), Phys. Rev. D **86**, 010001 (2012).

[51] I. G. Aznauryan, V. D. Burkert, and T.-S. H. Lee, arXiv:0810.0997.

[52] D. Drechsel, S. S. Kamalov, and L. Tiator, Eur. Phys. J. A **34**, 69 (2007).

[53] M. Dugger *et al.* (CLAS Collaboration), Phys. Rev. C **76**, 025211 (2007).

[54] J. Segovia, C. Chen, C. D. Roberts, and S. Wan, arXiv:1305.0292.

[55] B. Dey, M. E. McCracken, D. G. Ireland, and C. A. Meyer, Phys. Rev. C **83**, 055208 (2011).

[56] R. L. Workman, M. W. Paris, W. J. Briscoe, L. Tiator, S. Schumann, M. Ostrick, and S. S. Kamalov, Eur. Phys. J. A **47**, 143 (2011).

[57] H. Kamano, S. X. Nakamura, T.-S. H. Lee, and T. Sato, Phys. Rev. D **84**, 114019 (2011).

[58] S. X. Nakamura, H. Kamano, T.-S. H. Lee, and T. Sato, Phys. Rev. D **86**, 114012 (2012).

[59] V. D. Burkert and T.-S. H. Lee, Int. J. Mod. Phys. E **13**, 1035 (2004).

[60] I. G. Aznauryan *et al.*, Int. J. Mod. Phys. E **22**, 1330015 (2013); arXiv:0907.1901.

[61] S. X. Nakamura, Y. Hayato, M. Hirai, H. Kamano, S. Kumano, M. Sakuda, K. Saito, and T. Sato, arXiv:1303.6032.

[62] T. Sato, D. Uno, and T.-S. H. Lee, Phys. Rev. C **67**, 065201 (2003).

[63] K. Matsui, T. Sato, and T.-S. H. Lee, Phys. Rev. C **72**, 025204 (2005).

[64] H. Kamano, S. X. Nakamura, T.-S. H. Lee, and T. Sato, Phys. Rev. D **86**, 097503 (2012).

[65] H. Kamano and T.-S. H. Lee, AIP Conf. Proc. **1432**, 74 (2012).

[66] M. Betz and T.-S. H. Lee, Phys. Rev. C **23**, 375 (1981).

[67] J. D. Bjorken and S. D. Drell, *Relativistic Quantum Field Theory* (McGraw-Hill, New York, 1964).

[68] Y. Oh, K. Nakayama, and T.-S. H. Lee, Phys. Rep. **423**, 49 (2006).

[69] M. Jacob and G. C. Wick, Ann. Phys. **7**, 404 (1959); **281**, 774 (2000).